RELIABLE MULTIPHASE INDUCTION MOTOR DRIVES

A Dissertation

by

VIVEK MEENAKSHI SUNDARAM

Submitted to the Office of Graduate and Professional Studies of
Texas A&M University
in partial fulfillment of the requirements for the degree of

DOCTOR OF PHILOSOPHY

Chair of Committee,	Hamid Toliyat
Committee Members,	Mehrdad Ehsani
	Shankar Bhattacharyya
	Won-Jong Kim
Head of Department,	Miroslav Begovic

August 2016

Major Subject: Electrical Engineering

ABSTRACT

A motor is said to be reliable if it can run at its rated operating condition for a specified period of time. With the widespread use of electric motors in newer applications, reliability is a major concern in terms of safety as well as revenue. About 30-40% of reported failures in induction motors are due to stator faults. It is well known that a stator fault starts as an inter-turn fault within a phase and then propagates into phase-to-phase and phase-to-ground faults that can then lead to complete shutdown of the motor. Two approaches have been taken in this dissertation to make an induction motor drive system more tolerant to stator faults; integration of an inter-turn fault detection method into a five-phase induction motor drive and design of fault-tolerant induction motors.

The phase redundancy of five-phase motors makes it possible to achieve continued operation of the motor with an open phase. However, for true fault tolerance the drive must be able to detect an incipient fault and then transition to post fault operation. A low-cost diagnostic method based on DC voltage injection has been developed for detection of inter-turn faults in five-phase induction motor drive systems. It has been shown that difference in DC current response to an injected voltage before and after an inter-turn fault serves as a reliable fault indicator. The diagnostic is non-intrusive, requires no additional hardware and effectively integrates both fault detection and fault-tolerant control into the motor controller. The method has been successfully implemented and tested on low-cost microcontroller.

The propagation of a stator inter-turn fault into a phase-to-phase fault is worsened in distributed winding induction motors where the different phase windings overlap each other at the end connections. Tooth wound or fractional slot concentrated winding (FSCW) stators have non-overlapping end connections and hence more physical and thermal isolation between the phases as compared to distributed winding stators. While FSCW configurations have been widely used for permanent magnet motors, their adoption for induction motors is a challenge. An FSCW configuration has been designed for outer rotor induction motors by using a dual slot layer stator structure and multilayer windings. Comparison with a conventional induction motor shows an 11% reduction in the copper usage in addition to having non-overlapping phase windings.

To my wife, Suhasini and my parents

ACKNOWLEDGEMENTS

First, I thank my advisor Dr. Hamid A. Toliyat, with whom I spent the last six years of my graduate life, for all the advice, encouragement and support he has given me throughout the course of this research. He is my role model and a source of inspiration, and I feel honored to have had to opportunity to work under him.

I thank my committee members Dr. Mehrdad Ehsani, Dr. Shankar Bhattacharyya and Dr.Won-Jong Kim for their valuable time. I have learned a lot from their courses. I thank my colleagues at the Advanced Electric Machines and Power Electronics Lab, Yateendra, Matthew Johnson, Jae-Bum, Siavash, Mahshid, Morteza, Ajay, Babak, Robert, Hussain, Hamidreza, Khaled, Abdulkadir, Amir, Niloofar, Bahar, Matthew Gardner and Yongqi. I learnt a great deal from my countless interactions with them. I also thank all my friends and roommates who made my life at Texas A&M University fun and memorable.

Finally I thank my parents, my brother and my wife Suhasini who patiently supported and encouraged me throughout this endeavor.

TABLE OF CONTENTS

Page

LIST OF FIGURES

Page

LIST OF TABLES

Page

1. INTRODUCTION

Electric motor drives are now being used in a wide variety of newer applications. Motor drive reliability is an important driving factor where safety and/or revenue are a major concern. Some examples are

- Applications where motor or drive failure is a safety hazard – Traction motors used in electric and hybrid electric vehicles,
- Applications where accessibility to the motor is difficult; Off-shore wind turbine generators and sub-sea oil pump motors and drives,
- Applications where failure of the motor can cascade into failure of the entire system; Motors used in appliances and HVAC systems.

A highly reliable system is one where the components of the system have a longer mean time to failure. The term reliability in the context of motors is defined as the ability of the motor to perform under its rated operating conditions for a specified amount of time. From the point of view of motor drives some common ways to improve the reliability of the system are;

- Designing high efficiency motors and inverters to improve their thermal overload capabilities - Since overheating is the most common source of failure, improving the efficiency of the motor reduces the heat generated by losses.
- Avoiding the use of components that are prone to failure - From the mechanical side, components like belts and gear boxes are more susceptible to failure and

require routine maintenance or replacement. Electrolytic capacitors have been identified as the reliability-limiting component in inverters.

- Designing motors and inverters that are inherently tolerant to faults – Using stators with magnetically/physically decoupled phase windings helps contain a fault to the affected phase and isolate the faulty phase for post fault operation.
- Adding non-intrusive condition monitoring systems to monitor and detect incipient faults – Motor current signature analysis (MCSA) correlates specific frequency components in the current with faults in the winding or bearings. Alternatively vibration monitoring can also be used for detecting mechanical faults.
- Adding redundancies to the motor drive system that enable continued operation after a failure- With additional phases over three, it is possible to make the motor tolerant to faults while simultaneously improving the efficiency and performance of the overall motor drive system. Driving the motor phases with full bridge inverters also allows for seamless fault-tolerant operation.
- Performing scheduled maintenance to prolong the life of the system and minimize operating costs,

Most of the above methods add additional cost and complexity to the system but can still be justified depending on the application. While making the motor drive inherently tolerant to faults is not always feasible it is an attractive way to achieve fault-tolerant ability without adding cost and complexity. However achieving this fault tolerance at the cost of degraded performance of the motor under healthy operating condition is seldom justifiable. In contrast, adding redundancies is a definite method of

improving the reliability of motor drives without affecting or sometimes even improving its performance under healthy operation.

A true fault-tolerant motor drive system should perform the following steps

- Condition monitoring – Identifying incipient faults usually through non-intrusive methods,
- Fault detection – Detecting the type and location of the fault after it has occurred,
- Fault isolation – Isolating the faulty winding/component to prevent propagation of the fault,
- Fault-tolerant control – Continued post-fault operation of the motor albeit at reduced capacity.

1.1 Faults in Induction Motors

The first step to improving the reliability of an induction motor drive system is to identify the most common sources of failure. Faults in induction motors are broadly classified into the following:

Stator faults – These faults constitute 30-40% of motor faults and are always the result of failure in the stator winding insulation system [1]. Deterioration of the insulation is usually the combined effect of thermal loading, mechanical vibrations, voltage stresses and external contamination. Stator faults can be classified into several types depending on the nature of the fault, as shown in Figure 1.

- Phase-to-ground faults - Caused by short circuit between the stator phase winding and the stator core due to the breakdown of the ground wall insulation in the slot. The stator core is grounded through the housing making this a phase-to-ground fault.
- Phase-to-phase faults – Caused by short circuit between two or more phases of the stator. The location of this type of fault is usually in the end windings of the motor where the different phases of the motor overlap each other.
- Inter-turn faults – Faults caused by a short circuit between the turns of a particular phase. The inter-turn fault eventually cascades into a phase-to-phase or phase to ground fault.

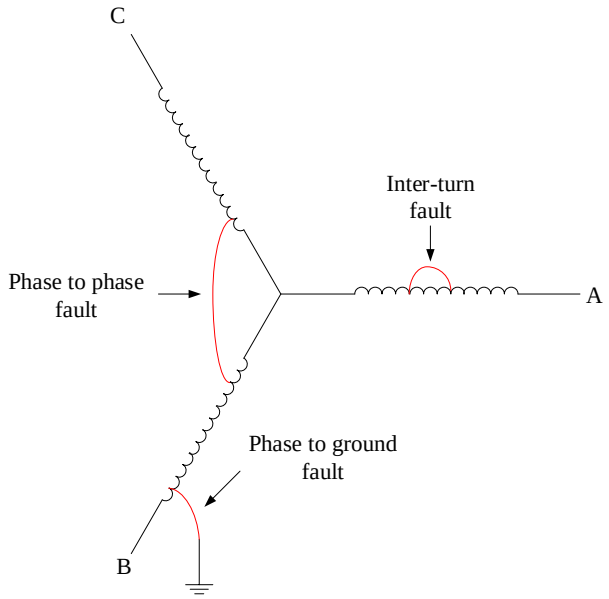

Figure 1. Types of stator winding faults in a three-phase motor

Rotor Faults – Rotor electrical faults are classified into broken bar and end ring faults both of which are primarily caused by mechanical stresses acting on the rotor cage. These faults account for 5-10% of induction motor failure [1].

Mechanical Faults – Bearings used in electrical motors are either ball or roller bearings and mechanical faults results from faults in the bearing which are sub-classified into:

- Inner bearing race defects
- Outer bearing race defects
- Ball defects

40-50% of motor faults are caused by bearing failure [1]. Rotor faults can also be caused by rotor ellipticity, or misalignment.

1.2 Stator Inter-Turn Faults Detection

Among the above discussed stator faults inter-turn faults are the hardest to detect but the most severe and can lead to a catastrophic failure in a very short span of time. Inter-turn shorts are generally recognized as the beginning stage of a phase to phase or phase to ground fault although there is little to no information available on the lead time to failure [14].

An inter-turn fault results in a circulating current that flows through the shorted turns. The amplitude of this circulating current is a function of the following,

- Number of shorted turns, often called fault severity
- Location of the shorted turns in the slot
- Speed of operation of the motor

- Mutual coupling between the phases

Counterintuitively the lesser the number of shorted turns the larger the short circuit current [2]. The voltage induced in the shorted turns increases proportional to the number of turns but while the resistance is directly proportional to the number of turns, the inductance has a square proportionality. This effect has been confirmed in the literature [3], [4].

For conventional distributed winding induction motors the mutual coupling between the phases is significant, and they are not inherently fault-tolerant like tooth wound permanent magnet motors [5] and switched-reluctance motors. Traditionally, since induction motors are symmetric an incipient inter-turn fault in the phase winding is accompanied by the following effects

- Unbalanced currents and voltages
- Torque pulsation resulting in noise and vibration
- Excessive localized heating and increased losses
- Saturation harmonics caused by the short circuit current

A lot of work has gone into detection of inter-turn faults in the past [6]-[10] but most of the work thus far has been on grid-fed machines. The focus of this review has been restricted to on-line, non-intrusive condition monitoring methods that rely on measurable electrical or mechanical quantities like currents, voltages, flux, and torque. Such methods are more relevant for drive-fed motors especially from the standpoint of fault-tolerant operation. The unbalanced phase impedances created in the stator as a result of the turn fault and its effects on various electrical quantities has been studied extensively. Due to the asymmetry created in the motor windings a negative sequence component is

introduced in the current. In [11], it is proposed to use this negative sequence current component as a fault indicator. Several other effects of this unbalance have also been used as fault indicators such as the:

- Ellipticity in the park vector of the current [12] [13] - This is derived from the fact that in the presence of unbalanced currents, the stationary frame d- and q-axes current components have different amplitudes and trace an ellipse in the stationary d-q plane.
- Envelope of the stator current [15]
- Multiple reference frames [16] – An alternate reference frame rotating at negative of fundamental frequency i.e. in a direction opposite to the synchronous frame, is used for separation of the negative sequence component. This method is suitable for digital implementation and can be implemented on the microcontroller that controls the motor.

Additionally, some secondary effects of the impedance unbalance such as second order harmonics in the instantaneous power [17] and torque [18] can also serve as fault indicators. All these methods are unreliable when considering the fact that the negative sequence current can be created by other factors such as saturation, unbalanced supply voltages and rotor eccentricity. One way of separating the effect of unbalanced supply voltage is discussed in [19] where the negative sequence impedance is used as a fault indicator. The negative sequence impedance is calculated from the negative sequence voltage and current and is shown to vary when a winding fault occurs in the motor. The

cross admittance between the negative sequence current and positive sequence voltage has also been used in [20] and shown to be related to the number of shorted turns.

Another alternative method explored in the literature is the use of zero sequence voltage which occurs if there is an unbalance in the phases of the motor with star connected windings [21]. This fault index, though reliable, requires access to the neutral as well as voltage sensors to measure the phase voltages. The use of high frequency current components caused due to slotting has also been investigated in the literature [22] for detection of turn faults. Such an approach however, requires additional hardware for data acquisition and spectral analysis to capture the higher order frequency components. In [23], high frequency signal injection is used with limited success as a method for stator inter-turn fault detection.

For drive-fed motors with closed loop current and speed control, the dynamics of the current controller presents additional challenges for the effective implementation of a condition monitoring method. The controller tries to cancel the negative sequence current produced by the inter-turn fault by applying a negative sequence voltage. In [24], this negative sequence voltage has been used to detect winding faults. If the control loop is implemented in the synchronous reference frame, which is the case in most drives, the negative sequence current appears in the control loop as a sinusoidal signal at double the fundamental frequency. This second order harmonic introduced in the measured d-axis current as calculated by the controller has also been proposed as a fault indicator in [24]. A similar cancelling effect of the controller can also be seen in the lower order saturation harmonics created by the inter-turn short circuit current.

A common requirement of all fault detection methods is the need to account for inherent asymmetries that may already be present in the healthy motor. Additionally, for methods that are intended for drive-fed motors, the non-linearity in the inverter switches as well as in the sensing and signal conditioning circuits, have to be taken into account. For a successful implementation of a diagnostic method and to avoid false positives it is necessary to compensate for these effects. Artificial neural networks and pattern recognition techniques have been utilized effectively in the literature for this purpose [25]. However these methods are complicated to implement and require additional sensing. A simple alternative that has been widely used and is ideal for low-cost fault diagnostic systems is a look-up table based method. The premise of this method is to measure and store the fault index of the healthy motor over its entire operating range. The availability of fast microcontrollers with larger memory capacities has made this relatively easy from a drive perspective. The look-up table then serves as the reference, based on which the fault decision is made when the motor is operating. The accuracy of the fault detection is dependent on the resolution of the look-up table. A successful implementation of the look-up table based method can be seen in [26].

1.3 Fault-Tolerant Operation

1.3.1 Control of Five-Phase Motors

In safety critical and cost sensitive applications, early detection of the fault followed by a fault-tolerant control is required to maintain uninterrupted operation and prolong the life of the system. Multiphase machines are an attractive alternative due to the

redundancies introduced in the system by the presence of additional phases. Apart from having the ability to operate post fault due to the additional degrees of freedom, they have several other benefits over conventional three-phase motors [27].

- Higher torque density
- Reduced torque ripple
- Fault-tolerant capability
- Reduced rating of inverter switches

Operation of an inverter-fed three-phase motor with an open phase requires access to the neutral point, a divided DC bus and injection of a zero sequence current. In general, an *m*-phase motor can continue to operate with up to *(m-3)* phases opened, without any hardware modifications. From the point of view of the drive, the number of inverter legs increases with the number of phases, introducing additional sources of failure into the system as shown in Figure 2.

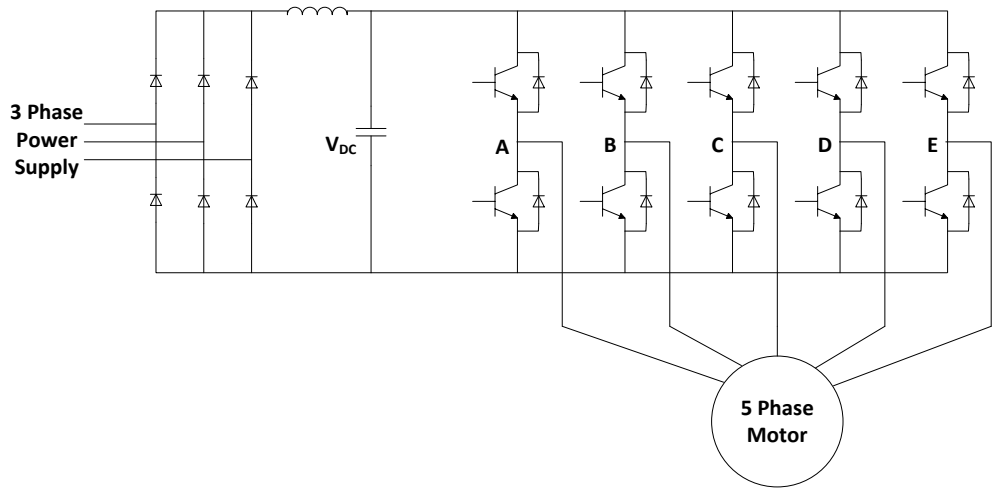

Figure 2. A five-phase motor driven using five leg inverter

The choice of five phases provides a good compromise between adding complexity in terms of motor control implementation, and the ability to operate with up to two open phases. For five-phase motors with concentrated stator windings, it has also been shown that torque enhancement can be achieved by injecting a third harmonic and creating a trapezoidal air gap flux [28]. The earliest papers on the control of five-phase motors used hysteresis current controllers with the control loop set up in the stationary reference frame [29]. However, similar to a conventional three-phase motor the vector control of a healthy five-phase motor can be performed in the synchronous frame using a synchronous frame transformation to convert the phase variables a-b-c-d-e to d-q-x-y-0. For a balanced motor, it can be shown that only the d- and q- components are coupled with the rotor and can independently control the torque and flux.

Figure 3 shows the implementation of stationary reference frame V/f control and Figure 4 shows synchronous reference frame indirect field oriented control in a five-phase motor. It has also been shown that constant and variable switching frequency DTC (direct torque control) schemes can be applied to five-phase induction motors [30]. It is worthwhile to note that x-y current components will still exist despite setting the corresponding voltage components to zero due to dead-times introduced in the switching signals of the IGBTs. This is also true in a motor where the phases are not perfectly balanced. While there is no effect on the torque performance of the motor, it results in current harmonics and hence additional losses. Complete elimination of x-y current would require separate control loops for the x and y currents, with the reference commands set at zero.

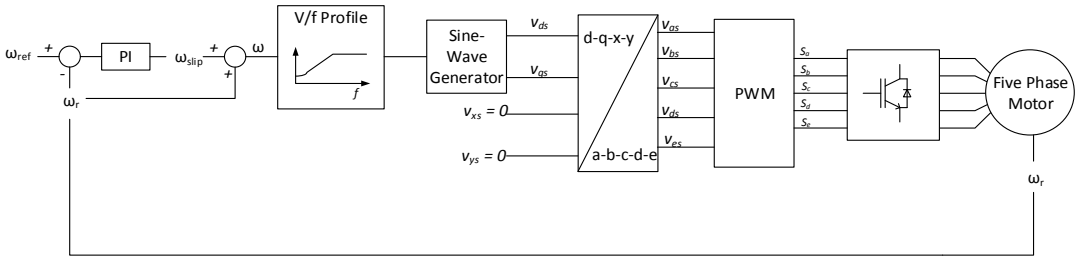

Figure 3. Closed loop V/f control of five-phase induction motor

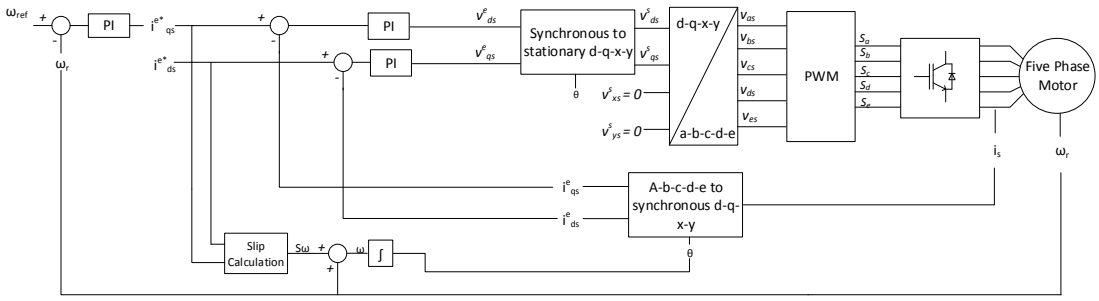

Figure 4. Indirect FOC of five-phase induction motor in synchronously rotating reference frame

Irrespective of the control method used, the PWM signal generation can be achieved through conventional sine PWM (SPWM) or the space vector PWM (SVPWM). Additionally, analogous to the third harmonic injection PWM scheme used for three-phase inverters, a fifth harmonic injection PWM switching scheme can be used for five-phase inverters to reduce the peak voltage and improve the DC bus utilization. The different PWM methodologies, just as in the three-phase inverter, result in different levels of DC bus utilization [31]. The number of switching states in a five-phase motor is increased from 8 to 32, two of which are zero states. The 32 space vectors are arranged into 10 sectors as shown in Figure 5 with large, medium, and small vectors. When compared to the three-phase inverter, there are more degrees of freedom in choosing the switching

states for a given voltage reference. The strategy that is usually adopted to choose the right switching states is to ensure that the 3^{rd} and 7^{th} order harmonics are minimized. The maximum attainable output phase voltage using SVPWM scheme for a five-phase inverter is 5.15 % higher than obtainable using SPWM. The 4-vector SVPWM switching scheme that uses two medium and two large vectors results in the lowest amplitude of third harmonic at the expense of higher number switching transitions for a five-phase inverter [32].

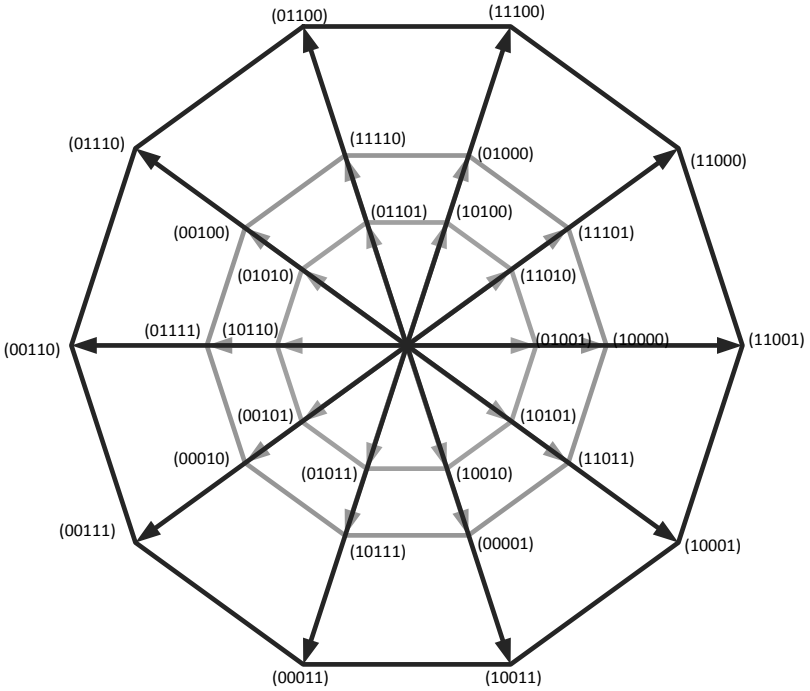

Figure 5. Switching states for SVPWM of a five-phase motor. Voltage vectors are of three different amplitudes

1.3.2 Fault-Tolerant Operation of Five-Phase Motors

With the gradual penetration of multiphase motor in critical applications like traction and aerospace, fault-tolerant operation of the five-phase motor has been extensively studied in the recent literature. The basic idea behind fault-tolerant operation is to apply current references in the x-y space to ensure that the fundamental component of the stator flux exists in the air gap even with four or three phases [33]. The applied x and y components can be selected based on different post fault operating criteria:

- Minimum drive derating [33]
- Minimum copper loss [34],[35]
- Minimum torque ripple [36]

The control of the motor post fault is complicated by the fact that the motor is asymmetric after loss of a phase. The initial work on fault-tolerant control uses simple hysteresis current controllers [29] which operate with a variable switching frequency. The use of synchronous frame controllers is proposed in [37] but with additional complexity as compared to healthy operation. The reason for the added complexity is that, while the orthogonality of the d- and q-axes is maintained after loss of phase A, the decoupling between the d-q and x-y reference frames is lost. This introduces cross coupling terms in the voltage equations in the synchronous reference frames. In [38], model predictive control (MPC) has been adopted for post fault operation of a five-phase induction motor. By modifying the transformation matrix it has been shown that the model of the motor can be maintained the same before and after the fault making it possible to adopt the same MPC strategy. This control method however creates a heavy burden on the microcontroller

and requires a significant change in the control scheme between pre and post fault operation. Another factor that has to be taken into consideration during post fault operation is the shift in the neutral voltage due to the back-EMF induced in the opened faulty phase [39]. This affects PWM-based switching methods, since the inverter leg voltage is no longer equal to the phase-to-neutral voltage of the motor and the neutral shift has to be indirectly compensated. In [39], a fault-tolerant control scheme that uses conventional synchronous frame controllers for the d-q current tracking and proportional resonant (PR) controllers for x-y current tracking has been used. The justification for this is based on the fact that the maximum-torque-post-fault-operation strategy requires that the fundamental components of stator currents are balanced. However due the asymmetry in the faulty motor, this would require unbalanced x- and y-axis current references in the stationary frame which then appear as oscillating components in the synchronous frame. The effective tracking of these oscillating x and y currents would depend on the bandwidth of the PI controller. On the other hand, tracking unbalanced currents is relatively easier with stationary frame PR controllers [40].

It is thus evident that, while several different strategies for calculating the post fault operating currents are available, the type of control adopted can be of varying complexity. The fact that the post fault system is inherently asymmetric adds additional sophistication to the control. With the availability of fast microcontrollers, it has become possible to implement some of the more advanced control methods involving predictive control and higher order controllers. By adopting proper discretization methods for digital implementation of these control methods, it can be shown that the post fault steady state

performance is mostly similar. The best control strategy for fast seamless transition should involve minimum change to the control loop when switching from healthy to fault-tolerant operating condition.

1.4 Fault-Tolerant Induction Motor Design

A few of the more commonly used approaches to make a motor inherently fault-tolerant are:

- Electrical isolation between phase windings
- Magnetic isolation between phase windings
- Physical separation between phase windings

Electrical isolation from the converter side is achieved by using a modular topology with independent H-bridges for every phase [41] as shown in Figure 6. However this increases the cost and complexity of the drive and in only justified in highly sensitive applications like military and aerospace.

Magnetic and physical isolation between the phases can be achieved by adopting fractional slot concentrated winding (FSCW) configurations where each stator coil is wound around a single tooth as shown in Figure 7(a). FSCW configurations provide additional thermal and physical isolation between the phases when compared to distributed winding motors which have overlapping end connections as shown in Figure 7(b). For these motors, the number of slots per pole per phase is less than one making them suitable for high pole count designs. While complete isolation requires that the windings are single layered with only one coil side per slot, single layer windings affect the

performance of the motor. The stator MMF of a motor with single layered windings is rich in space harmonics creating high tooth and magnet lossses [5] **.** Tooth wound stators can also be found in switched-reluctance motors (SRMs) shown in Figure 8 which exhibit a very high level of fault tolerance due to very low magntic coupling between the phases and no magnets on the rotor. However, despite this advantage SRMs commonly suffer from low efficiency, noise and vibrations and are more complicated to control.

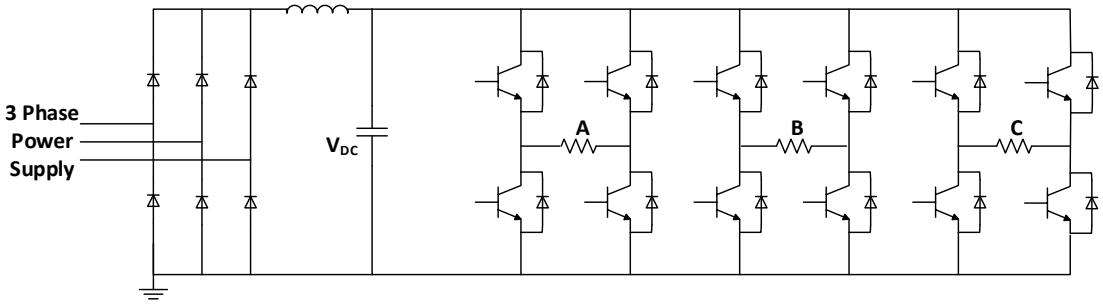

Figure 6. Three-phase inverter using a modular motor drive topology with independent H-bridges for each phase

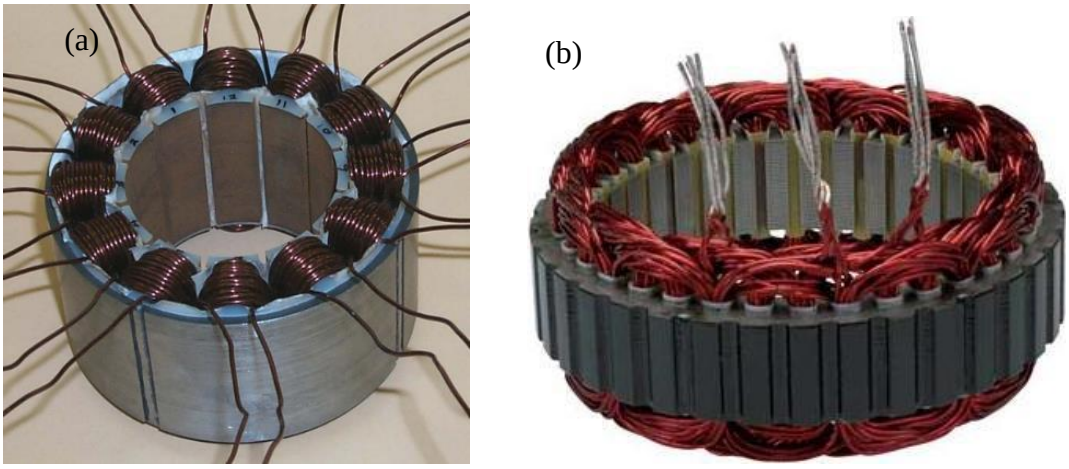

Figure 7. Comparison of stator windings (a) fractional slot concentrated winding and (b) a distributed winding [42]

Figure 8. Commercially available switched-reluctance motor *(Source: Bulletin NAAC - 009 US Motors Industrial SR Range Catalog)*

FSCW configurations have been widely adopted for permanent magnet and specifically interior permanent magnet motors due to their ability to provide extremely torque dense designs. The copper utilization in an FSCW stator is much higher than a conventional distributed winding stator due to reduced overhang at the end connections. They also provide several additional advantages over conventional distributed windings such as higher fill factor and easier manufacturability [5]. In terms of inter-turn faults, while in an FSCW it is not possible to prevent the fault from spreading to more turns of the same phase coil due to the voltage induced in the faulted turns by the rotor magnets, they provide some means to contain the fault in the affected phase of the motor.

Due to these merits, there have been many recent but mostly unsuccessful attempts to apply FSCW to induction motors in the literature. The air gap flux density distribution created by using FSCW configurations is rich in sub and higher order space harmonics. Although this only translates to rotor and magnet losses in PM motors, in induction motors these harmonics induce currents in the cage rotor. This results in low average torque, high rotor copper loss as well as torque pulsations at different rotor speeds. In [42], the most commonly used FSCW slot-pole combinations for PM motors; the 1/2 slot per pole per

phase (SPP) and 2/5 SPP are used with induction motors with limited success. Although the double layered 1/2 SPP is shown to provide promising results it is not in par with a conventional integral SPP distributed winding in terms of average/ripple torque and rotor losses.

Multi-layer FSCW configurations have been used in PM motors to minimize losses by reducing or cancelling some of the sub and higher order space harmonics [43]. In [44], this idea is extended to induction motors while also using a multi-layer tooth wound rotor. Although this helped minimize some of the harmonics in the air gap flux and their interaction with the rotor, the resulting configurations still show to exhibit high torque pulsations. Additionally, the manufacturing advantage provided by using a rotor cage that can be die cast with aluminum or copper, is lost.

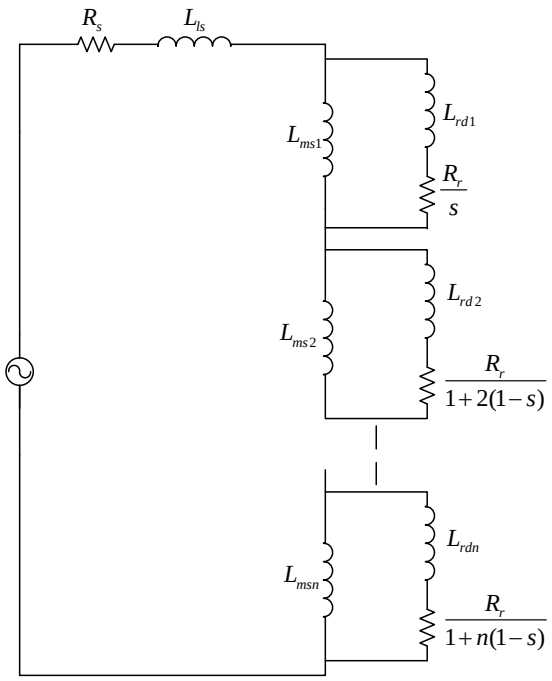

Figure 9. Harmonic equivalent circuit of an induction motor

Conventional design methods for induction motors use the simplified equivalent circuit model [45] that fails to capture these effects, which are negligible in distributed winding configurations, resulting in non-optimal designs. The effect of stator space harmonics on the steady state performance of induction motors can be analyzed by using the harmonic equivalent circuit shown in Figure 9. The torque speed curve obtained for a ½ SPP induction motor with 12 stator slots, 8 poles and a 44 bar rotor is shown in Figure 10. The Figure 10(a) also shows the average steady state torque due to each space harmonics. It is clear that the effect of the space harmonics degrades the performance of the motor. Adopting FSCW winding configurations for induction motors is a challenging problem.

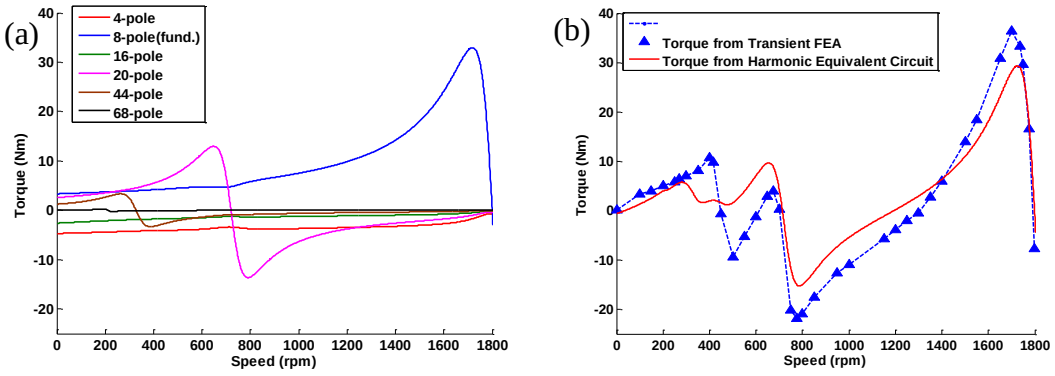

Figure 10. Torque speed characteristics of a ½ SPP FSCW induction motor obtained from the harmonic equivalent circuit (a) average torque due to individual harmonics (b) net average torque compared with results from Finite Element Analysis (FEA)

1.5 Problem Statement

Based on the above literature, stator inter-turn faults have been identified as the most difficult to detect and the most destructive to the motor. While it may be not be possible to design an induction motor that is tolerant to inter-turn faults, adding redundancies in the form of additional phases seems to be a promising way to deal with the impacts of the fault for high reliability applications. Five-phase induction motors are an attractive option for high performance, safety critical and cost sensitive applications. Not only do they provide fault-tolerant capability but also improved performance as compared to equivalent three-phase motors. Widespread adoption of five-phase motors for practical applications has been limited due to the additional requirements in the inverter side and the relatively complicated control system. However, with the availability of low-cost high speed microcontrollers equipped with fast and high resolution ADCs, digital implementation of the control system is no longer an issue. Extensive work has been done with the fault-tolerant control of five-phase induction motors, but to benefit from the fault-tolerant capability, the motor drive system should include prognostics, detection, and isolation of the fault and finally fault-tolerant operation. Most of the methods used in the existing literature for fault diagnostics of stator windings rely on MCSA which, while shown to be effective requires additional hardware for data acquisition and spectral analysis. This is difficult to justify for five-phase motor drives in most applications considering the already added complexity in the drive with the addition of two phases. The aim of this dissertation is to integrate a low-cost non-intrusive inter-turn fault detection method with a fault-tolerant control scheme for five-phase induction

motors. Specifically the method should be easy to implement on the digital signal processor (DSP) or microcontroller that drives the motor.

The literature also suggests that there have been very few attempts to extend the benefits of FSCW configurations that provide better physical isolation between the stator phases to induction motors. The main issue has been the identified to be abundance of the lower order space harmonics in the air gap. While this only results in additional magnet losses in a PM rotor it significantly impacts the torque performance and increases the rotor losses with an induction rotor. Several modifications have been introduced to the stator windings of FSCW permanent magnet motors to minimize the magnet losses by eliminating the space harmonics using multilayer windings or adopting varying turns per slot. This direction seems promising because it requires no additional changes to the rotor or the motor control system. This dissertation also explores alternate methods for adopting FSCW configurations for induction motors.

1.6 Dissertation Outline

This dissertation has been organized into seven chapters. Chapter 2 covers control of five-phase induction motors before and after a fault, focusing on stationary frame controllers. The purpose for adoption of stationary frame control is to reduce the complexity of the control algorithm to allow for incorporation of an on board inter-turn fault diagnostic. Chapter 3 develops a detailed model of a multiphase induction motor with inter-turn fault. The purpose of the model is to understand the dynamics of the five-phase induction motor with an inter-turn fault in one of its phases and to test and validate the

fault detection method. Chapter 4 introduces a voltage injection based fault diagnostic method for detection of inter-turn fault. The fundamental basis of the method is developed and simulation results showing its effectiveness are presented. The drawbacks and possible complications with practical implementation and as well as methods to deal with these issues have been identified. Chapter 5 details a new multilayer FSCW configuration suitable for outer rotor induction motors. The proposed design eliminates the end winding overlap between the phases of the motor. Chapter 6 validates the proposed DC injection based diagnostic method through experimental results conducted on a 7.5 HP lab prototype motor with taps in the phases to create inter-turn faults. Chapter 7 presents the conclusions of this work.

2. CONTROL OF FIVE-PHASE INDUCTION MOTORS

Five-phase motors provide several advantages over three-phase motors.

- They can operate at reduced capacity with up to two of its five phases opened. For cost sensitive applications like electric submersible pumps (ESPs), this translates into reduced production but avoids exponential costs associated with downtimes and unscheduled maintenance.
- For the same kVA and phase voltage rating, a five-phase motor requires lesser current per phase. This reduces the switching and conduction losses in the inverter switches, increasing their reliability.
- With increase in the phase number, torque pulsation and acoustic noise problems are much less compared to conventional three-phase, current regulated induction motor drives.
- The air gap flux harmonics of a five-phase motor are of higher order and smaller amplitude as compared to a three-phase motor. This results in lower harmonic currents in the rotor reducing the average rotor copper loss and improving the overall efficiency of the motor.

2.1 Control of Five-Phase Induction Motors Using Resonant Controllers

The first step to developing the control algorithm for a five-phase motor is the construction of a motor model. Just like a d-q transformation is used to remove the position dependence of the mutual inductance terms and decouple the flux equations, a similar d-

q-x-y transformation can be applied to a five-phase motor. For a five-phase motor the spatial distribution between the different phase windings is 72 degrees. The voltage and flux equations of a five-phase motor are given by (1)-(4)

$$v_{abcdes} = R_s i_{abcdes} + \frac{d\psi_{abcdes}}{dt} \tag{1}$$

$$v_{abcder} = R_r i_{abcder} + \frac{d\psi_{abcder}}{dt} \tag{2}$$

$$\psi_{abcdes} = L_{ss} i_{abcdes} + L_{sr} i_{abcder} \tag{3}$$

$$\psi_{abcdes} = L_{rs} i_{abcdes} + L_{rr} i_{abcder} \tag{4}$$

where,

R_s – Stator resistance matrix

R_r – Rotor resistance matrix

L_{ss} – Stator self inductance matrix

L_{rr} – Rotor self inductance matrix

L_{sr}, L_{rs} – Mutual inductance matrices

Similar to a conventional 3 phase motor the mutual inductance matrices are time dependent functions of rotor position. To simplify the above model a decoupling transformation of five orthogonal basis vectors (d-q-x-y-n) is defined by (5):

$$T_s = \sqrt{\frac{2}{5}} \begin{bmatrix} \cos(\theta) & \cos(\theta-\alpha) & \cos(\theta-2\alpha) & \cos(\theta+2\alpha) & \cos(\theta+\alpha) \\ -\sin(\theta) & -\sin(\theta-\alpha) & -\sin(\theta-2\alpha) & -\sin(\theta+2\alpha) & -\sin(\theta+\alpha) \\ 1 & \cos(2\alpha) & \cos(4\alpha) & \cos(4\alpha) & \cos(2\alpha) \\ 0 & \sin(2\alpha) & \sin(4\alpha) & -\sin(4\alpha) & -\sin(2\alpha) \\ \frac{1}{\sqrt{2}} & \frac{1}{\sqrt{2}} & \frac{1}{\sqrt{2}} & \frac{1}{\sqrt{2}} & \frac{1}{\sqrt{2}} \end{bmatrix} \tag{5}$$

where $\alpha = \frac{2\pi}{5}$ and $\theta = \omega t$ is the instantaneous angular position of the d-axis with respect to the 'a' phase magnetic axis.

On applying the transformation, the voltage and flux equations of a five-phase motor reduce to (6)-(13)

$$v_{dqs} = R_s i_{dqs} \mp \omega \psi_{qds} + p\psi_{dqs} \tag{6}$$

$$v_{dqr} = R_r i_{dqr} \mp (\omega - \omega_r)\psi_{qdr} + p\psi_{dqr} \tag{7}$$

$$v_{xys} = R_s i_{xys} + p\psi_{xys} \tag{8}$$

$$v_{xyr} = R_s i_{xyr} + p\psi_{xyr} \tag{9}$$

$$\psi_{dqs} = L_s i_{dqs} + L_m i_{dqr}, \text{ where } L_s = L_{ls} + L_m \tag{10}$$

$$\psi_{dqr} = L_r i_{dqr} + L_m i_{dqs}, \text{ where } L_r = L_{lr} + L_m \tag{11}$$

$$\psi_{xys} = L_{ls} i_{xys} \tag{12}$$

$$\psi_{xyr} = L_{lr} i_{xyr} \tag{13}$$

Since the motor is star connected with no neutral wire, zero sequence components do not exist. From the above equations, it can be seen that the x-y space is completely decoupled from the d-q space and there exists no coupling between the stator and rotor flux in the x-y space. The five dimensional vector space is thus divided into 2 sub-spaces with the following characteristics:

- d-q space - components that produce the air gap flux that links the rotor and are responsible for energy conversion
- x-y space – components that do not produce a coupling flux and add only leakage fluxes and copper losses

Different space harmonics map into different subspaces as seen from Table 1.

Table 1. Space harmonic mapping

COMPONENT	HARMONICS
DQ	10j ±1 (j = 0,1,2,….)
XY	10j ±3 (j = 0,1,2,….)
N	10j ±5 (j = 0,1,2,….)

The torque production is only due to the d-q components and is given by (14)

$$T_e = PL_m\left(i_{dr}i_{qs} - i_{qr}i_{ds}\right) \tag{14}$$

The control of a five-phase motor can now be accomplished similar to a conventional three-phase motor where by orienting the rotor flux along the d-axis, it is possible to independently control the flux and torque using the d-axis and q-axis stator currents respectively. The transformation given in (5) is generalized for an arbitrary reference frame. The choice of the controller depends on the nature of the reference frame used to build the control loop and can be classified as follows:

- Synchronous frame $\omega = \omega_e$ – The frame rotates at synchronous speed which corresponds to the fundamental operating frequency (ω_e) of the motor.
- Stationary frame $\omega = 0$ – The frame is fixed with the q-axis aligned with the magnetic ‘a’ phase axis.

In the synchronous frame all the variables like current, voltages and flux have constant DC values and so a conventional proportional integral (PI) controller can be used for current control to track a current reference. In the stationary frame, all the variables are sinusoidal functions at the fundamental frequency and a proportional resonant (PR)

controller can be used to track the current reference [46]. The transfer function of the PR controller is given by (15)

$$C(s) = K_p + \frac{K_i}{s^2 + \omega^2} \tag{15}$$

where,

ω = resonant frequency or the frequency of tracking signal

PR controllers are capable of achieving a zero steady state error at the selected resonant frequency. A PR controller is chosen for control for the following reasons:

- Simpler reference frame transformation makes digital implementation easier.
- The only coupling term in the voltage equations (6) is the back-EMF voltage which can be treated as a simple disturbance.
- Enables on-line stator resistance estimation through DC injection. This is further discussed in Chapter 4.
- Enables tracking of unbalanced current references which is required for fault-tolerant control.

Hence using a PR controller allows minimal change in the control loop between healthy and fault-tolerant operation. The overall current control loop with a PR controller is shown in Figure 11.

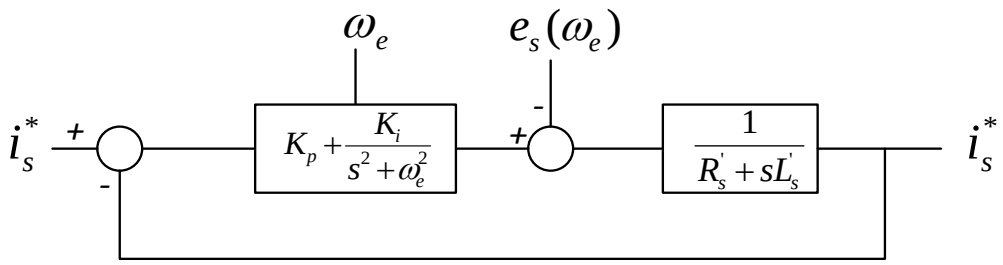

Figure 11. Current control loop with PR controller; $e_s(\omega_e)$ is the back emf

The gains of the PR controller, K_p and K_i can be designed from the Bode plot of the open loop system. Figure 12 shows the frequency response of the open loop system for varying K_p and K_i. The proportional gain K_p controls the gain crossover frequency and is chosen to ensure that the system has a sufficiently large phase margin, as shown in Figure 12(a). The resonant term causes the gain to increase significantly at the resonant frequency. Varying the resonant gain K_i controls the width around the resonant frequency. This can be seen in Figure 12(b). As a result, K_i has almost no impact on the stability of the closed loop system. The complete vector control loop of the system is shown in Figure 13.

Under balanced condition with no neutral connection the x-y-n components of the current are kept zero by commanding $V_{xs} = 0$ and $V_{ys} = 0$. However in a practical system, the dead times of the inverter and switching non-linearity result in finite x and y-axis current components even when V_{xs} and V_{ys} are set to zero.

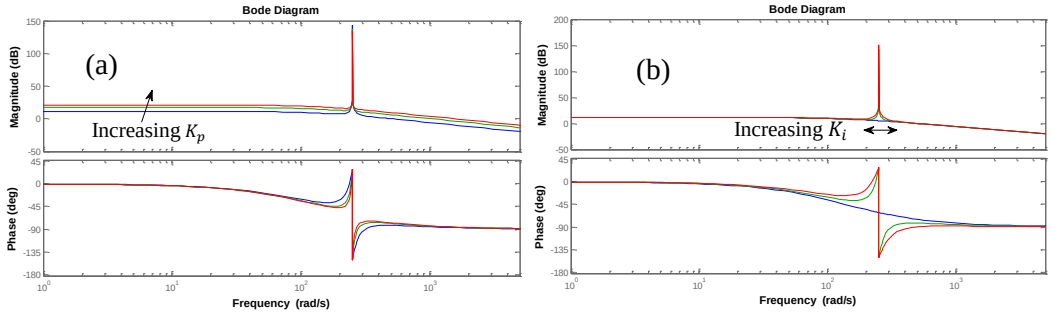

Figure 12. Change in the frequency response with increasing (a) K_p (b) K_i

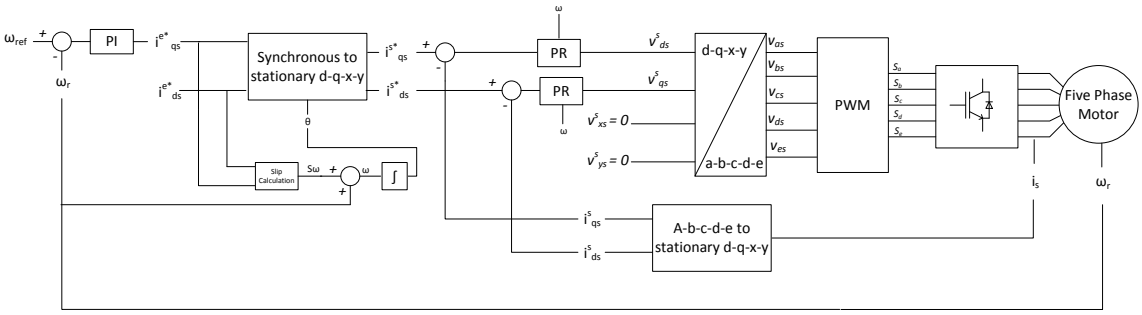

Figure 13. Complete vector control loop of five-phase induction motor with PR controller

When using digital microcontrollers to control the motor the choice of discretization method affects the control performance. Based on [40], the zero-order hold based discretization method is used for practical implementation of the control loop. The discrete form of the resonant term of the PR controller is given by (16). The control loop shown in Figure 13 is simulated in MATLAB Simulink. A summary of the simulation results is shown in Figure 14.

$$R(z) = \frac{\sin(\omega_0 T_s)}{\omega_0} \frac{z^{-1} - z^{-2}}{1 - 2z^{-1}\cos(\omega_0 T_s) + z^{-2}} \tag{16}$$

2.2 Fault-Tolerant Control of Five-Phase Induction Motors

In general, fault tolerance is the ability of the motor to continue its operation in the event of a fault. For any multiphase motor with three or more phases, applying phase shifted currents to the phases creates a rotating magnetic field in the air gap of the motor, which is the primary requirement for torque production. For multiphase motors with more than three phases fault tolerance is possible due to the ability of the motor to operate after failure in one or more phases. In other words, the rotating magnetic field can still be created after loss of one or more phases.

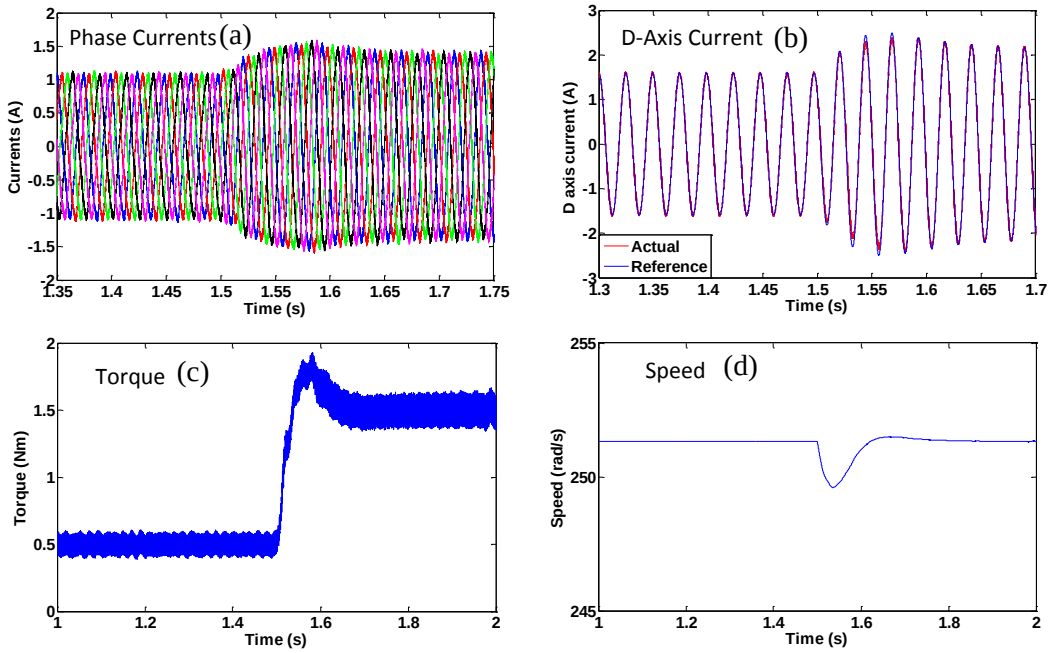

Figure 14. Simulation results of five-phase motor with PR controller with load change at t = 1.5s (a) Phase currents (b) d-axis current (c) torque (d) speed.

Specifically, five-phase motors can safely operate with loss of up to two phases without any additional hardware requirements. This is achieved by simply modifying the

control algorithm, which is generally implemented digitally on a microcontroller. While it is possible to operate three-phase motors with just two phases, this would require a neutral connection, a divided DC bus voltage, and applying a zero sequence component to the remaining healthy phases. Additionally, from a reliability standpoint, zero sequence currents have detrimental effect on the motor bearing and rapidly reduce the life of the motor. On the other hand zero sequence currents are not required for fault-tolerant operation of a five-phase motor.

It has been established in Section 2.1 that to create a sinusoidal air gap flux at fundamental frequency that links the rotor, a d-axis and a q-axis component of the current is required. The inverse transformation of currents from the d-q-x-y-n frame to the a-b-c-d-e frame is given by (17):

$$i_{abcde} = \sqrt{\frac{2}{5}} \begin{bmatrix} 1 & 0 & 1 & 0 & \frac{1}{\sqrt{2}} \\ cos\left(\frac{2\pi}{5}\right) & sin\left(\frac{2\pi}{5}\right) & cos\left(\frac{4\pi}{5}\right) & sin\left(\frac{4\pi}{5}\right) & \frac{1}{\sqrt{2}} \\ cos\left(\frac{4\pi}{5}\right) & sin\left(\frac{4\pi}{5}\right) & cos\left(\frac{8\pi}{5}\right) & sin\left(\frac{8\pi}{5}\right) & \frac{1}{\sqrt{2}} \\ cos\left(\frac{4\pi}{5}\right) & -sin\left(\frac{4\pi}{5}\right) & cos\left(\frac{8\pi}{5}\right) & -sin\left(\frac{8\pi}{5}\right) & \frac{1}{\sqrt{2}} \\ cos\left(\frac{2\pi}{5}\right) & -sin\left(\frac{2\pi}{5}\right) & cos\left(\frac{4\pi}{5}\right) & -sin\left(\frac{4\pi}{5}\right) & \frac{1}{\sqrt{2}} \end{bmatrix} i_{dqxyn} \qquad (17)$$

Assuming that 'a' phase is opened, from the first row of the matrix in (17), it can be inferred that for $i_a = 0$ and no neutral connection ($i_n = 0$),

$$i_x = -i_d \qquad (18)$$

Equation (18) implies that the d-q and x-y components are no longer independent and the x-axis current component is constrained by the system once the d-axis current is

fixed by the controller. On the other hand the y-axis current can be chosen based on the either for the following two conditions:

- Phase currents in the remaining phases (b, c, d, and e) have the same amplitude – this ensures that the losses in the inverter switches are balanced and the drive derating is minimum. From (17) and (18) this condition results in (19)

$$i_y = -0.236 i_d \tag{19}$$

- Total copper loss is minimum – this condition, given by (20)(*19*) , creates unequal phase currents, thereby reducing the reliability of the switches due to unbalanced loss distribution.

$$i_y = 0 \tag{20}$$

The condition (19) is preferable and the phase shifts between the currents in the a-b-c-d-e frame under this condition are shown in Figure 15.

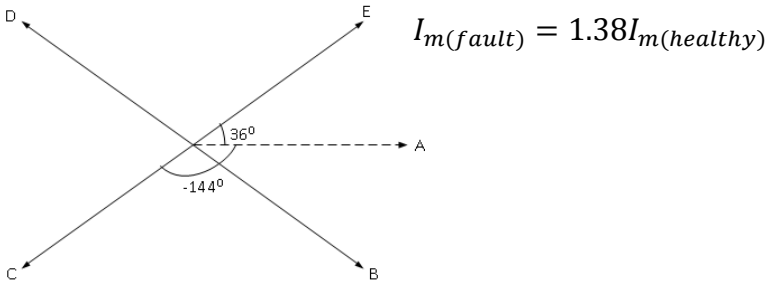

Figure 15. Phase shifts between the currents for fault-tolerant operation with one phase opened

In terms of the control loop, it may seem that the only modification from healthy operating condition is the addition of a current controller for the y-axis current. However since the phase A is left open it can be shown that the neutral voltage is no longer zero or

equal to the negative DC bus voltage [39]. For a drive-fed motor this would mean that the phase voltages of the motor cannot be controlled by modulating the corresponding leg voltages of the inverter. To compensate for this neutral shift the x-axis current has to be forced to be equal to the negative d-axis current. Thus a fault-tolerant operation can be achieved with one open phase. If any phase other than 'a' is opened, the transformation (5) can be rearranged such that the stationary q-axis is aligned with the magnetic axis of the opened phase. The control of d- and q-axis current components in the stationary reference frame remains unchanged since even after loss of phase 'a', the orthogonality and hence decoupling between the d and q axes is still retained. This is evident from the transformation matrix (5) after removing the first row and column and setting θ to be equal to zero.

When two phases 'a' and 'b' are opened, it is observed from (17) that once the d-axis and q-axis currents are fixed, constraints are imposed on both the x-axis and y-axis current components, given by (21), (22):

$$i_x = -i_d \tag{21}$$

$$i_y = \ -1.902 i_d - 1.618 i_q \tag{22}$$

The phase shifts between the currents in the a-b-c-d-e frame under the above conditions is shown in Figure 16. Similar to the single phase fault condition, for a drive-fed motor, the x-axis and y-axis currents have to be forced to track the above values, (21) and (22) to compensate for the shift in the neutral voltage and facilitate tracking of the d and q-axis reference currents.

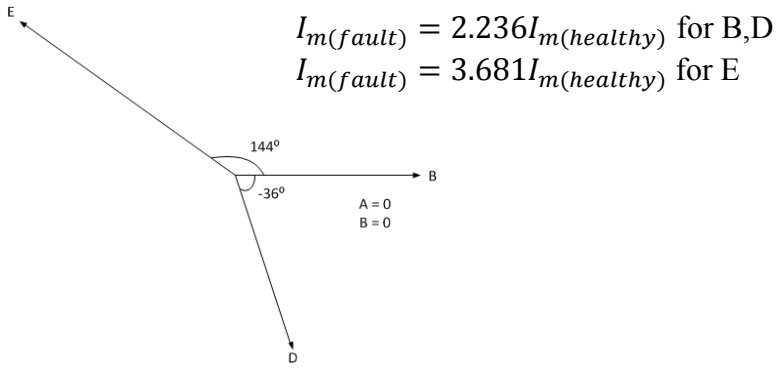

$I_{m(fault)} = 2.236 I_{m(healthy)}$ for B,D
$I_{m(fault)} = 3.681 I_{m(healthy)}$ for E

Figure 16. Phase shifts between the currents for fault-tolerant operation with two phases opened

It is observed, form the above discussion, that for the same sinusoidal air gap flux, the amplitudes of the currents have to be increased above the rated value during faults and additionally, the resulting phase current amplitudes are unbalanced when there are two faulty phases. The modified control loop for fault-tolerant operation is shown in Figure 17.

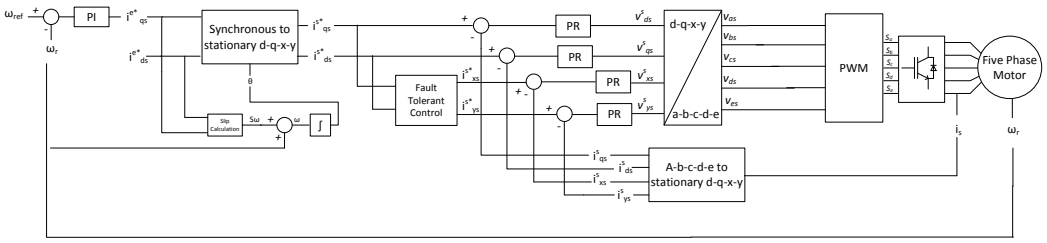

Figure 17. Complete vector control loop of five-phase induction motor for fault-tolerant control

This method ensures minimal change to the controller enabling a seamless transition from healthy to fault-tolerant operation. In actual practice, in the absence of a "sinusoidal" winding distribution, non-zero x-y currents create harmonic flux in the air gap that result in some torque pulsations.

2.3 Chapter Summary

The control of five-phase induction motors in the stationary frame with resonant controllers is presented in this chapter. Implementation of the control loop in the stationary frame eliminates the need for a rotating frame transformation and also ensures that the modification to the control loop is minimal when transitioning to fault-tolerant operation. Irrespective of the post fault operating criteria it can be seen that two additional PR controlled current loops are required to ensure that a fundamental rotating magnetic field exists in the airgap after the loss of a phase. Another added advantage of implementing the control loop in the stationary frame is seen when performing a DC voltage injection for diagnostic purposes since the resonant controllers offer low gains outside of the resonant frequency. The method is discussed in detail in Chapter 4.

3. MODELING OF INDUCTION MOTORS WITH INTER-TURN FAULTS

A generalized model of the induction motor is developed to serve as a tool for fault analysis. The following factors are taken into account to develop the model

- The effect of space harmonics due to slotting on the air gap flux
- Adaptability to multiphase stator winding configurations
- Accounting for skew in the rotor or stator
- Adaptability to include inter-turn fault in the winding phases

3.1 Generalized Model of an Induction Motor

Based on the above requirements Modified Winding Function Theory (MWFT) is identified as a suitable method [47]. MWFT provides a simple method of calculating the self and mutual inductances of the motor from the winding functions of the phases. The winding function of a phase is defined as the MMF created in the air gap due to unit current flowing through the phase. The assumptions made when using winding function theory are:

- Saturation in the core is negligible
- The inter-bar current is negligible
- Eddy current, friction and windage losses are neglected

Mutual inductance L_{ij} calculated from winding function is given by the equation (23)

$$L_{ij} = l \int_0^{2\pi} M_i(\varphi)\, n_j(\varphi) dP(\varphi) \tag{23}$$

where,

$M_i(\varphi)$ = Modified Winding Function of winding *i*

$n_j(\varphi)$ = Turns function of winding *j*

$P(\varphi)$ = Specific permeance

l = effective stack length

The modified winding function is given by,

$$M_i(\varphi) = n_i(\varphi) - \frac{1}{2\pi\langle P(\varphi)\rangle} \int_0^{2\pi} n_i(\varphi)\, dP(\varphi) \tag{24}$$

To take into account the change in the reluctance due to the presence of slots on the stator and rotor, the specific permeance is modeled as a piecewise linear function along the air gap periphery for every rotor position. Some of the possible types of flux paths depending on the relative position of the stator and rotor slots are shown in Figure 18.

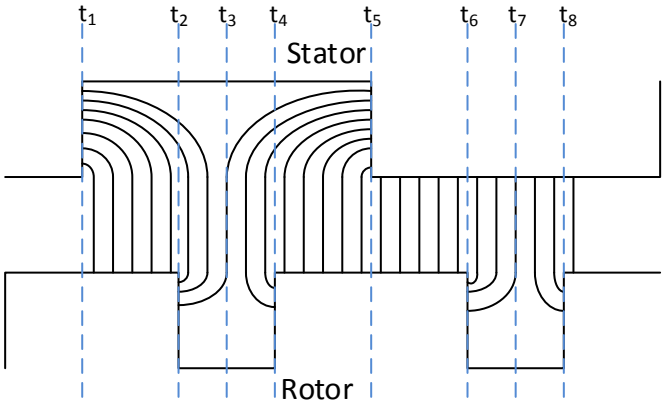

Figure 18. Fringing of the air gap flux due to stator and rotor slotting effects

The air gap is divided into sections formed by either of stator or rotor tooth edge and the mid points of the stator or rotor slots. Assuming that the flux lines trace a quarter circle before entering a tooth; a closed form expression for the specific permeance can be derived for each section. For example for the single sided fringing shown in Figure 19 (a) the expression for the specific permeance is given by (25). Similar expressions can be derived for all sections.

$$P(\varphi) = \int_0^{b_0} \frac{\mu_0}{g + \frac{\pi x}{2}} dx \tag{25}$$

Three different types of fringing are shown in Figure 19.

- Single sided fringing

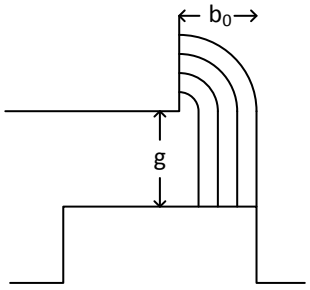

(a)

- Double sided fringing

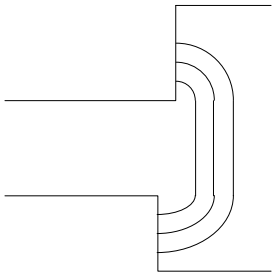

(b)

Figure 19. Different types of flux fringing between the stator and rotor teeth

- ‘S’ shaped fringing

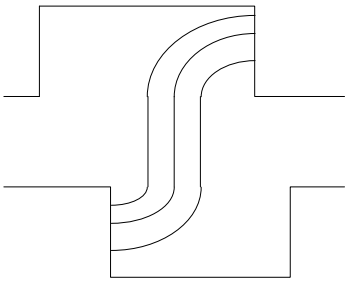

(c)

Figure 19. (Continued)

The rotor cage is modeled as individual loops as shown in Figure 20 with adjacent bars and the connecting end ring segments representing a phase. This makes it possible to apply the model to motors with non-integral bars per pole [47]. The specific permeance function is then used to calculate the self and mutual inductances between stator and rotor phases as a function of rotor position (or time for constant speed operation) for one complete mechanical revolution of the rotor.

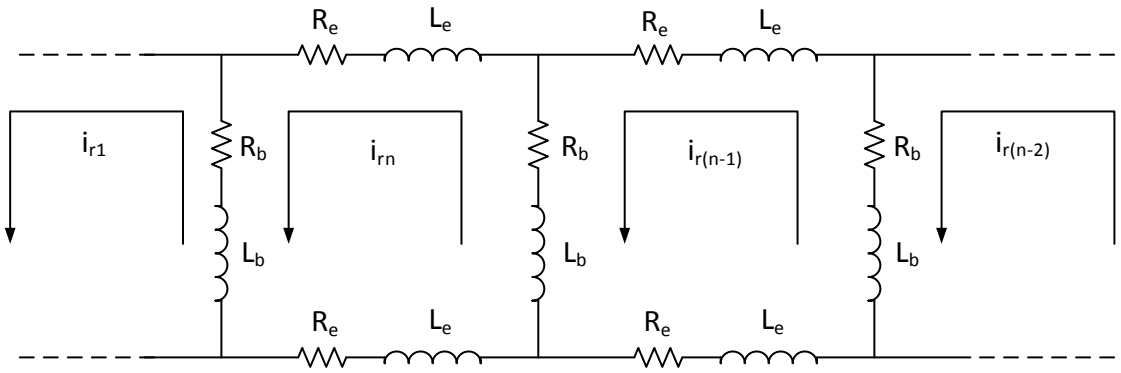

Figure 20. Rotor cage modeled as individual loops

Assuming a Voltage Source Inverter (VSI)-fed induction motor the magnetic coupled circuit model of the motor can be used to solve for the stator and rotor currents. The voltage equation of the stator is given by,

$$[v_s] = [R_s][i_s] + [L_{ls}]\frac{d[i_s]}{dt} + \frac{d[\lambda_s]}{dt} \tag{26}$$

For an *m* phase motor with *n* rotor bars the matrices are given by

$$[R_s]_{m\,\mathrm{X}\,m} = \begin{bmatrix} R_{ph} & 0 & 0 \\ 0 & \ddots & 0 \\ 0 & 0 & R_{ph} \end{bmatrix}$$

$$[L_{ls}]_{m\,\mathrm{X}\,m} = \begin{bmatrix} L_{lph} & 0 & 0 \\ 0 & \ddots & 0 \\ 0 & 0 & L_{lph} \end{bmatrix}$$

$$[v_s]_{m\,\mathrm{X}\,1} = \begin{bmatrix} V_{s1} \\ \vdots \\ V_{sm} \end{bmatrix}$$

An important point has to be made on the calculation of the leakage inductances L_{lph} of the phases of the induction motor. Conventionally the leakage inductance is divided into the following components [48]

- Slot leakage
- End winding leakage
- Differential or air gap leakage
- Tooth-tip leakage
- Skew leakage

Among the above components the differential or air gap leakage component is the only flux component that crosses the air gap and links the rotor. It is comprised of the space harmonics in the air gap flux other than the fundamental that do not contribute to the average fundamental torque and are hence included as a leakage flux component. These space harmonics are created by a combination of both slotting effects on the air gap permeance and a non-sinusoidal winding distribution which results from placing the phase coils in a finite number of slots. Since the MWFT specific permeance model includes these effects in calculating the self and mutual inductances the leakage inductance should only comprise of the other four components namely slot leakage, end winding leakage, skew leakage and tooth tip leakage. All these components can be determined from standard analytical formulations [48].

The rotor voltage equation is given by,

$$0 = [i_r][R_r] + [L_{lr}]\frac{d[i_r]}{dt} + \frac{d[\lambda_r]}{dt} \tag{27}$$

For an *n* slot rotor, from Figure 20, the equation of the n^{th} loop is given by

$$\begin{aligned} 0 = {} & R_b\left(i_{rn} - i_{r(n-1)}\right) + L_b\left(\frac{di_{rn}}{dt} - \frac{di_{r(n-1)}}{dt}\right) + R_b(i_{rn} - i_{r1}) \\ & + L_b\left(\frac{di_{rn}}{dt} - \frac{di_{r1}}{dt}\right) + 2R_e i_{rn} + 2L_e\frac{di_{rn}}{dt} + \frac{d\lambda_{rn}}{dt} \end{aligned} \tag{28}$$

The rotor resistance and leakage inductance matrix can thus be written as

$$[R_r]_{n\,\mathrm{x}\,n} = \begin{bmatrix} 2(R_b + R_e) & -R_b & \cdots & -R_b \\ -R_b & 2(R_b + R_e) & -R_b & \vdots \\ \vdots & \vdots & \vdots & \vdots \\ -R_b & \cdots & \cdots & 2(R_b + R_e) \end{bmatrix} \tag{29}$$

$$[L_{lr}]_{n\,\mathrm{x}\,n} = \begin{bmatrix} 2(L_b + L_e) & -L_b & \cdots & -L_b \\ -L_b & 2(L_b + L_e) & -L_b & \vdots \\ \vdots & \vdots & \vdots & \vdots \\ -L_b & \cdots & \cdots & 2(L_b + L_e) \end{bmatrix} \tag{30}$$

Combining the flux and voltage equations for the stator and rotor,

$$[v_s] = [R_s][i_s] + [L_{ls}]\frac{d[i_s]}{dt} + [L_{ss}]\frac{d[i_s]}{dt} + \frac{d[L_{ss}]}{dt}[i_s] + [L_{sr}]\frac{d[i_r]}{dt} + \frac{d[L_{sr}]}{dt}[i_r] \tag{31}$$

$$0 = [R_r][i_r] + [L_{lr}]\frac{d[i_r]}{dt} + [L_{rs}]\frac{d[i_s]}{dt} + \frac{d[L_{rs}]}{dt}[i_s] + [L_{rr}]\frac{d[i_r]}{dt} + \frac{d[L_{rr}]}{dt}[i_r] \tag{32}$$

Since the model uses a piecewise linear specific permeance function the time differential of L_{ss} and L_{rr} are not zero. Both these terms contribute to harmonics in the torque which can be obtained from co-energy as shown below

$$\tau = \frac{\partial W_{co}}{\partial \theta}\Big|_{fixed\ i} = \frac{1}{2}[i_s]^T \frac{d[L_{ss}]}{d\theta}[i_s] + \frac{1}{2}[i_r]^T \frac{d[L_{rr}]}{d\theta}[i_r] + [i_s]^T \frac{d[L_{sr}]}{d\theta}[i_r] \tag{33}$$

To solve the above system of equations the equations (26), (27) can be combined to give

$$\begin{bmatrix} v_s \\ 0 \end{bmatrix} = \begin{bmatrix} R_s & 0 \\ 0 & R_r \end{bmatrix}\begin{bmatrix} i_s \\ i_r \end{bmatrix} + [L]\begin{bmatrix} pi_s \\ pi_r \end{bmatrix} + [pL]\begin{bmatrix} i_s \\ i_r \end{bmatrix} \tag{34}$$

where,

$$[L] = \begin{bmatrix} L_{ls} + L_{ss} & L_{sr} \\ L_{rs} & L_{lr} + L_{rr} \end{bmatrix}$$

$$[pL] = \begin{bmatrix} pL_{ss} & pL_{sr} \\ pL_{rs} & pL_{rr} \end{bmatrix}$$

Here, $'p'$ denotes differentiation with respect to time. In the equation (34) the inductance matrix L is a function of rotor position formed from the inductance functions obtained

using MWFT. The inductance matrices can be stored in a look-up table as a function of rotor position. However to improve the computational speed, the inductances calculated from MWFT for one complete rotor rotation are converted to the frequency domain using Fast Fourier Transform (FFT). The significant harmonic components are then used to reconstruct L and pL in the time domain at each time step.

Before solving the above set of equations two constraints have to be imposed:

- $i_{s1} + i_{s2} + \cdots + i_{sm} = 0$, for a star connected stator. This condition is enforced by combining the first $(m - 1)$ rows of the stator voltage equation [49].
- $i_{r1} + i_{r2} + \cdots + i_{rn} = 0$, the total end ring current is zero. This condition is enforced by an additional row to the rotor voltage equation [47].

Solving the above ODE requires inversion of the inductance matrix L. Since the rotor is modeled as individual loops; for a conventional distributed winding induction machine, the mutual inductance between each rotor loop and stator phase is low compared to the mutual inductance between the stator phases. The matrix L is thus a sparse matrix and has to be inverted using a suitable sparse matrix inversion algorithm such as LU decomposition, QR factorization or Cholesky's method. The torque can then be calculated from the stator and rotor currents using (33).

The presented model can be generalized for any number of phases and rotor slots although the solving complexity increases with increase in either. The remainder of this dissertation will focus on adopting the model for a five-phase motor.

3.2 Modeling an Inter-Turn Short Circuit

To accurately develop and validate a strategy for inter-turn fault detection a model of the motor with inter-turn fault has to be developed. The model presented in the previous section can be easily adopted for this purpose. As discussed in Chapter 1, the term inter-turn fault usually refers to a short circuit between the turns of the same phase. An inter-turn fault is the result of the break down in the insulation between the turns. This is illustrated in Figure 21 for a motor with a five-phase star connected stator and series connected coils. The resistance R_f is the resistance of the insulation between the shorted turns.

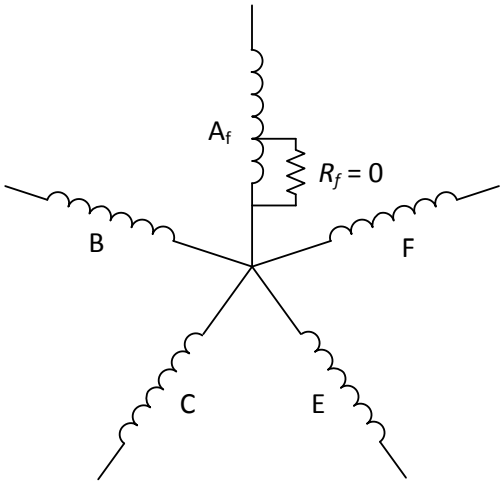

Figure 21. Five-phase star connected stator with inter-turn fault in phase A

The term bolted turn fault is used in the literature [50] to refer to the case when $R_f = 0$. The model developed in this chapter focuses on incorporating a bolted turn fault of varying severity. The severity of the fault is determined by the ratio of the number of

shorted turns to the total number of turns in the phase. For a fault severity of σ, the resistance of the shorted turns is given by

$$R_{sh} = \sigma R_{ph} \tag{35}$$

where R_{ph} denotes the per phase resistance of the healthy motor. For the case of a bolted turns fault the Figure 21 can be modified into Figure 22 where the shorted turns occurring in phase A are represented as a separate phase A_{sh} and the number of turns in the faulty phase, now represented as A_f, is the same as the healthy condition less by the number of shorted turns. The advantage of this type of representation is that, irrespective of the spatial location around the rotor or the severity of the turn fault, MWFT can now be used to determine the self and mutual inductances of the faulty motor, now with one additional phase. As mentioned earlier the leakage inductance of the shorted turns can be calculated from standard analytical formulations.

When calculating the leakage it is assumed that the severity of the inter-turn fault is low enough that the following assumptions can be made:

- The shorted turns are contained in a single pair of slots
- The shorted turns are evenly distributed through the entire slot.

The first assumption is justified in developing a condition monitoring scheme since increasing the percentage of shorted turns results in unbalance in the motor phase windings, and a high current in the faulty phase. For a very large number of shorted turns, such a situation would most likely trigger an over current protection scheme that is a standard feature in all line connected and drive-fed induction motors. The second assumption is valid for random wound induction motors.

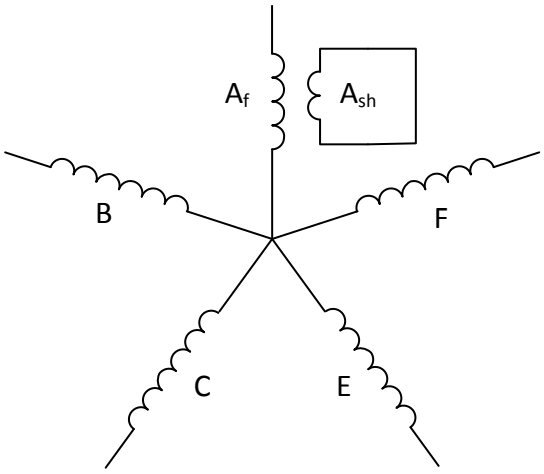

Figure 22. Equivalent circuit of five-phase star connected motor with bolted inter-turn fault

Based on the above considerations the following equation is written for the shorted turn

$$0 = R_{sh} i_{sh} + (L_{lsh} + L_{shsh}) \frac{di_{sh}}{dt} + \frac{dL_{shsh}}{dt} i_{sh} + [L_{shs}] \frac{d[i_s]}{dt} + \frac{d[L_{shs}]}{dt} [i_s] + [L_{shr}] \frac{d[i_r]}{dt} + \frac{d[L_{shr}]}{dt} [i_r] \quad (36)$$

where,

$[L_{shs}]_{1 \text{ X } m}$ = mutual inductance of shorted turns with all the stator phases

$[L_{shr}]_{1 \text{ X } n}$ = mutual inductance of shorted turns with all the rotor loops

L_{lsh} = leakage inductance of the shorted turns

L_{shsh} = magnetizing inductance of the shorted turns

The torque equation remains the same as (33) with the effect of shorted turns being incorporated into the inductance and current matrices. It can be inferred that the presence of the inter-turn fault adds only an oscillating component to the torque at twice the

fundamental frequency. This is due to the interaction between the pulsating field created by the current flowing through the shorted turn and the air gap field.

To verify the MWFT model the inductances of the 7.5 HP prototype motor are calculated using the above model and compared with results obtained from 2D Finite Element Analysis (FEA) using infinite permeability iron. Figure 23 and Figure 24 show the plot of the mutual inductance between the faulty phase and a rotor loop and between the shorted turns (for 5.55% shorted turns) and rotor loop respectively. The model is found to show a close match especially with the incorporation of slotting effects.

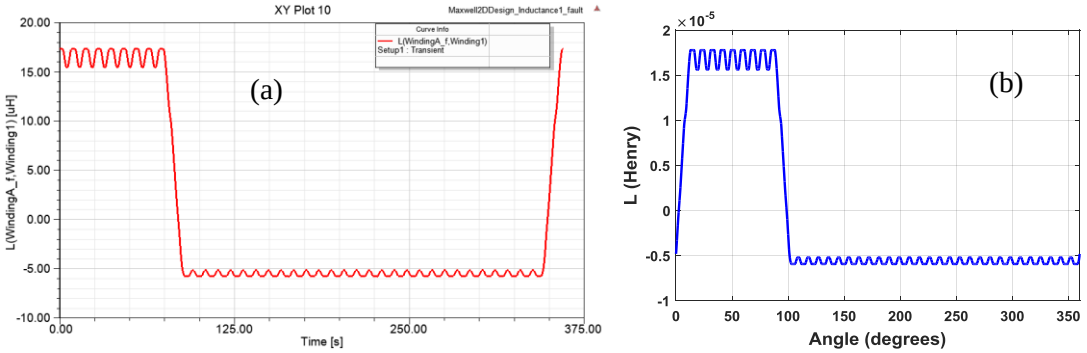

Figure 23. Mutual inductance between the shorted turns (5.55%) and a rotor loop(a) from FEA with infinitely permeable core (b) from model

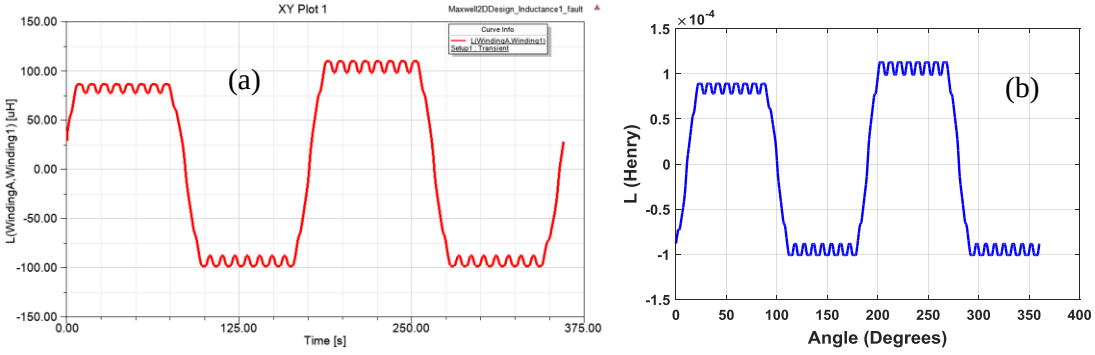

Figure 24. Mutual inductance between the faulty phase and a rotor loop (a) from FEA with infinitely permeable core (b) from model

The developed model is used to simulate a 5.55% inter-turn short in phase A when operating at slip = 0.0361 and applying a peak phase voltage of 100v. Figure 27 shows the comparison of the torques between healthy and faulty operating condition obtained from the model and 2D FEA (using a saturable core material). Figure 25 shows the phase currents and Figure 26 illustrates the current in the shorted turns. In the presence of an inter-turn fault the phase currents in the motor are unbalanced and a torque pulsation at double the synchronous frequency is created due to the current induced in the shorted turns. The results from the model are found to be in good agreement with FEA; although it should be noted that core saturation affects the accuracy of the model.

The use of such a model is however justified in this study of inter-turn faults since the proposed fault detection method, discussed in Chapter 4, does not rely on harmonic frequency components in the current, that are heavily impacted by the change in the magnetic flux distribution caused by the fault . An FEA simulation illustrating this effect is shown in Figure 28. The extent of unbalance in the phase currents depends on the severity of the fault. The current in the shorted turns depends on the mutual coupling between the phases and this is usually the highest for a conventional distributed winding induction motor which is also the case for the prototype motor.

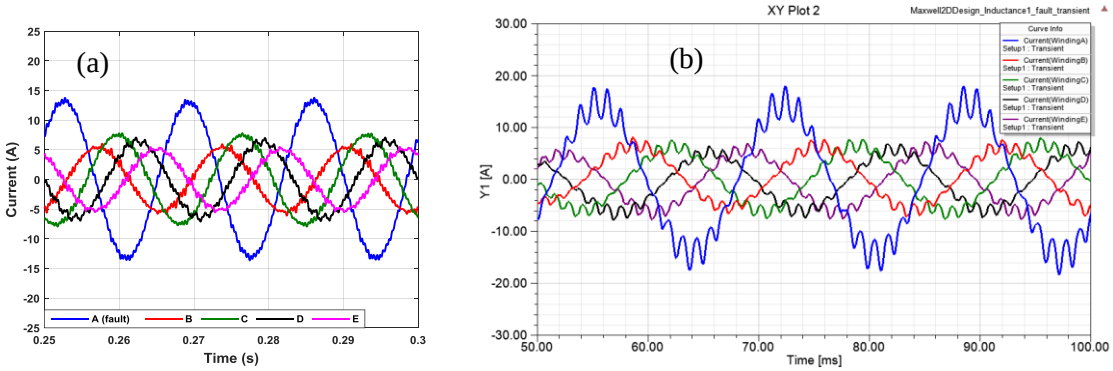

Figure 25. Phase currents for 5.55% inter-turn fault (a) model (b) FEA

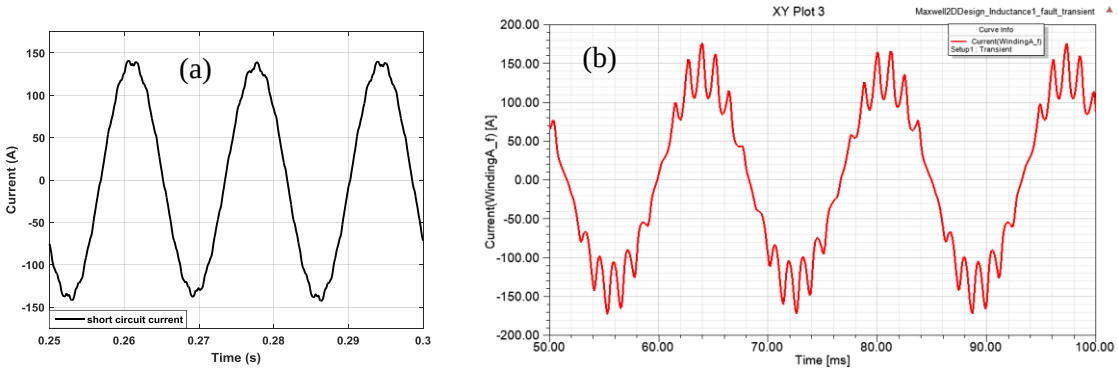

Figure 26. Short circuit current for 5.55% inter-turn short (a) model (b) FEA

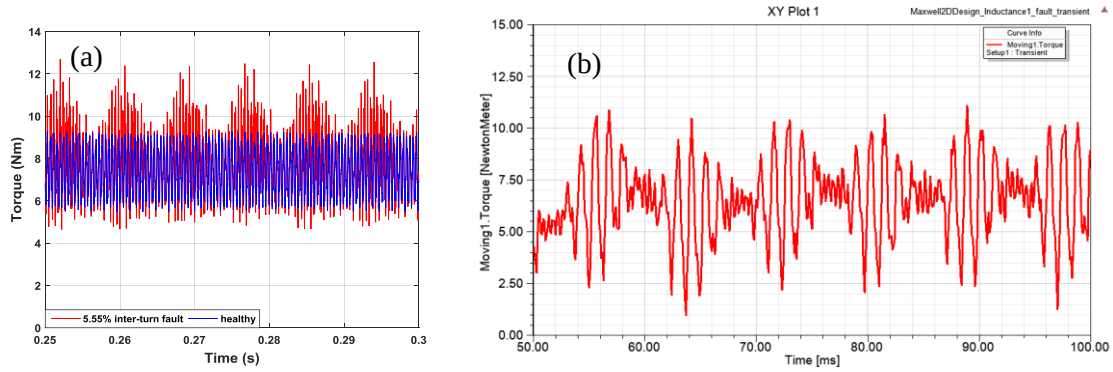

Figure 27. Torque developed during 5.55% inter-turn fault (a) model (b) FEA

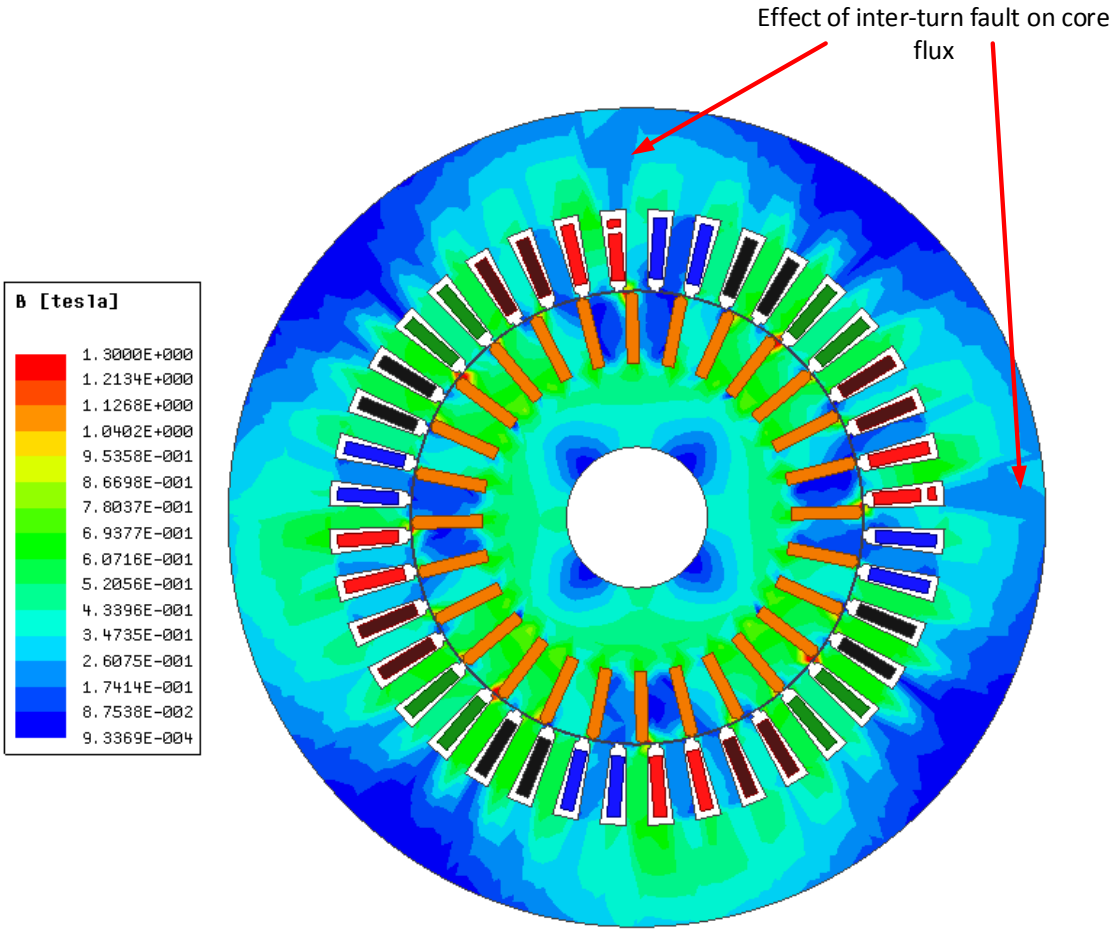

Figure 28. Flux density distribution in the presence of inter-turn short

3.3 Chapter Summary

A detailed generalized model of the motor has been developed in this chapter. The model which is based on modified winding function theory (MWFT) takes into account space harmonics created by slotting effects and can be adopted to incorporate inter-turn fault as well as extended to any number of phases. Simulation results show a very close match to 2D FEA. The model is used to serve as a tool for developing and testing the DC injection based fault diagnostic method. It is important to note that, models that do not

incorporate saturation effects are ineffective for testing inter-turn fault detection methods that are based on stator current signature analysis. However for the fault detection method used in this dissertation the level of complexity provided by this model is sufficient.

4. ON-LINE INTER-TURN FAULT DETECTION USING DC INJECTION

Seamless fault-tolerant operation of a motor consists of the following steps:

- Condition monitoring – This process involves monitoring the health of the motor winding, bearings, etc. It helps in identifying incipient faults in the motor and can be accomplished by intrusive or non-intrusive methods.
    - Intrusive method – requires installation of additional sensors in the motor. e.g.: search coils to measure flux or RTDs (Resistance Temperature Detectors) to measure winding temperature
    - Non-intrusive method – uses measurements that are used for controlling the motor and does not require additional sensing. e.g.: currents and voltages
- Fault detection - This is the process of detecting a fault after it has occurred. Typically over current, over voltage and vibrations are methods of fault detection in a motor.
- Fault isolation - This is the process of separating the faulty component to prevent the fault from propagating to the healthy parts. Fault isolation helps stop a cascading process that can completely stall the motor drive system.
- Fault-tolerant operation – This is the process of continuing operation of the motor albeit at reduced capacity after the fault has been detected and isolated.

Non-intrusive condition monitoring methods are cheaper to implement, but suffer from problems like fault identification, due to low signal to noise ratio. The employed

method should also have little to no effect on the performance of the healthy motor. The most commonly used non-intrusive method is Motor Current Signature Analysis (MCSA) which involves studying the frequency components of the line currents of the motor that are already sensed for control purposes. For inter-turn faults that cause unbalance between the stator phases, the negative sequence current component can be used as an indicator. However negative sequence currents can be caused by other sources like unbalanced voltages and switching non-idealities. Frequency domain methods also require large scale data logging to yield meaningful results from the FFT.

4.1 DC Voltage Injection for Three-Phase Motors

As seen from the model developed in Chapter 3, an inter-turn fault in a phase of the motor introduces an unbalance in the impedance of the phases. This unbalance creates negative sequence components at fundamental frequency and second harmonic component in the instantaneous power, torque and speed. It has been shown in Chapter 1 that the presence of negative sequence has been the basis of many inter-turn fault detection strategies in the literature. An alternative to this is the use of the zero sequence component in the fundamental voltage which is also the result of impedance unbalance. This is observed only in star connected motors and requires voltage sensing and access to the neutral point.

For an inverter-fed induction motor, the effect of the PI controller has to be taken into consideration when developing fault detection methods. In the presence of an impedance unbalance the controller applies a negative sequence voltage to cancel the

negative sequence current created by the motor. The extent of compensation depends on the bandwidth of the controller and is a function of the controller gains. This negative sequence that is created in the controller output voltage commands has also been reported as a useful diagnostic index [24]. Diagnostic methods that rely on higher frequency current components created by slotting effects or use axial flux measurements have also been shown to be effective [1], [51]. However, these techniques need additional external hardware in the form of data acquisition systems and search coils as well as accurate knowledge of motor geometry. In general, it is difficult to propose a universal fault detection method that works for all inverter driven motors.

The reduction in the DC resistance of the faulty phase from the normal operating condition forms the basis of fault detection method used in this work. The effect is indirectly captured in the current response to a DC voltage applied across a pair of phases. This also eliminates the need for additional sensors since the phase currents are already sensed by the drive and the DC offset calculation can be easily implemented on the controller. DC voltage or current injection has been used extensively in the recent literature [52] as a method for on-line estimation of stator resistance or thermal protection. For inverter fed motors the injection of a DC voltage can be accomplished at the output of the control loop by adding a DC offset to the phase voltage commands generated by the controller; while current injection is achieved by adding the transformed DC offset current to the reference currents in the synchronous d-q frame. The DC current appears as a sine function in the synchronous reference frame. A practical issue with DC current injection is that it requires measurement of the DC voltage response which is usually very small

compared to the fundamental phase voltage. This is due to the relatively small stator resistance of motors. On the other hand the current response to a small applied DC voltage is easily measurable through the current sensors on the output of the drive. For an inverter using sinusoidal PWM switching (SPWM) connected to a balanced load, (37) would result in a DC current flowing into phase A and returning through phase B and C.

$$\begin{aligned} v_{a-out} &= v_a^* + V_{DC} \\ v_{b-out} &= v_b^* - {}^{V_{DC}}/_{2} \\ v_{c-out} &= v_b^* - {}^{V_{DC}}/_{2} \end{aligned} \tag{37}$$

Some of the known issues with DC voltage injection in motors are

- DC current appears as a sine function in the synchronous reference frame acting as a disturbance for the PI current controller. Since the disturbance frequency changes with speed, the compensation will be different for different speeds and has to be taken into consideration,
- For a three-phase motor the resulting DC current creates an output torque oscillating at the fundamental frequency [52]. This can adversely affect the performance of the motor,
- Since the stator resistance is small the DC voltage required is usually a small percentage of the phase voltage and is difficult to measure.

All the above issues can be overcome in a five-phase motor by introducing a modification to the control loop.

4.2 DC Voltage Injection for Inter-Turn Faults– Basic Principle

Before explaining this method it is useful to analyze the current response to an applied DC voltage for a balanced five-phase star connected inverter-fed resistive network when a fault is introduced in a phase. The use of a resistance (R) as a load is justified since this is the only load seen by the applied DC voltage. For a five-phase inverter shown in Figure 29 a DC voltage is applied across phases A and B.

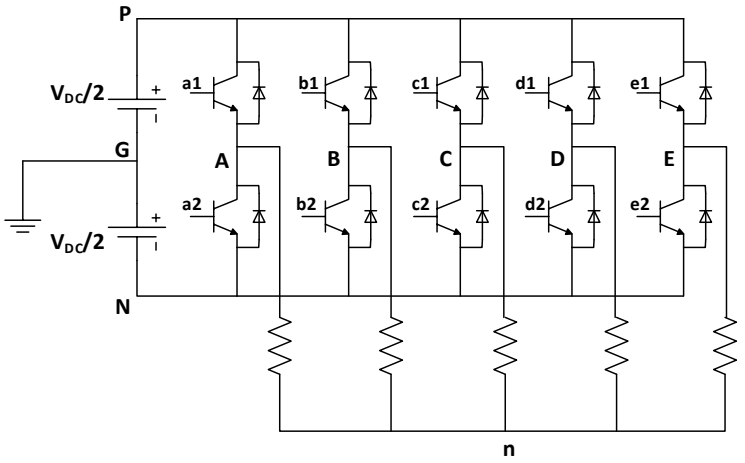

Figure 29. Five-phase five leg inverter with resistive load

Each switching cycle is divided into 4 modes; Figure 30 shows the average phase to ground voltages for each mode and the average phase to ground voltage over a switching cycle. To study the path of the DC current, the average voltage of each phase over the entire switching cycle is used to formulate the equivalent circuit shown in Figure 31. From Figure 30:

$$v_{jG} - v_{nG} = I_j R \tag{38}$$

where $j = A, B, C, D, E$

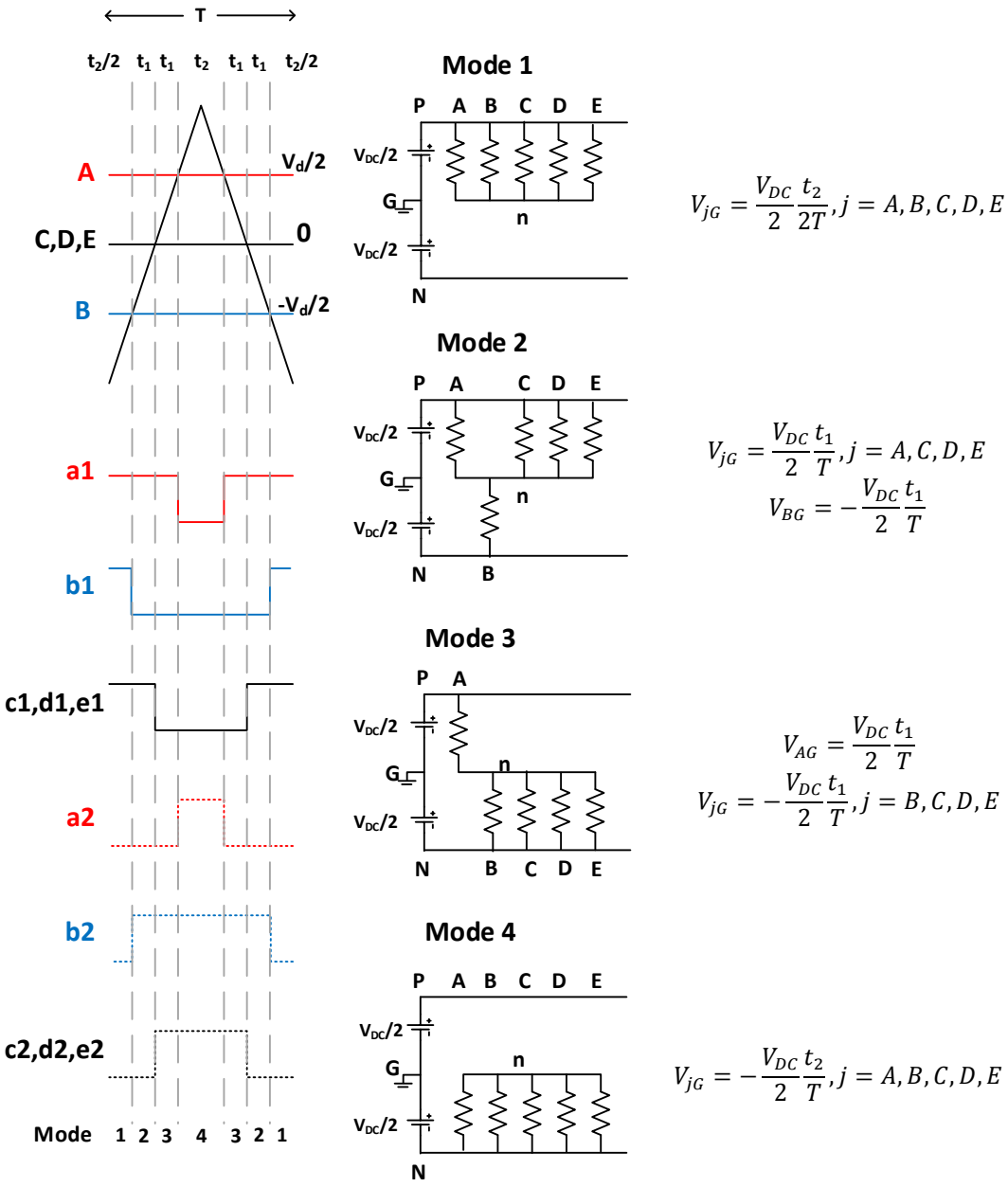

Figure 30. Average voltage applied to the phases of over a switching cycle, during DC injection across A and B

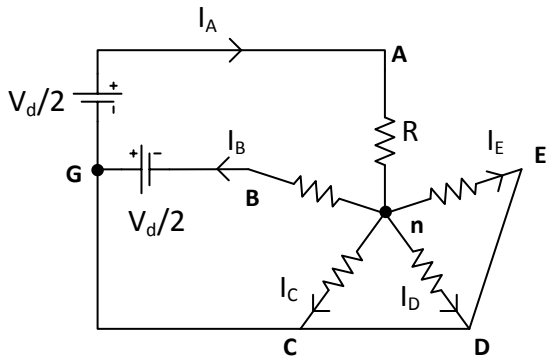

Figure 31. Five-phase star connected resistive load with DC applied across A and B

From (38) the neutral voltage is given by

$$v_{nG} = \frac{1}{5}(V_{AG} + V_{BG} + V_{CG} + V_{DG} + V_{EG}) = \frac{1}{5}\left(\frac{V_d}{2} - \frac{V_d}{2}\right) = 0 \tag{39}$$

For a balanced load the neutral voltage is equal to the ground voltage. Assuming that there is a turn fault in phase A, the resistance reduces from R to R_f. The neutral voltage v_{nGf} for the system is now given by

$$\begin{aligned} v_{nGf} = {} & \frac{1}{5}(V_{AG} + V_{BG} + V_{CG} + V_{DG} + V_{EG}) \\ & - \frac{1}{5}\left(I_{af}R_f + R\left(I_{bf} + I_{cf} + I_{df} + I_{ef}\right)\right) \end{aligned} \tag{40}$$

$$v_{nGf} = \frac{I_{af}}{5}\left(R - R_f\right) \tag{41}$$

where $I_{jf}, j = A, B, C, D, E$ denotes the phase currents in the fault condition and $R > R_f$

From (41) the application of a DC voltage to the faulty phase results in a positive DC shift in the neutral voltage. This causes a DC current to flow through all the phases. It should be noted that the neutral shift occurs only when the DC voltage is applied to the faulty phase. The currents in the different phases are given by

$$I_{Af} = \frac{5I_A R}{4R_f + R} \tag{42}$$

$$I_{Bf} = \frac{5I_A R_f}{4R_f + R} \tag{43}$$

$$I_{Cf} = I_{Df} = I_{Ef} = \frac{I_A\left(R - R_f\right)}{4R_f + R} \tag{44}$$

The change in the DC currents between healthy and faulty operation is given by

$$\Delta I_A = \frac{4I_A(R - R_f)}{4R_f + R} \tag{45}$$

$$\Delta I_B = \frac{I_A(R - R_f)}{4R_f + R} \tag{46}$$

$$\Delta I_C = \Delta I_D = \Delta I_E = \frac{I_A\left(R - R_f\right)}{4R_f + R} \tag{47}$$

From (45) since $R > R_f$ for an inter-turn fault, the change in the DC current between healthy and faulty operation is highest for the faulty phase. This provides a method for identifying the faulty phase.

While the above example assumed a perfectly balanced load, in reality there exists inherent unbalance between the phases of the motor. It is possible to show that the above inference still holds for an unbalanced load. However, in this case, when a DC voltage is applied across two phases, a DC current flows through all the phases even under healthy operating condition. Figure 32 shows a typical case of an unbalanced five-phase star connected resistive load. Similar to before a DC voltage V_d is assumed to be applied across phases A and B.

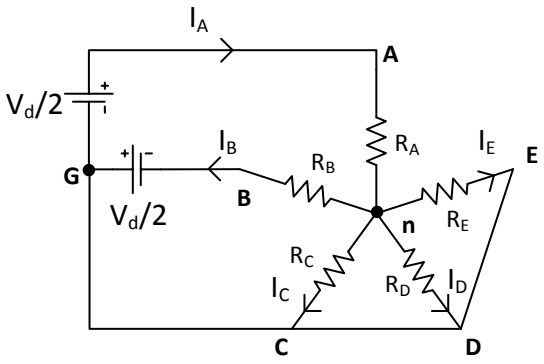

Figure 32. Five-phase star connected unbalanced load with DC applied across A and B

The resulting DC currents in the phases are giving by the following expressions,

$$I_A = K_h(R_B + 2R_P) \tag{48}$$

$$I_B = K_h(R_A + 2R_P) \tag{49}$$

$$I_j = K_h(R_D - R_A)\, {R_P}\Big/{R_j}\,, j = C, D, E \tag{50}$$

where,

$K_h = \frac{V_D}{R_P(R_A+R_B)+R_A R_B}$

$R_P = R_C \parallel R_D \parallel R_E$

When a fault occurs in phase A and the resistance of phase A decreases to a new value R_f, $R_f < R_A$. The change in the DC offset currents between the healthy and fault condition is given by

$$\Delta I_A = \Delta \mathrm{K}.\, 2R_P + \Delta \mathrm{K}.\, R_B \tag{51}$$

$$\Delta I_B = \Delta \mathrm{K}.\, 2R_P + \left(K_f R_f - K_h R_A\right) \tag{52}$$

$$\Delta I_j = {R_P}/{R_j}\left(\Delta \mathrm{K}.\, R_B + \left(K_f R_f - K_h R_A\right)\right), \qquad j = C, D, E \tag{53}$$

where,

$K_f = \frac{V_D}{R_P(R_f+R_B)+R_f R_B}$

$\Delta \mathrm{K} = \left(K_f - K_h\right),\ K_f > K_h$

From the circuit it is clear that $R_P < R_j$ and hence phase A produces the maximum change in the DC current from the healthy operating condition. . The change in the DC offset current, ΔI_{DC} can hence serve as a fault index to identify the faulty phase. It can also be inferred from the above calculations that ΔK, or the extent of deviation of the current from the healthy operating condition is dependent on the number of shorted turns.

4.3 Balanced DC Voltage Injection

An effective diagnostic method should have minimum to no interference with the operation of the motor. However, a DC current flowing through two phases of the motor creates a stationary MMF in the air gap. The interaction of this MMF with the air gap flux causes torque pulsations at the fundamental frequency [52]. For this reason, thermal monitoring schemes using DC injection apply the offset voltage or current at low frequency intervals to ensure that the disturbance caused to the operation of the motor is minimal.

For five-phase motors the presence of two additional degrees of freedom makes it possible to apply a balanced DC voltage offset across two pairs of phases at the same time. By appropriately choosing the DC voltages the stationary flux produced in the air gap can

be canceled, removing the torque pulsation created by the resulting DC current. The expression for the torque of a five-phase motor in a stationary d-q reference frame is given by

$$\tau = \frac{5P}{2} L_m \left(i_{dr} i_{qs} - i_{ds} i_{qr} \right) \tag{54}$$

By setting the stator d-axis (i_{ds}) and q-axis (i_{qs}) current components created by the applied DC voltage to zero, the pulsating torque can be cancelled. An assumption made here is that the DC voltage applied across two pairs of lines will create proportional DC currents, which is true only if the phases are perfectly balanced as shown in the previous section. However the unbalance between the phases under healthy condition is usually negligible making this a valid assumption. The stationary reference frame transformation for a five-phase motor is given by,

$$T_s = \sqrt{\frac{2}{5}} \begin{bmatrix} 1 & \cos(\alpha) & \cos(2\alpha) & \cos(2\alpha) & \cos(\alpha) \\ 0 & \sin(\alpha) & \sin(2\alpha) & -\sin(2\alpha) & -\sin(\alpha) \\ 1 & \cos(2\alpha) & \cos(4\alpha) & \cos(4\alpha) & \cos(2\alpha) \\ 0 & \sin(2\alpha) & \sin(4\alpha) & -\sin(4\alpha) & -\sin(2\alpha) \\ \frac{1}{\sqrt{2}} & \frac{1}{\sqrt{2}} & \frac{1}{\sqrt{2}} & \frac{1}{\sqrt{2}} & \frac{1}{\sqrt{2}} \end{bmatrix} \tag{55}$$

where,

$\alpha = \frac{2\pi}{5}$

Assuming that a DC voltage of V_{AD} is applied across phases A and D and a voltage of V_{CB} is applied across phases C and B, the corresponding d and q axes voltages are given by,

$$V_d = V_{AD} - V_{AD} \cos 2\alpha + V_{CB} \cos 2\alpha - V_{CB} \cos \alpha \tag{56}$$

$$V_q = V_{AD}\sin 2\alpha + V_{CB}\sin 2\alpha - V_{CB}\sin \alpha$$

To ensure that the stator d-axis (i_{ds}) and q-axis (i_{qs}) current components created by the DC voltage are zero, V_d and V_q are set to zero resulting in,

$$V_{CB} = \frac{1-\cos 3\alpha}{\cos \alpha - \cos 2\alpha} V_{AD} = \frac{\sin 2\alpha}{\sin \alpha - \sin 2\alpha} V_{AD} \quad (57)$$

If DC voltages are simultaneously applied across phase A and D and phase C and B satisfying the relation (57) the torque pulsation created by the resulting DC current is cancelled.

4.4 Simulation Results

The above results are verified with the developed model and using FEA and are summarized in Figure 33 and Figure 34. To account for the inherent unbalance in the motor windings the length of the end connections of the different phases are arbitrarily varied between ±0.5 percent. This creates unequal resistances and leakage inductances for the different phases.

It is clear that balanced DC injection, which is possible in five-phase motors eliminates one of the most important drawbacks of any DC injection based diagnostic. An additional advantage is that the DC offset measurement can be performed on four phases at the same time reducing the number of times the DC voltage has to be applied to perform the measurement on all the phases.

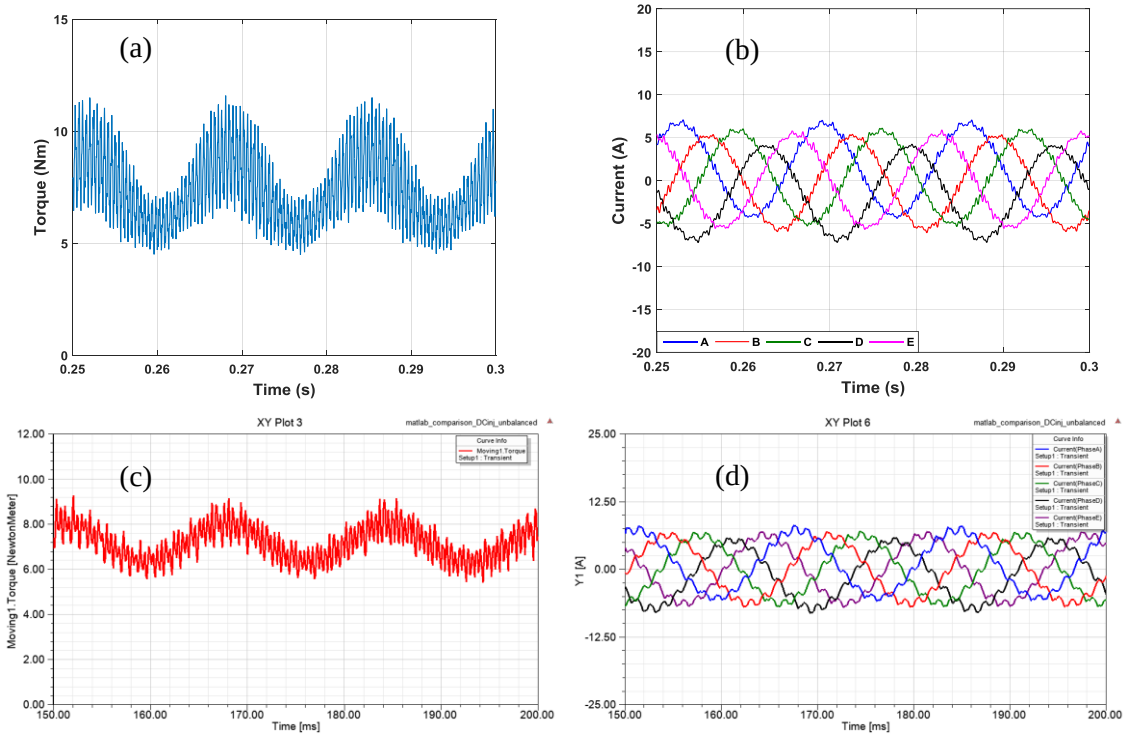

Figure 33. Torque and current waveforms with unbalanced DC injection (a) and (b) model (c) and (d) FEA

The simulation model is solved with a voltage input and a balanced DC offset applied across two pairs of phases. The simulation results of the change in the DC offset current from healthy condition ΔI_{DC} for different slips are shown in Figure 35 for 5.55% (6 turns) and 8.33% (9 turns) inter-turn fault in phase A. It can be clearly seen that ΔI_{dc} is maximum for the faulty phase. The magnitude of the fault index ΔI_{dc} increases with fault severity.

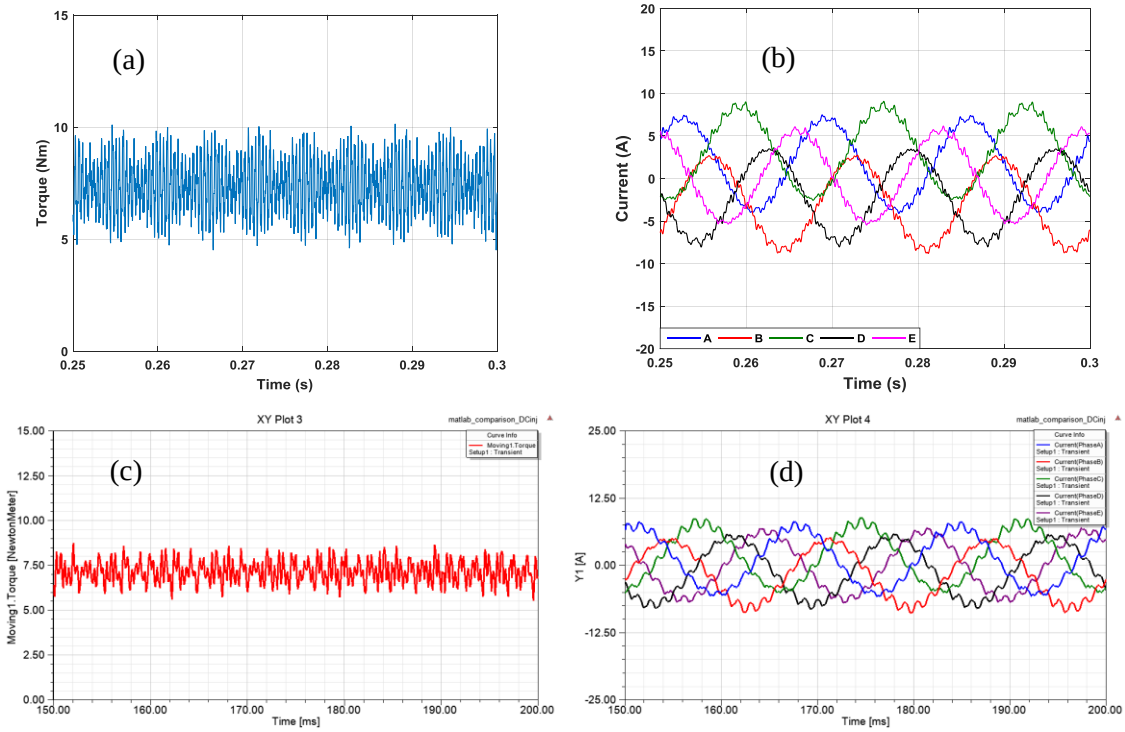

Figure 34. Torque and current waveforms with balanced DC injection (a) and (b) model (c) and (d) FEA

4.5 Practical Aspects of DC Voltage Injection

4.5.1 Fault Detection Sensitivity

The sensitivity or resolution of the DC voltage injection method in detecting an inter-turn fault is directly related to the accuracy of the DC current measurement. Since the method is intended for low-cost digital implementation in the microcontroller, the resolution of the analog to digital converter (ADC) and the effectiveness of the sensing and signal conditioning circuit play an important role. Several different techniques can be used to extract the DC offset information from the current. Once such method has been implemented and presented in Chapter 6.

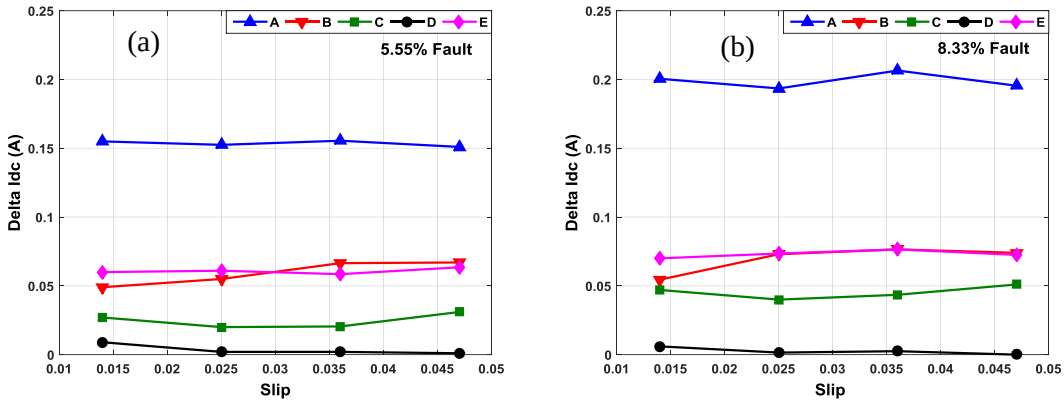

Figure 35. Change in the DC offset current ΔI_{DC} vs slip for (a) 5.55% (b) 8.33% inter-turn fault in phase A

While it is possible to increase the amplitude of the applied DC offset voltage to improve the resolution, this comes at the cost of increased copper loss as well as core loss due to iron saturation. The allowable DC offset voltage command is also limited by the PWM modulation index corresponding to the operating point. However, typically this is not usually an issue since the voltage is only a small fraction of the fundamental voltage. The ideal DC voltage command has to be determined during the commissioning stage for different motor drive systems. The selection of the DC voltage command is a compromise between sensitivity and some loss in performance. To avoid false positives it is also advisable to maintain a threshold in ΔI_{dc} above which the decision that a fault has occurred can be made.

4.5.2 Effect of Controller

Synchronous reference frame control of induction motors uses PI controller to track the d- and q-axes command currents that appear as constant or DC values at steady state in this frame. However, the DC offset added to the current appears as a sinusoidal

function at fundamental frequency. The high band width current controller tries to compensate for this sinusoidal signal, effectively reducing the applied DC offset voltage. The extent of compensation depends on the controller bandwidth and is a function of the fundamental operating frequency. Some solutions proposed in the literature include using DC current injection or suspending the current control loop when performing the DC injection [53]. DC current injection introduces challenges in measuring the small DC voltage signal and also requires additional voltage sensors while disabling the control loop interferes with the motor performance.

To avoid the effect of current loop dynamics on the injected DC voltage the control loop is implemented in the stationary reference frame using proportional resonant (PR) controllers. A detailed description of this implementation for a five-phase induction motor was presented in Chapter 2. Once tuned, the PR controllers offer a fixed, low gain at all frequencies other than the resonant frequency effectively minimizing, if not eliminating the impact of the controller on the applied DC voltage. The resonant frequency of the controller changes with the fundamental frequency. Implementation of the current control loop in the stationary frame has several other advantages that are discussed in Chapter 6. The overall current control loop with the DC injection is shown in Figure 36. As shown, a balanced DC voltage is applied at the output of the control loop which is implemented in the stationary reference frame.

4.5.3 Effect of Dead-Time and Switch Non-Linearity

The actual DC voltage that is applied across the phases is different from the command. This is attributed to the effect of dead-time and switch non-linearity that has

been well documented in the literature [54]. Dead-time is the period between an on-off transition when both the top and bottom switches of an inverter are turned off. Under such condition the polarity of the output phase voltage depends on the polarity of the current flowing through the leg as shown in Figure 37. In the absence of any DC offset in the current the net DC voltage applied to the phase as a result of dead-times is zero. However a positive DC offset in the current results in a net negative DC voltage contribution applied to the phase as a result of dead times. This voltage contribution reduces the effective DC voltage applied to the phase. The effect becomes an issue when the load current amplitude changes, since the negative voltage contribution due to dead time drops as shown in Figure 38.

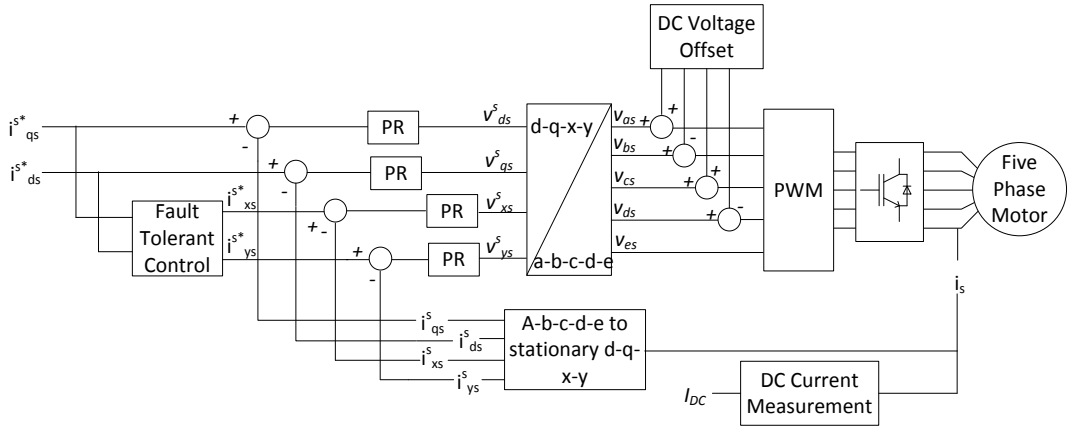

Figure 36. Five-phase motor control loop incorporating DC voltage injection

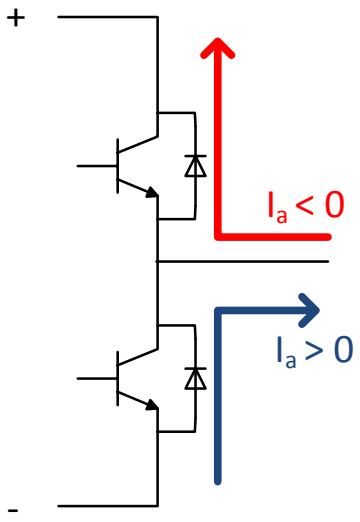

Figure 37. Current path during dead times for an inverter leg

Hence, for the same DC voltage command the actual DC voltage applied to the phase increases with increase in load (i_q). The plot shown in Figure 39 shows the variation of the DC current with change in load for the healthy motor obtained from experimental tests. It can be seen that while the offset current remains relatively constant with speed it varies with load. In addition to the dead-time effect, the forward voltage drop of the switch varies non-linearly with the current through the switch. To account for these effects in the fault detection algorithm, DC current offset data should be measured offline at varying loads (i_q) on a healthy motor to form a look-up table. The same DC voltage command has to be applied to perform the diagnostic when the motor is online. The look-up table then serves as the reference, based on which the fault decision is made.

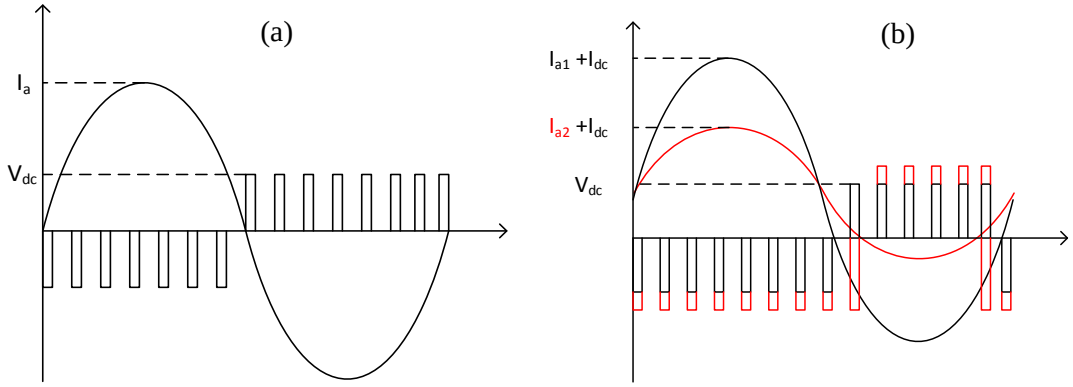

Figure 38. (a) DC voltage contributed by dead time effects without application of DC offset (b) comparison of effect of current amplitude on dead-time DC voltage contribution

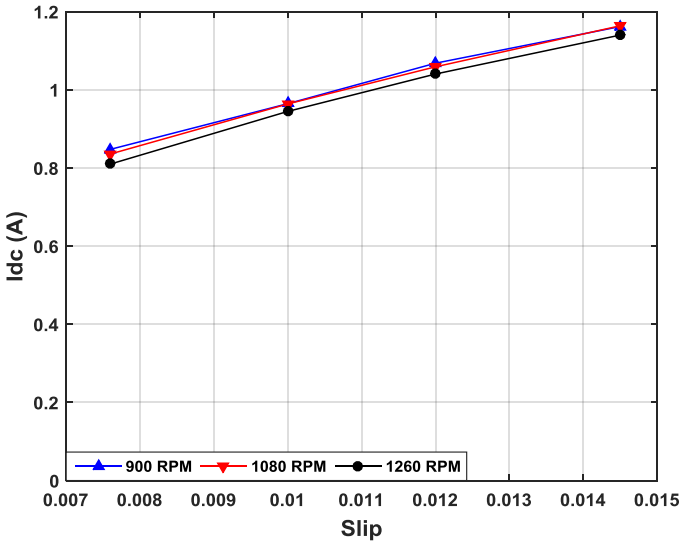

Figure 39. Experimental result showing change in I_{DC} with load for the same DC voltage command

It should also be pointed out that in the presence of an inter-turn short in a phase, the amplitude of the current flowing though the faulty phase increases due to the unbalanced impedances. Additionally for a vector controlled motor the q axis current command increases during the fault [3]. This occurs due to a reduction in the air gap flux caused by the large opposing current flowing through the shorted turns as shown in

Chapter 3. Both these effects increase the applied DC voltage across the phase further, resulting in increase in the DC offset current, in addition to increase caused due to lower resistance. The phase with the maximum change in DC offset current from the healthy operating condition (obtained from the look-up table) can be identified as the faulty phase.

4.5.4. Effect of Winding Asymmetries

As derived earlier, the asymmetry in the phase windings results in a DC offset current through all the phases. This effect however is taken into account when forming the reference DC current look-up table for the healthy motor.

4.5.5. Effect of Temperature

Temperature affects the phase resistance which in turn impacts the DC offset current. The impact of temperature is uniform on all the phases. The effect of temperature on the DC offset current can be accounted for by performing the reference DC current measurements at thermal steady state.

4.5.6. Effect of DC Bus Voltage

For successful implementation of this diagnostic method the DC bus voltage has to remain fixed when performing the DC current measurement and should be the same value used for calibrating the reference DC current offset table. Another alternative would be to sense the DC bus voltage before performing the diagnostic to avoid spurious detection of faults.

Detection of inter-turn fault using DC voltage injection requires no additional sensors since the current is already sensed by the drive. An algorithm for estimating the DC bias in the current can be digitally implemented on the microcontroller controlling the

motor. Additionally, for a five-phase motor this method has been shown to be truly non-intrusive in terms of its impact on the motor torque production. The method is also effective when the extent of inter-turn fault is not substantial enough to create significant unbalance between the phase currents, which is an important requirement for condition monitoring.

4.6 Chapter Summary

This chapter introduces a novel DC voltage injection method for detection of inter-turn faults in five-phase motors. By applying a balanced DC voltage across two pairs of phases it has been shown through simulations that the torque pulsation caused by the DC offset current can be cancelled. The difference in the current response to a DC offset voltage between healthy and faulty operating condition ΔI_{dc} is proposed as a fault index. Additionally, it has been shown that the maximum value of ΔI_{dc} will be seen in the faulty phase. A detailed study of the practical issues associated with this diagnostic method are presented and suitable solutions are recommended for each issue. Further validation of the diagnostic is presented through experimental results in Chapter 6.

5. FSCW CONFIGURATION FOR OUTER ROTOR INDUCTION MOTORS*

Tooth wound or fractional slot concentrated winding (FCSW) configurations have gained popularity over the last decade for PM motors for several reasons

- Better copper utilization – A FSCW has shorter and non-overlapping end connections when compared to a conventional distributed winding.
- High slot fill factor – For tooth wound coils this is achieved by using in-slot winding machines or a segmented stator structure pre-wound with coils.
- Higher stack length - A tooth wound coil has a shorter end extension resulting in a higher stack length for the same effective length.
- Fault tolerance - The end-windings of the different phase do not overlap each other impeding the propagation of a winding fault to other phases

5.1 Stator Winding Design

5.1.1 Feasible Slot-Pole Combinations

For a given choice of number of poles and number of slots, independent of the (slots per pole per phase) SPP, there exists in the air gap, step-harmonics produced as a result of arranging the winding in slots, which are given by (58):

* © 2015 IEEE. Reprinted, with permission, from V. M. Sundaram and H. A. Toliyat, "A Fractional Slot Concentrated Winding (FSCW) configuration for outer rotor squirrel cage induction motors," *2015 IEEE International Electric Machines & Drives Conference (IEMDC)*, Coeur d'Alene, ID, 2015, pp. 20-26.

$$\nu = (kZ \pm p), k = 0,1,2,3 \ldots \quad (58)$$

where,

ν = order of the step-harmonic

Z = number of stator slots

p = number of pole pairs

For a winding with a constant slot pitch, the winding factors for the step-harmonics are the same as the fundamental $(k = 0)$ [55]. Hence, the air gap MMF due to a step-harmonic of order ν has an amplitude that is p/ν of the fundamental.

For conventional FSCW the ratio of $Z/2p$ is chosen to be close to 1. This ensures that when using a tooth wound coil the fundamental pitch factor is close to unity. As a result, the first order step harmonics $(k = 1)$ are closer to the fundamental and hence create MMF components that are comparable in amplitude to the fundamental. Table 2 shows the amplitude of the first order step harmonics as percentage of the fundamental for some common FSCW slot-pole combinations.

Table 2. Step harmonic amplitudes for common FSCW configurations

SLOT /POLE /PHASE	$(\boldsymbol{Z - p})$ **(% OF FUNDAMENTAL)**	$(\boldsymbol{Z + p})$ **(% OF FUNDAMENTAL)**
3/8 *(9 slot 8 pole)*	80	30.8
1/2 *(12 slot 8 pole)*	50	25
2/5 *(12 slot 10 pole)*	71.4	29.4
5/14 *(15 slot 14 pole)*	87.5	31.8
3/7 *(18 slot 14 pole)*	63.6	28

The currents induced in the rotor due to step-harmonics produce asynchronous and synchronous parasitic torques that reduce the average torque and create torque pulsations

that are a function of rotor speed**.** When compared to a distributed winding where the step-harmonics are of a much higher order relative to the fundamental, an FSCW results in an inferior design.

Increasing $(Z - p)$ to minimize the step harmonics would increase $Z/2p$ well above one which in turn causes the fundamental pitch factor to reduce for a tooth wound coil when compared to a distributed winding where pitch factor is typically > 0.9. Although there is less copper used for the end connections more turns are now required in the slots for comparable torque production.

A suitable compromise is achieved by using a coil pitch of two slots and creating two layers of stator slots. This configuration, which is more suitable for outer rotor motors, makes it possible to create non-overlapping and hence shorter end connections that preserve the advantage provided by FSCW in terms of better copper utilization. At the same time, the two slot coil pitch ensures that the fundamental pitch factor is still comparable with distributed windings. Details of dual slot layer stator are explained in Section 5.2. For induction motors higher number of poles results in low magnetizing inductance and poor power factor. This in turn affects the efficiency by increasing the stator current required for a given torque and the kVA rating for the inverter driving the motor. Based on these considerations a 24 slot 10 pole winding with a two slot coil pitch and a dual slot layer stator is chosen for design. The pitch factor and amplitudes of the first order step harmonics are given in Table 3.

Table 3. Parameters of 24 slot 10 pole stator

PARAMETER	VALUE
Pitch Factor (K_{p5})	0.966
$19^{th}, (Z-p)$	26.3% of 5th harmonic
$29^{th}, (Z+p)$	17.24% of 5th harmonic

5.1.2 Stator Winding Configuration

Opting for a fractional SPP creates additional sub and higher order space harmonics in the air gap MMF that have the same effect on torque production of an induction motor as the step-harmonics. . However unlike the step harmonics that have the same winding factor as the fundamental, it is possible to minimize or cancel these MMF harmonics by several means.

In PM motors, minimizing or cancelling these harmonics improves the efficiency of the motor and has been explored in the literature. The methods include

- using multi-layer windings [43]
- different turns per coil side [56]
- different turns per coil [43]
- using multiple winding systems shifted in space [57]

In this chapter, a multi-layer winding with varying turns per coil is designed for the 24 slot 10 pole stator.

The star of slots theory [58] is used to design the winding. Since each coil has a two slot coil span the spokes on the star now correspond to the number of turns across two adjacent stator teeth instead of a single tooth. The angle between the spokes is given by:

$$angle\ between\ spokes\ \theta = \frac{360 \times GCD(Z,p)}{Z} \tag{59}$$

For the proposed slot-pole combination this angle is 15^0. The star of slots diagram for a 24 slot 10 pole motor is shown in Figure 40. For the above multi-layer winding the air gap MMF waveform around the rotor periphery and its space harmonics are shown in Figure 41**.** It can be seen that this winding has a high first order sub-harmonic. The other harmonics at 19, 29 and 43 are the step-harmonics produced due to placing the coils in 24 slots.

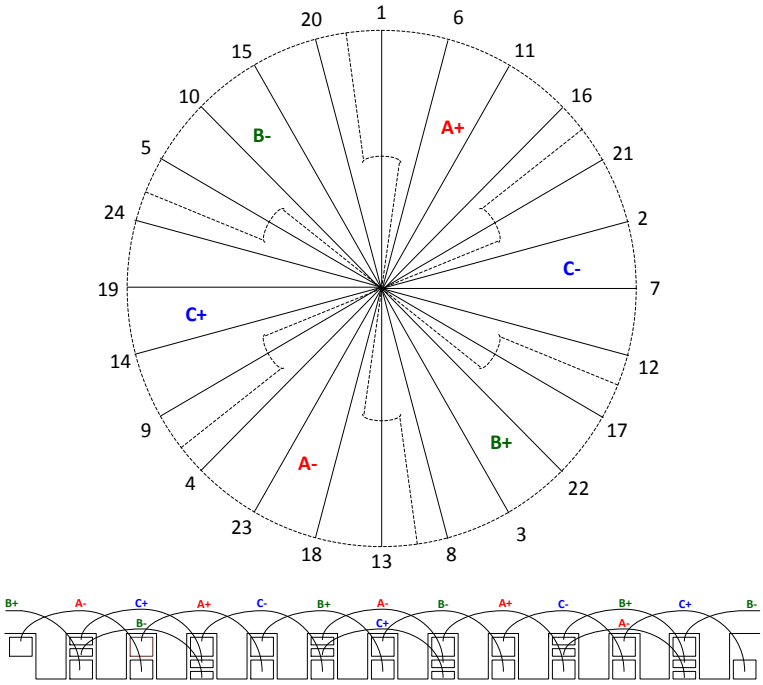

Figure 40. Star of slots for 24 slot 10 pole multi-layer configuration with uniform turns per coil.

While it is not possible to cancel the step harmonics additional degrees of freedom are introduced to minimize the first sub harmonic. Two variables x and y are used to denote

the fraction of the total turns per coil for certain selected coils. The modified star of slot diagram is shown in Figure 42. The values of x and y are now varied from 0 to 1. Figure 43 shows the variation in the first sub harmonic as x and y are varied from 0 to 1.

Based on the plot in Figure 43, it is possible to eliminate the first sub harmonic by setting $x = 0.7$ and $y = 0.5$. The resulting air gap MMF and its space harmonics are shown in Figure 44. It can be seen that the first order sub-harmonic is completely eliminated and the only significant harmonics in the air gap are the step harmonics at 19, 29 and 43. The pitch and distribution factor for this modified winding are given in Table 4.

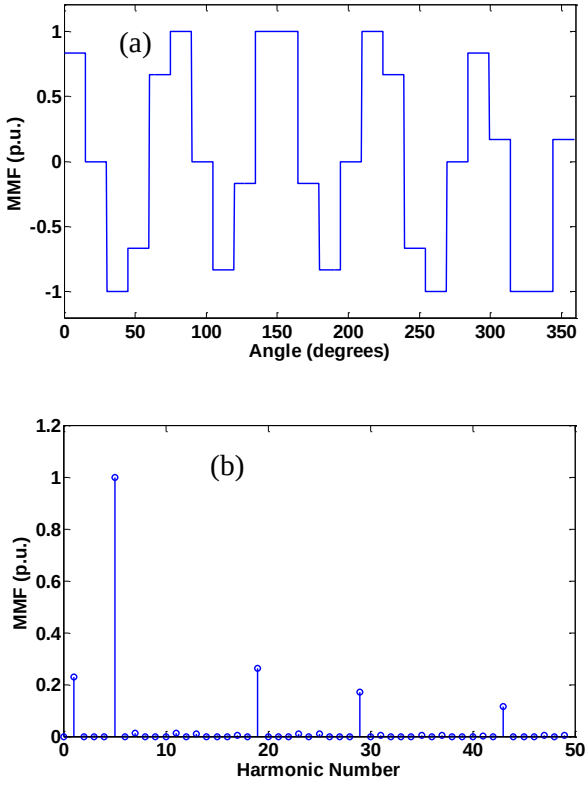

Figure 41. (a) Air gap MMF of 24 slot 10 pole winding with uniform turns per coil and, (b) its frequency components.

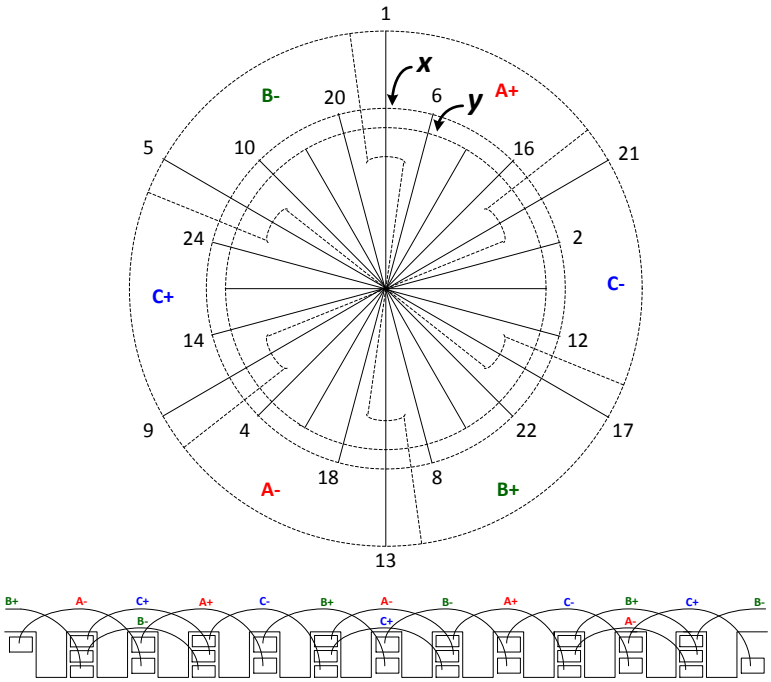

Figure 42. Star of slots for 24 slot 10 pole multi-layer configuration with varying turns per coil.

Table 4. Winding factor for 24 Slot 10 pole stator with varying turns per coil

PARAMETER	VALUE
Pitch Factor (K_{p5})	0.966
Distribution Factor (K_{d5})	0.9373
Winding Factor (K_{w5})	0.9054

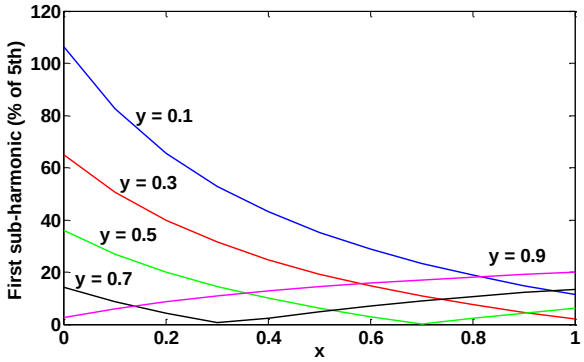

Figure 43. Variation of first order sub-harmonic with x and y.

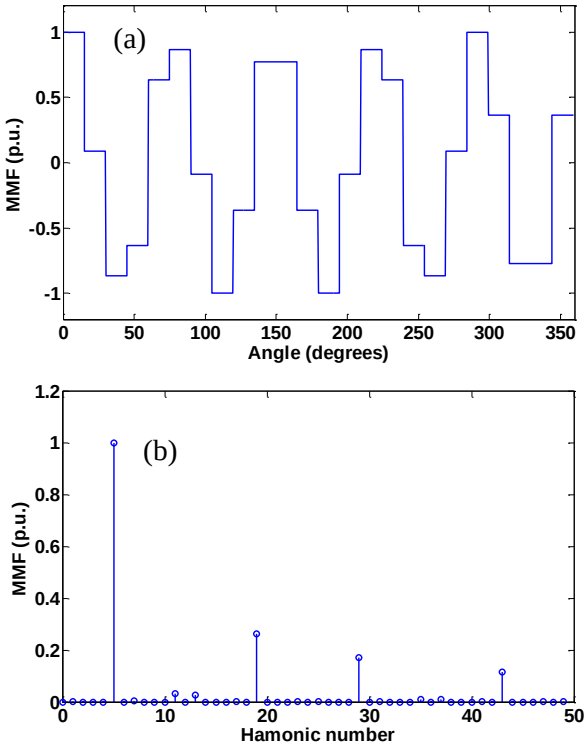

Figure 44. (a) Air gap MMF of 24 slot 10 pole winding with varying turns per coil and (b) its frequency components.

It is worthwhile to point out that the winding adopted in [57] is effectively a 24 slot 10 pole double layer winding with a two slot coil pitch. However, the resulting air gap MMF distribution in [57] additionally has a significant 17^{th} harmonic.

5.2 Dual Slot Layer Stator

The winding configuration for a 24 slot 10 pole stator has a coil pitch of two slots. This results in an overlapping end connection which affects the copper utilization. It can be seen from Figure 42 that the stator slots alternate between having two and three layers of coils. It is proposed to arrange the stator slots in two layers with alternate slots in a lower layer as shown in Figure 45.

For the above winding, such a dual slot layer stator structure and an outer rotor are advantageous for the following reasons,

- Non-overlapping end connections similar to a tooth wound FSCW, Figure 45(b),
- Lower end winding length due to shorter coil radius especially for the second layer,
- Reduction in overall motor volume due to shorter rotor back iron width required for a higher number of poles. For an external stator more back iron will be required to accommodate the second slot layer thereby increasing the total volume,
- Higher slot fill factor by using in-slot winding machines to wind both slot layers.

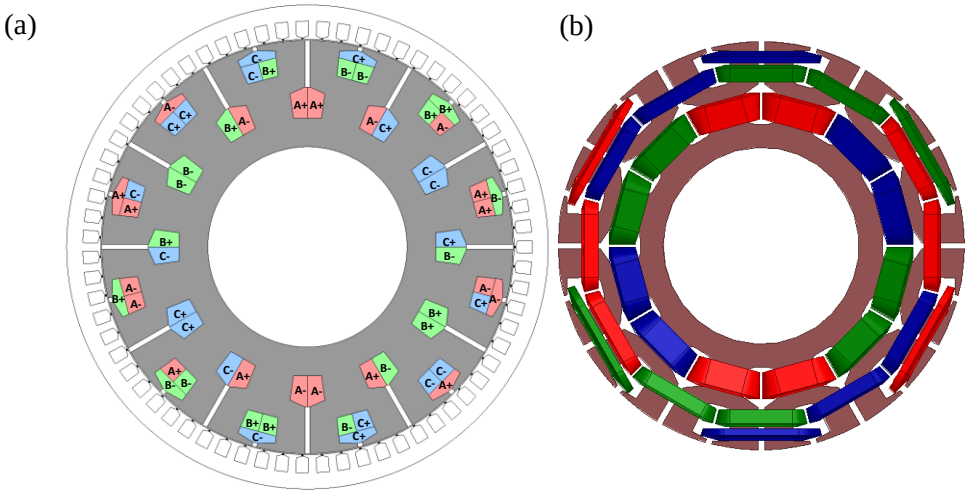

Figure 45. (a) Dual slot layer 24 slot 10 pole stator and (b) it end connections.

This type of stator slot arrangement is commonly used in single phase outer rotor induction motors for ceiling fans as shown in Figure 46 (a). The main winding is wound in the peripheral layer and the starting or auxiliary winding in the second layer. The number of poles per layer can vary from 8 to 18. Commercially, automated in-slot winding machines are used in this application to wind the coils around each tooth in a layer making

it possible to achieve higher fill factors. Figure 46 (b) shows the non-overlapping end connection created by using this stator structure.

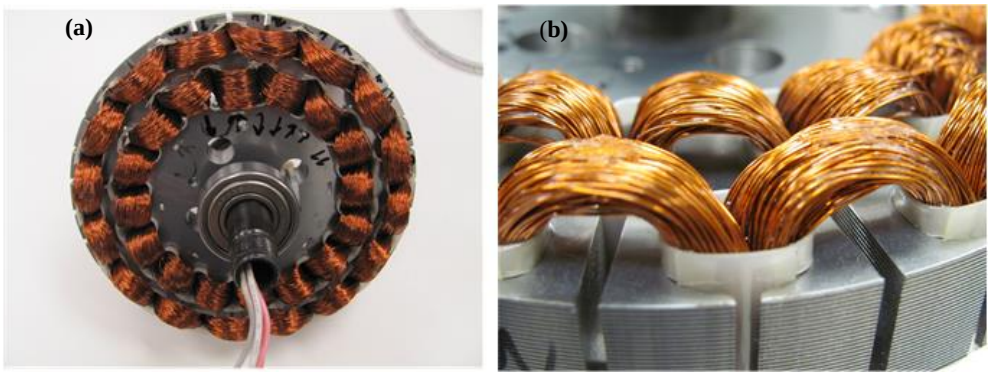

Figure 46. (a) Ceiling fan stator (b) non-overlapping end connections

It is important to note that, for the resulting non-overlapping 24 slot 10 pole winding with a two slot coil pitch, the end winding length is the same as a 12 slot 10 pole tooth wound 2/5 SPP winding that is widely used for PM motors.

5.3 Cage Rotor Design

For an induction motor, the stator and rotor slot combinations significantly impact the audible noise and the average/ripple torque production at different speeds. The rotor slot shape and the number of rotor slots is chosen to achieve a desired torque and efficiency characteristic by accounting for the parasitic torques caused by the stator sub and higher order MMF harmonics [55]. The change in rotor resistance and leakage inductance due to skin effect is obtained from circuit analysis by dividing the rotor slot into multiple layers [48] using a T-model equivalent circuit per layer.

For the 24 slot 10 pole stator, the dominant step-harmonics at 19 and 29 can be cancelled/reduced by skewing the rotor slots. However, the fundamental winding factor reduces as the skew angle is increased [48]. A skew angle of $2\pi/29$ radians or 12.414^0 is chosen to cancel the 29th step harmonic. Table 5 shows the fundamental winding factor with a skewed rotor and the amplitudes of the lower order step harmonics as a result of skewing.

Table 5. Winding factor for 24 slot 10 pole stator with skewed rotor slots

PARAMETER	VALUE
Winding Factor (K_{p5})	0.861
$19^{th}, (Z-p)$	11.86% of 5th harmonic
$29^{th}, (Z+p)$	0
$43^{rd}, (2Z-p)$	2.62% of 5th harmonic

5.4 Design Comparison

The performance of the proposed 24 slot 10 pole FSCW stator is compared to a conventional single layer concentric wound 60 slot 10 pole distributed winding stator for an outer rotor geared in-wheel hub motor for electrical two wheelers. The design constraints are

- Rotor outer diameter (OD) = 145 mm
- Stack length = 40 mm
- DC bus voltage = 48 V
- Output power = 1.1 kW at 2800 rpm (fundamental frequency = 240 Hz)

The winding factor of the 60 slot 10 pole distributed winding is given in Table 6.

The FSCW stator has an inferior winding factor as well as a higher leakage inductance caused by the deeper slot openings of the inner slot layer. For a fair comparison, it is necessary to exploit the shorter stator end connections that are characteristic of FSCW. The effective stack length is defined as the sum of the stack length and end extension on both sides of the stator as shown in Figure 47. The end extension and end winding length of the proposed FSCW and distributed winding are obtained from ANSYS Maxwell Modeler.

Table 6. Winding factor for 60 slot 10 pole stator

Parameter	***Value***
Pitch Factor (K_{p5})	1
Distribution Factor (K_{d5})	0.9659
Winding Factor (K_{w5})	0.9659

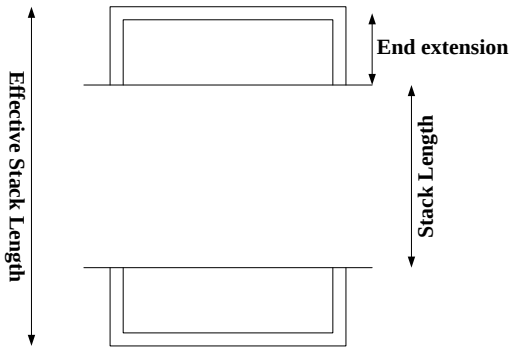

Figure 47. Effective stack length of a stator

It is observed that for the same effective stack length, the stack length of the FSCW stator is 48 mm as compared to 40 mm stack length for the distributed winding stator. It is worthwhile to note that concentric coils provide the lowest end extension for a distributed winding. The comparison of the stack length for the two motors is shown in

Figure 48.

A 67 slot rotor with copper bars and a 0.3 mm air gap is used for both motors. The rotor of the FSCW motor additionally has a skew of 12.414^0 as explained in the previous section. The rotor slot shape is designed for the fundamental 10 pole MMF harmonic using the standard induction motor equivalent circuit and is the same for both designs. The stator slots are designed for an RMS current density of 5.6 A/mm^2. The air gap flux density distribution, including the saturation effects, obtained from transient finite element analysis (FEA) of the two motors in Cedrat Flux2D/FluxSkew is shown in Figure 49.

(a)

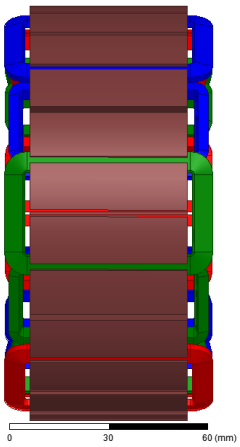

(b)

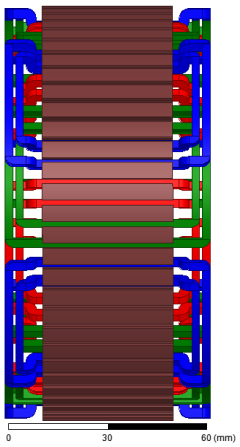

Figure 48. Comparison of stack lengths of (a) FSCW and (b) distributed winding for the same effective stack length.

The FSCW motor is simulated using a layered quasi-3D model with skewed rotor slots in Cedrat FluxSkew. As expected, step harmonics exist in the air gap flux but the amplitudes of the step harmonics are modulated by the slot permeance harmonics which occur at the same frequencies [55]. A comparison of the two designs is shown in Table 7**.** The loss calculations are obtained from FEA simulations.

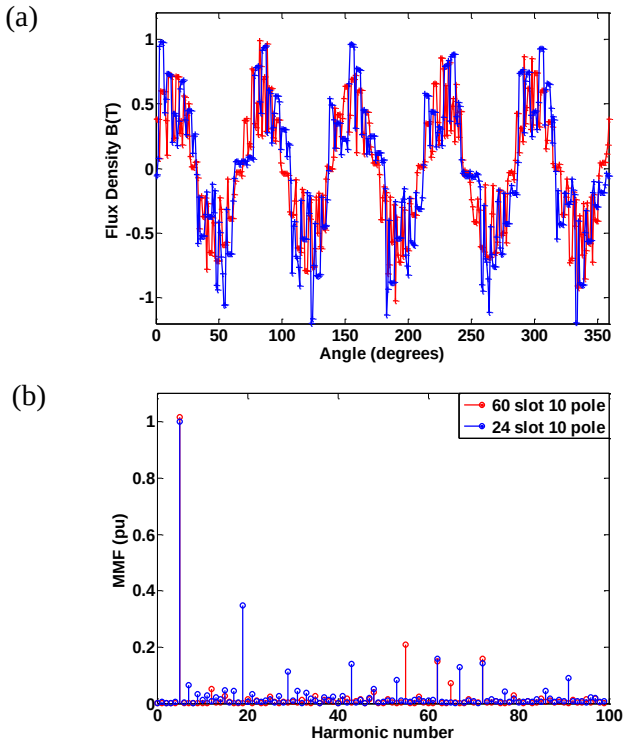

Figure 49. (a) Air gap flux density of the FSCW and distributed winding designs from FEA and, (b) their frequency components.

The following observations can be made

- The FSCW has a low magnetizing inductance due to low fundamental winding factor when compared to the distributed winding resulting in a higher rated slip and higher rotor copper losses,

- The choice of turns per coil in the FSCW configuration is restricted by the condition that was derived to eliminate the first sub-harmonic in Section 5.2,
- Due to the non-overlapping and shorter end connection, the end winding leakage and stator resistance of the FSCW are lower compared to the conventional distributed winding. However, the presence of deep slot openings especially for the inner slot layer, increases the slot leakage,
- The additional core loss in the FSCW motor is attributed to the higher slot leakage and harmonic leakage as well as the increase in core volume created by the longer stack length. The flux density distribution of the two designs is shown in Figure 50.

Table 7. Comparison of FSCW and distributed winding

PARAMETER	**24 SLOT 10 POLE**	**60 SLOT 10 POLE**
Stack length (mm)	48	40
Turns per phase	24 (26 strands of 22 AWG per turn)	30 (22 strands of 22 AWG per turn)
Rated Current (A)	48	40
Rated Slip	2.5%	2.25%
Stator copper loss (w)	84.5	90
Stator core loss (w)	133.69	63.81
Rated efficiency (%)	81.5	86.1
Copper volume in stator (m^3)	0.0942	0.1227
Copper volume in rotor (m^3)	0.0522	0.0424

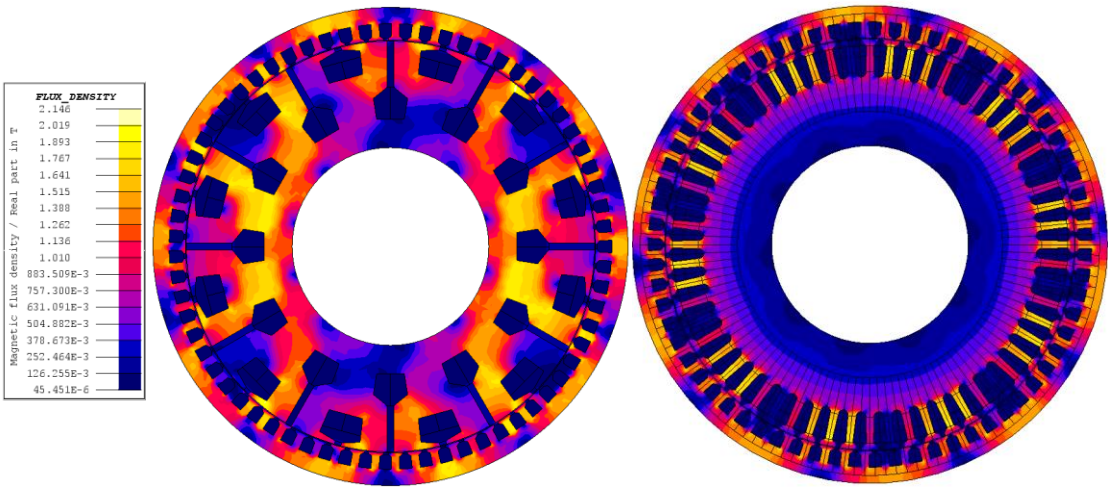

Figure 50. Comparison of flux density distribution in the FSCW and distributed winding motors.

- Even after accounting for the increased rotor bar length due to skewing; the shorter overhang and end winding length of FSCW results in an 11.3% reduction in the copper volume for the FSCW motor when compared to the distributed winding motor.
- A comparison of the torque ripple at rated condition for the two motors obtained from transient FEA is shown in Figure 51. The distributed winding motor has a marginally lower torque ripple but the use of multi-layered winding and a skewed rotor significantly lowers the torque pulsation for the FSCW motor.

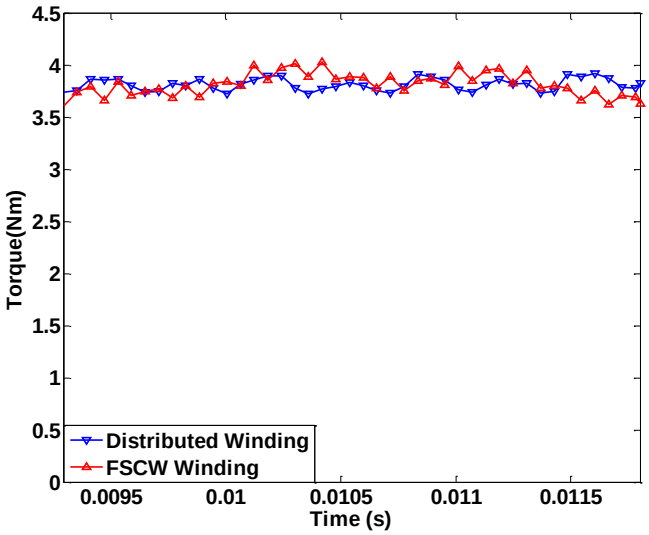

Figure 51. Instantaneous torque of the FSCW and distributed winding motors at rated slip.

5.5 Chapter Summary

An FSCW configuration suitable for outer rotor squirrel cage induction motors has been presented. The proposed design uses a multi-layer winding with varying turns per coil and a skewed rotor to minimize the space harmonics in the air gap MMF. A dual slot layer stator construction that is commonly used for single phase ceiling fan motors is adopted to create a non-overlapping end-winding and a high slot fill factor, similar to the tooth wound FSCW. A cost effective winding method using in-slot winding machines has been identified.

A 24 slot 10 pole outer rotor motor with the proposed FSCW stator is compared to a 60 slot 10 pole distributed winding motor designed for the same specification. It is shown that when taking into account the effective stack length the FSCW motor can

provide comparable performance in terms of average/ripple torque with a significant reduction in total copper usage. However, the comparatively lower fundamental magnetizing inductance and increased slot and harmonic leakage of the FSCW affects its efficiency.

Nevertheless, for an induction motor the proposed stator configuration gives the best of both worlds in terms of easy manufacturability of the cage rotor and stator winding as well as better copper utilization and non-overlapping end connections of an FSCW without compromising torque performance.

6. EXPERIMENTAL RESULTS

6.1 Details of Experimental Set-Up

The proposed fault-tolerant control method and inter-turn fault detection scheme are tested on a prototype five-phase motor with taps provided on the stator winding to create an inter-turn fault. The overall experimental set up is shown in Figure 52 and component descriptions are provided in Table 9.

The specifications of the motor are provided in Table 8. The equivalent circuit parameters of the five-phase motor are obtained from the following measurements [59]:

- Standstill test with x-y plane excitation – L_{ls} and R_s
- No load test – L_s or (L_{ls}+L_m)
- Locked rotor test - L_{lr} and R_r

6.2 Digital Implementation of the Motor Control Loop

The stationary frame PR controller is implemented on the F28335 Delfino Micrcontroller. A block diagram of the control loop is shown in Figure 53**.** The five-phase induction motor is controlled using indirect field oriented control (FOC) with speed sensing. The d-axis current command is kept fixed for all tests. Although the Delfino has a floating point core the entire control is performed using fixed point math to show that it can be applied to her low-cost microcontrollers. The switching signals are generated using

conventional sine PWM (SPWM). The PR controllers are discretized using ZOH as explained in Chapter 2.

Table 8. Parameters of 7.5 HP prototype five-phase induction motor

TYPE	QUANTITY	UNITS	VALUE
NAMEPLATE	Rated Power	HP	7.5
	Rated Speed	RPM	1735
	Pole Number		4
	Voltage	V	460
	Frame		C213T
STATOR	Slot Number		40
	Stack length	Inches	4
	Parallel Connection		1
	Wire Gauge	AWG	19
	Stands		4
	Turns/coil		27
	Winding Layers		1
	Winding Taps (A,B,C)		5 per phase
ROTOR	Slot Number		28
	Cage Material		Al
EQUIVALENT CIRCUIT	L_m	H	0.117
	L_{ls}	H	0.0127
	R_s	Ω	0.6424
	L_{lr}	H	0.0063
	R_r	Ω	0.373

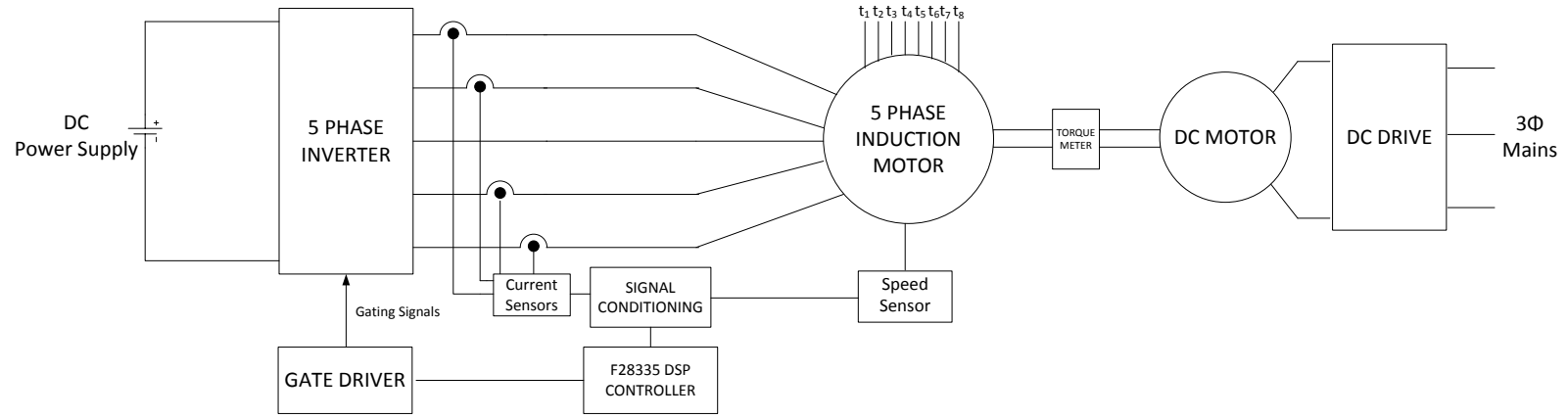

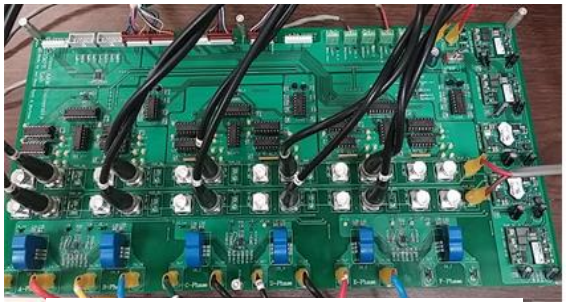

Sensing and signal conditioning

F28335 DSP Control Card

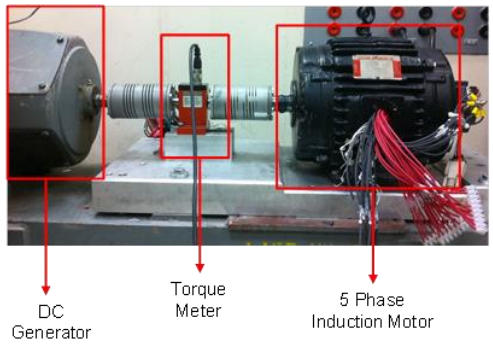

Figure 52. Layout of experimental set-up

Table 9. Components of the five-phase motor drive test system

COMPONENT	SPECIFICATION
5 PHASE INVERTER	2 SEMIKRON SEMITEACH 20kVA (5 of 6 six legs used)
IGBT	SKM 50GB 123 D
DC BUS	250V
GATE DRIVER	SKHI 22A
CURRENT SENSORS	LEM LTS 15-NP
DSP/MICROCONTROLLER	Texas Instruments F28335 Delfino
SHAFT ENCODER	Hohner 88 2048ppr
DC MOTOR	4.5kW , 1750 RPM
DC DRIVE	ABB DCS800

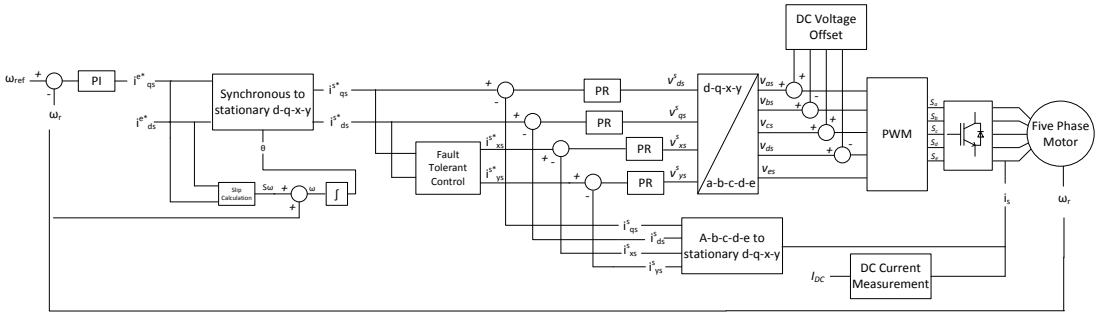

Figure 53. Block diagram of motor control loop implemented in F28335 DSP

The DC offset measurement by the DSP forms the basis of the proposed diagnostic. To ensure that the signal measured by the DSP is free from high frequency switching noise that may be entering the system, the output of the current sensors are over sampled at a high sampling rate of 350kHz. The mean of 32 successive samples is calculated to represent the sensed currents resulting in a net sampling rate of 10.93 kHz. The PWM switching frequency is fixed at 5.47 kHz. For digital implementation, the control loop is

divided into three separate interrupt service routines (ISR) – control ISR, DC measurement ISR, and sampling ISR. The timing diagram for each routine is given in Figure 54 and the flow charts for the ISRs are given in Figure 55, and Figure 57.

6.2.1. Sampling ISR

This represents the innermost and fastest ISR which over samples the current signals from the sensors.

6.2.2. DC Measurement ISR

32 successive current samples from the sampling ISR are averaged in this loop. The calculation of the DC offset in the current is performed in this ISR by calling the DC Calculation function shown in Figure 56. After adding the commanded DC offset voltage to the controller output, the loop waits for 1000 cycles or approximately 100ms to allow the transient in the DC current to settle. The DC offset calculation is then performed by averaging the current samples between two successive positive zero crossings. To eliminate errors that may occur due to noise the DC calculation function checks for 5 successive positive current samples after a negative current sample to confirm that a positive zero crossing has occurred. A similar routine is followed for the negative zero crossing detection. The calculated DC offset is averaged over 8 such measurements. To account for already existing DC bias in the current; for every DC measurement, the calculation of the offset in the current is performed twice, once before the application of a DC voltage and once after. The difference between these two values is taken to be the DC current offset resulting from the applied DC voltage. Note that for simplicity this part is not shown in the flow charts.

6.2.3. Control ISR

This is the outermost and slowest ISR which executes the motor control loop. The ISR is triggered every PWM cycle to perform the control loop calculations and update the PWM compare values.

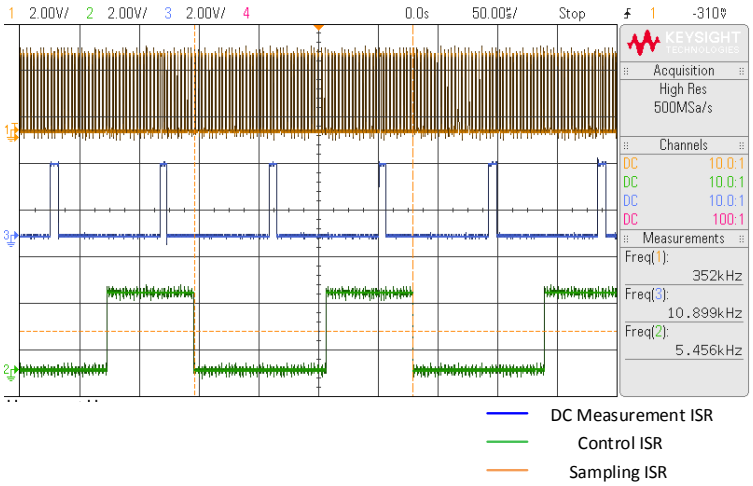

Figure 54. Timing diagram showing the frequency of execution of each service routine

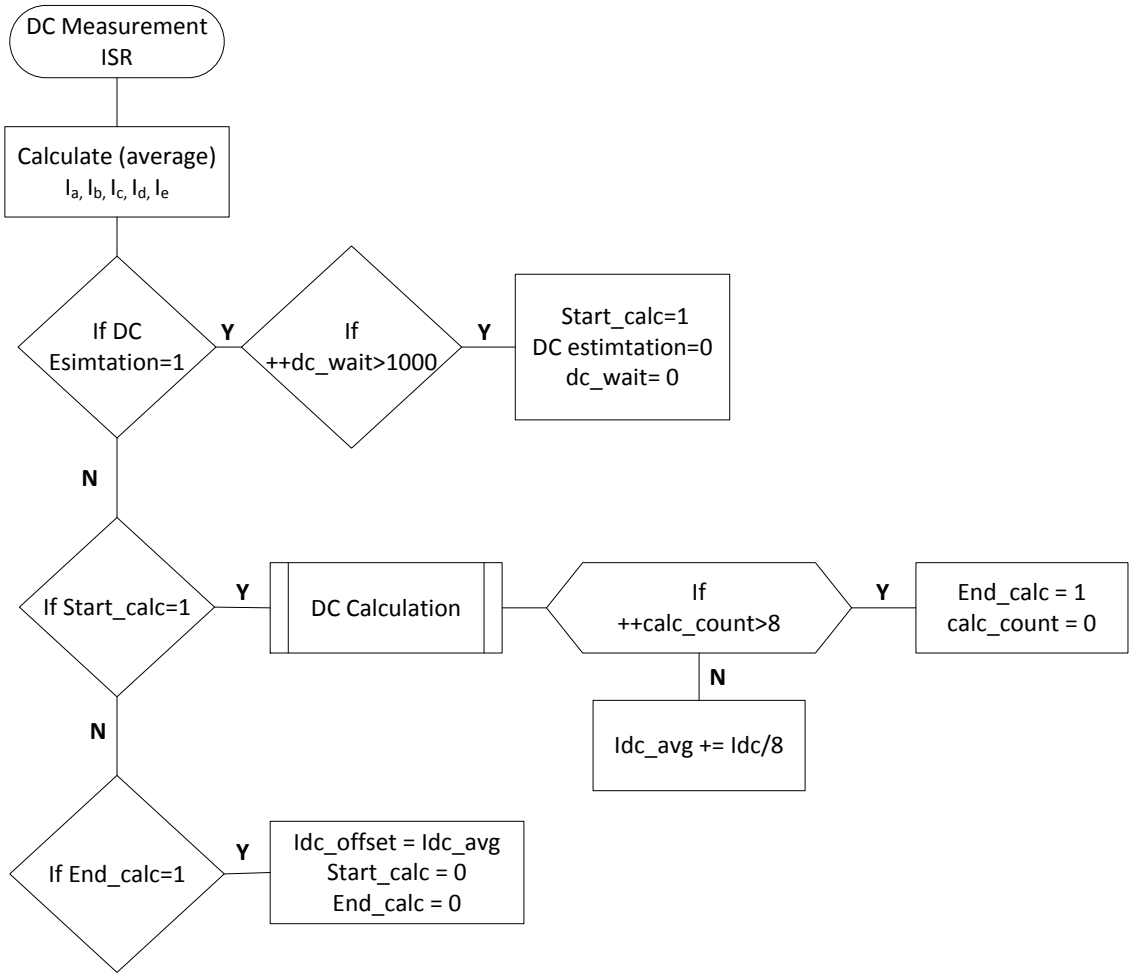

Figure 55. Flowchart for DC measurement ISR

DC Calculation

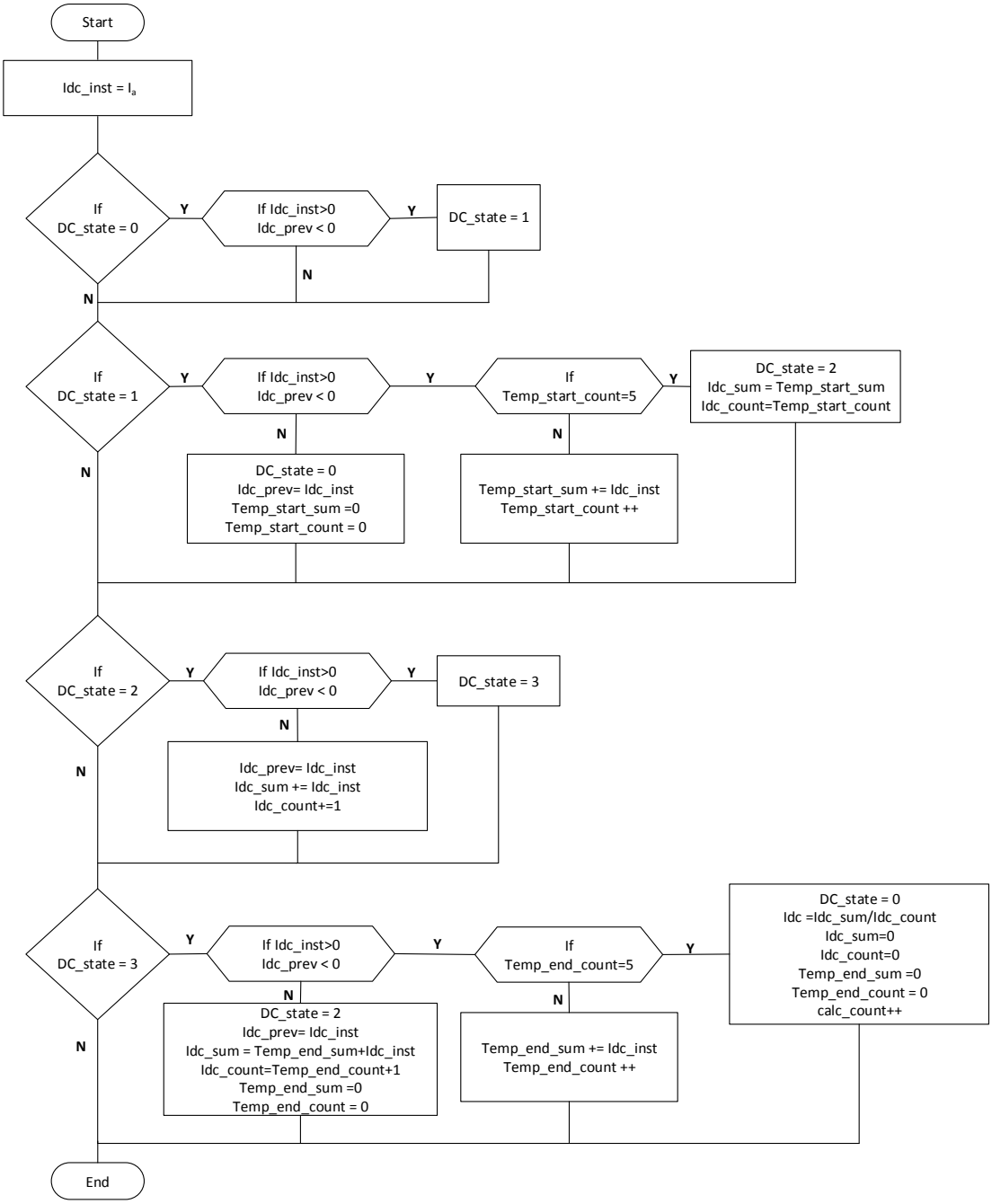

Figure 56. Flowchart for DC calculation by the DSP

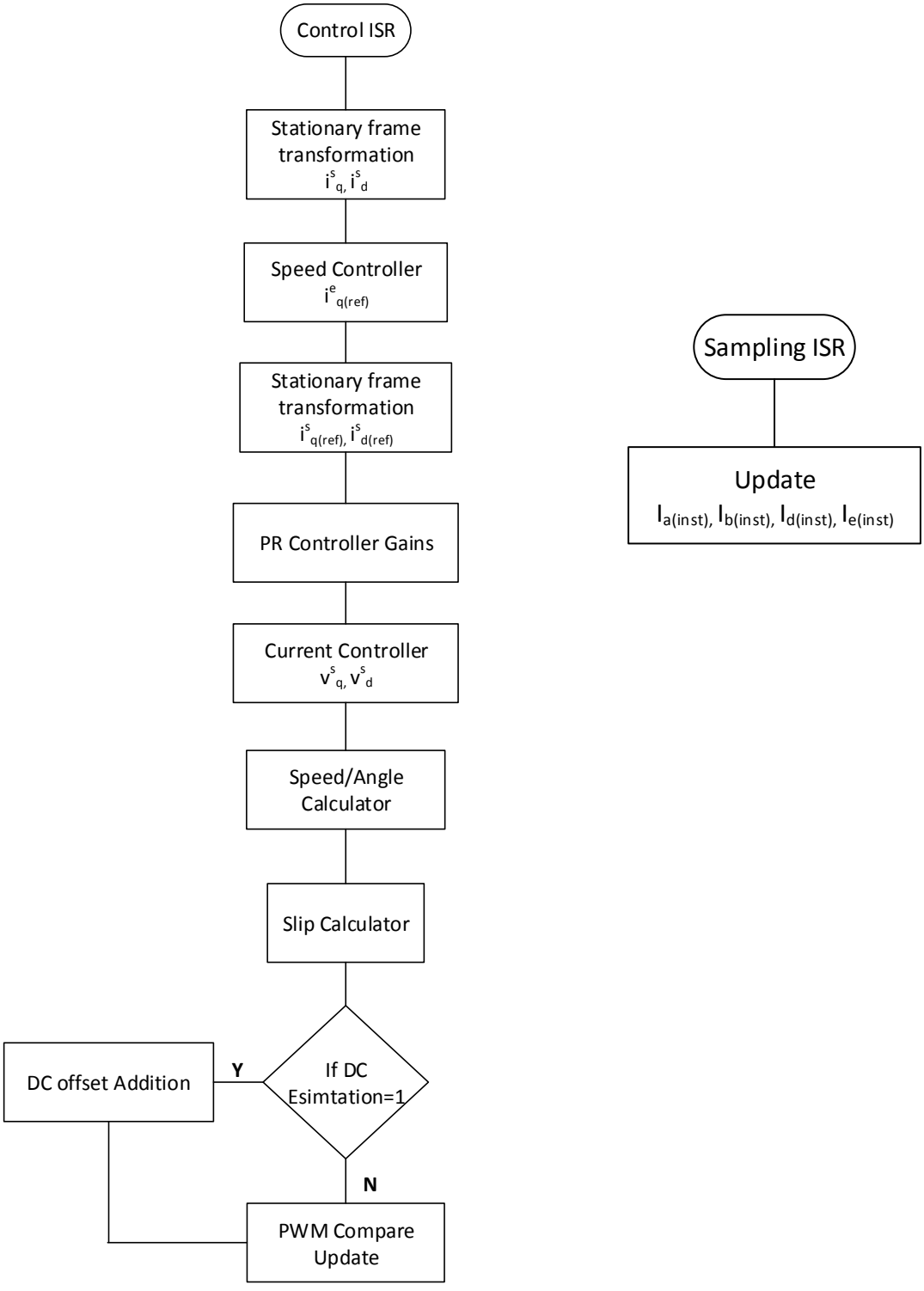

Figure 57. Flowchart for control ISR and sampling ISR

6.3 Experimental Verification of Fault Detection Algorithm

The effectiveness of the DC injection method for detecting inter-turn faults is verified at varying speeds and slips for a fault severity of 5.55% or 6 turns which is the first tap in the motor phase winding. Under the fault condition, the shorted turns are bypassed completely as shown in Figure 58 and a 2.5Ω resistor is connected across the shorted turns to limit the short circuit current. To eliminate errors due to temperature effects, all the DC offset current measurements before and after fault are performed after the motor reaches thermal steady state.

Before application of the turn fault the reference DC offset currents are measured at various operating points (slip/i_q, speed) for a given DC voltage command. This serves as the reference DC offset current for the healthy motor. After application of the fault, the DC offset in the current is once again measured for the same DC voltage command. The deviation in DC offset current (ΔI_{DC}) from the reference DC offset value corresponding to the same operating point is then determined. For all the tested cases a balanced DC voltage as explained in Chapter 4 is applied across phases AD and phases CB. It should be pointed out that all plots of ΔI_{DC} shown are based on the DC offset measured by the F28335 Microcontroller using the algorithms illustrated before.

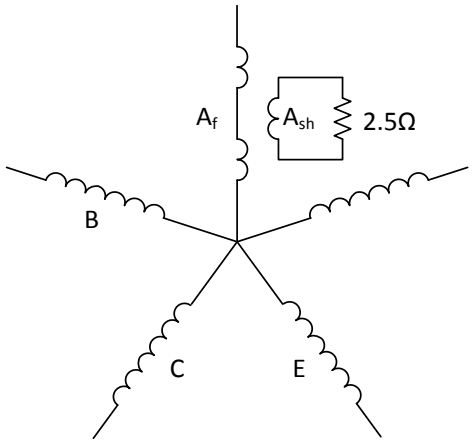

Figure 58. Experimental connection of motor windings for inter-turn fault

Figure 59 shows the variation in the torque pulsation of the motor with unbalanced and balanced DC voltage applied across the phases. The results show that torque pulsation is close to normal operation when using balanced DC injection. A small ripple exists since the ratio of applied DC voltages across phases AD and CB derived in Chapter 4, assumed perfectly balanced condition. The inherent unbalance is also evident in the rise in DC current in phase A when a voltage is applied across C and B. Figure 60 shows the phase currents during balanced DC injection. The output from a vibration sensor mounted on the motor housing is shown in Figure 61 and is in agreement with the result.

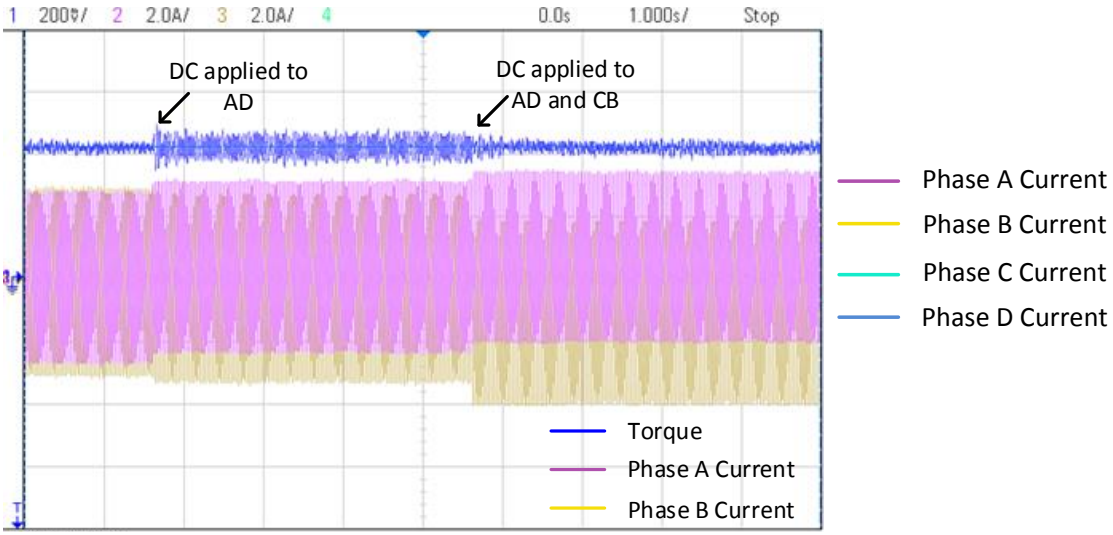

Figure 59. Comparison of torque with balanced and unbalanced DC voltage application (Speed =900rpm T = 5Nm)

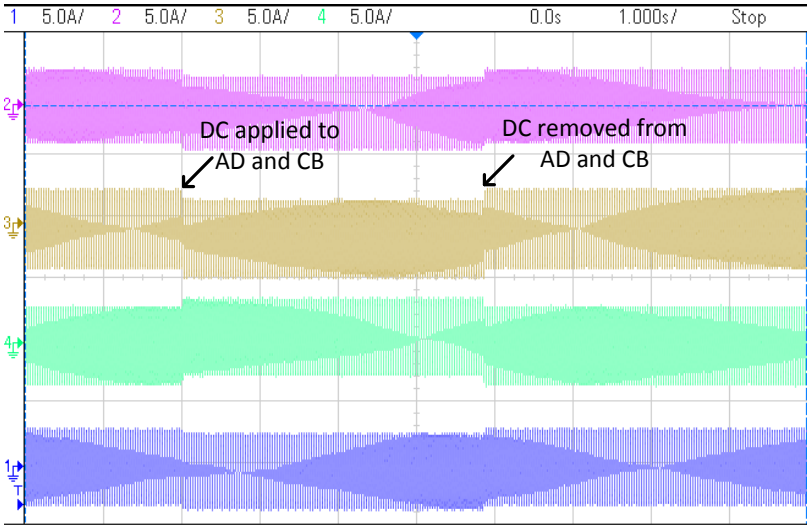

Figure 60. Currents with balanced DC voltage application

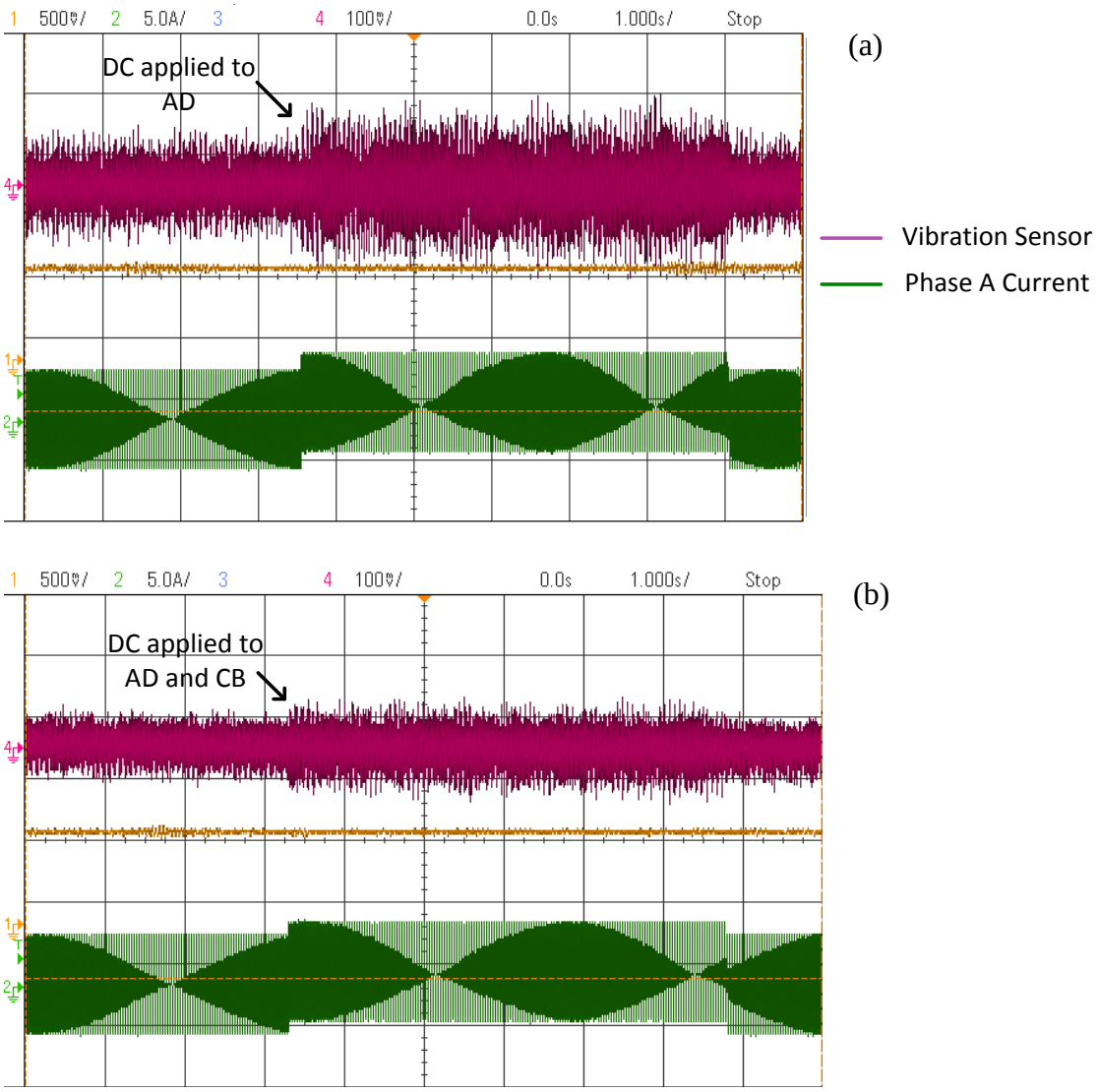

Figure 61. Comparison of vibration measured on motor casing with (a) balanced and (b) unbalanced DC voltage application

Figure 62 shows the change in the DC offset current in phase A created by a 5.55% inter-turn fault in phase A. The DC component of the current is obtained by filtering the phase A current on the oscilloscope.

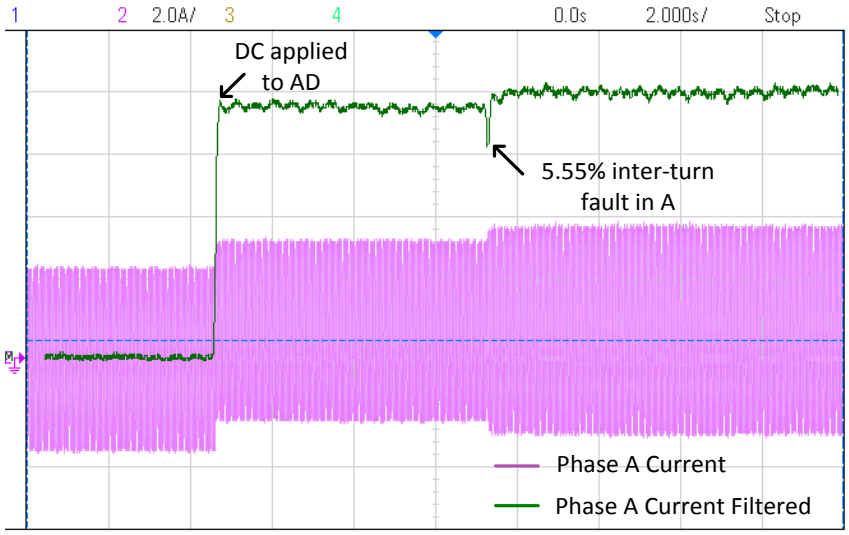

Figure 62. DC offset in the current in phase A before and after a 5.55% turn fault is applied to the phase

To verify the effectiveness of the fault index ΔI_{DC} in detecting inter-turn fault for different operating points, ΔI_{DC} is calculated for all phases from the DC offset current measured by the DSP before and after a 5.55% inter-turn fault in phase A. Note that the reference DC value is modified depending on the loading condition (i_q) obtained from tests on the healthy motor. Figure 63, Figure 64, and Figure 65 show that the fault index is highest for the faulty phase A. Figure 66 shows the variation in the fault index measured for phase A at random time points after the motor reaches thermal steady state.

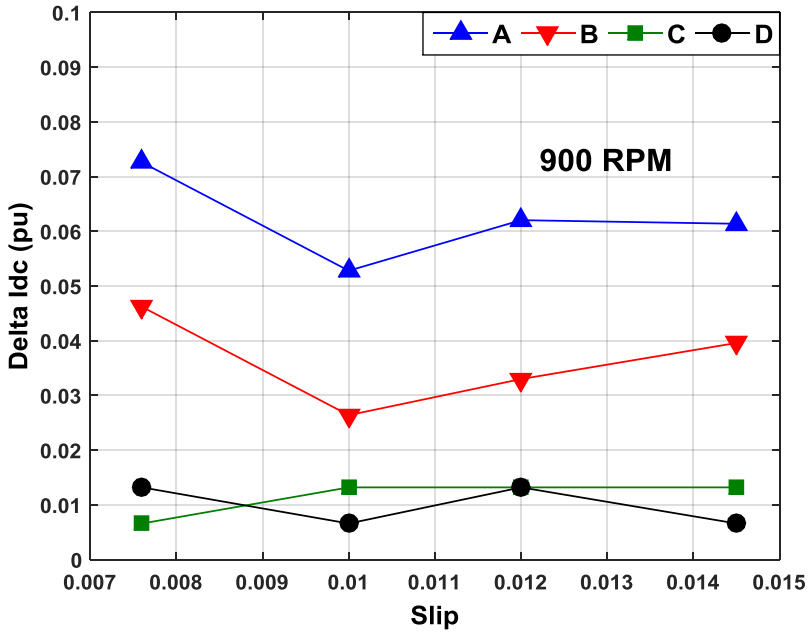

Figure 63. ΔI_{DC} after a 5.55% turn fault in phase A at 900rpm for different loads

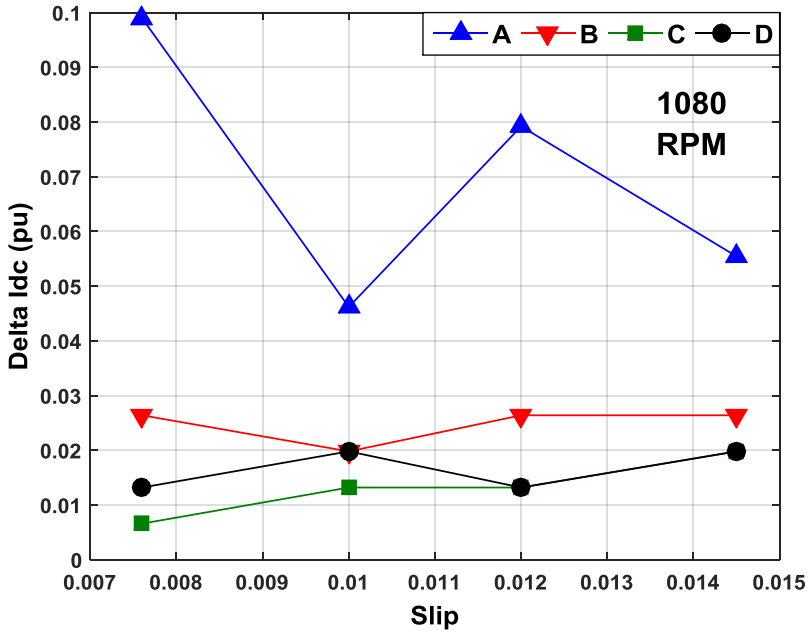

Figure 64. ΔI_{DC} after a 5.55% turn fault in phase A at 1080rpm for different loads

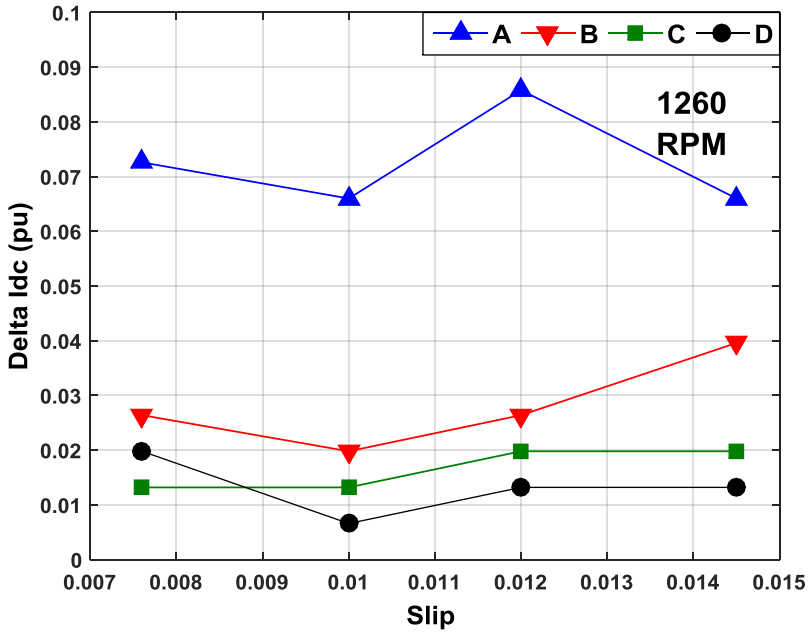

Figure 65. ΔI_{DC} after a 5.55% turn fault in phase A at 1260rpm for different loads

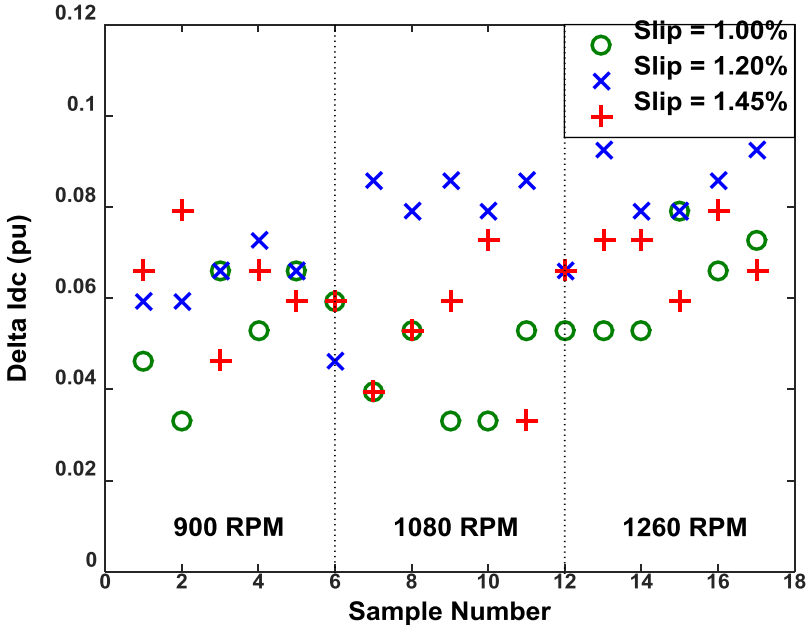

Figure 66. ΔI_{DC} for phase A after a 5.55% turn fault in phase A calculated by the microcontroller at random time points

6.4 Experimental Verification of Fault-Tolerant Control

The fault-tolerant control scheme assumes that after detection and identification the faulty phase is opened by some external means. For the experimental test set-up a switch (SPST), is used to open phase A as shown in the Figure 67. The DSP is programmed to modify the x- and y- axis commands for fault-tolerant operation by setting a flag which occurs after the switch is opened. A light load is applied to ensure that over modulation does not occur during the fault-tolerant operation when the DC bus utilization increases [39]. The load torque is kept the same before and after the fault.

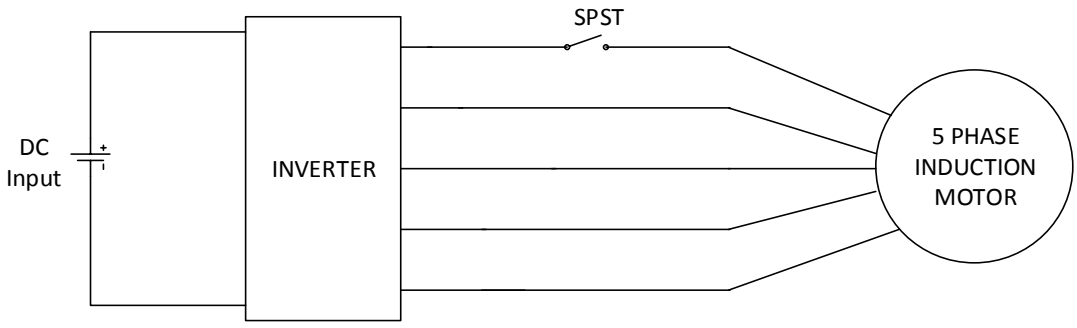

Figure 67. Schematic for experimental testing of fault-tolerant operation

Figure 68 shows the operation of the motor under healthy operating condition. Due to limitations in the number of channels in the oscilloscope only currents in phase A, B, C, and D are shown. Figure 69 shows the change in the current after phase A is opened but the control loop is unmodified and x and y voltages are 0. A clear distortion can be seen in the currents due to introduction of non-zero x and y- axis current components in the faulty motor. The lack of compensation for shift in the neutral voltage also introduces current distortion. Additionally, the phase currents are unbalanced. Figure 70 shows the

same operating condition when fault-tolerant control is applied to the motor. The phase currents are now balanced.

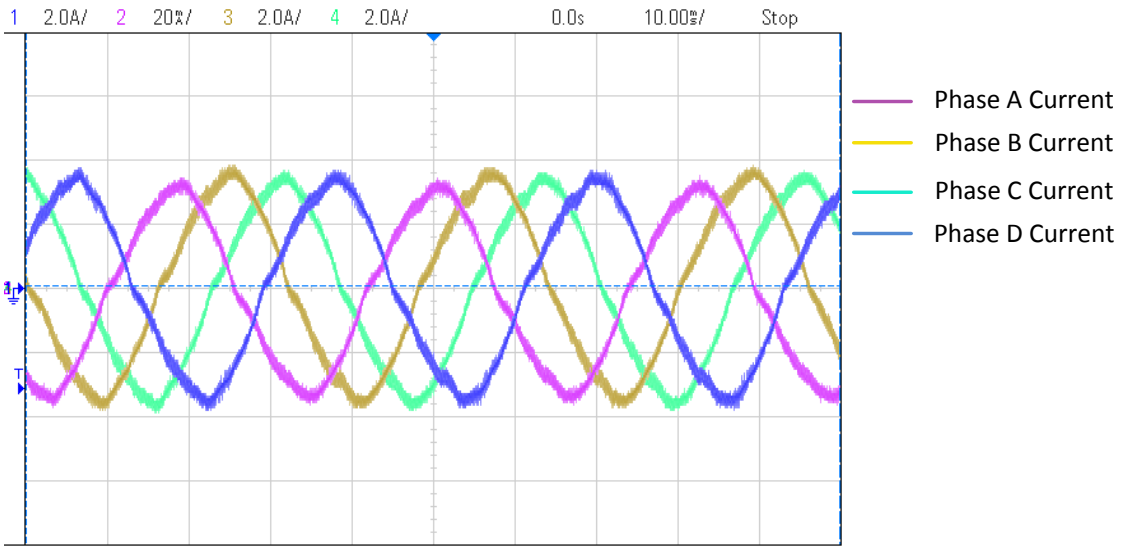

Figure 68. Operation of the motor under healthy condition at 900rpm

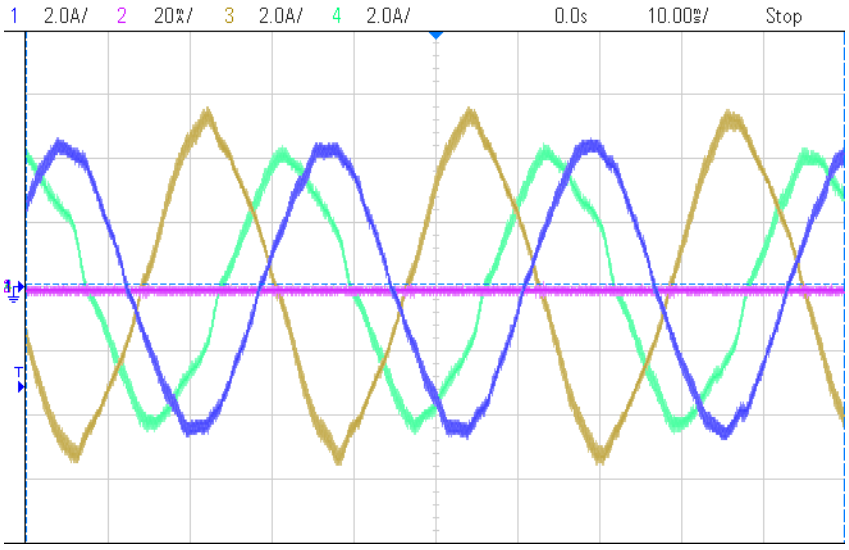

Figure 69. Operation of the motor with phase A opened using the conventional control loop

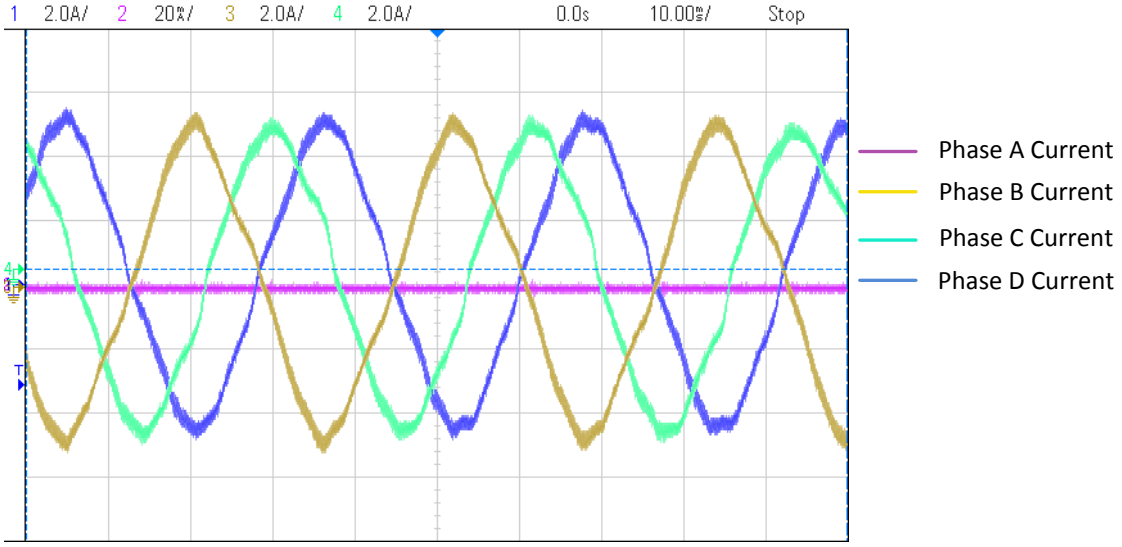

Figure 70. Operation of the motor with phase A opened applying fault-tolerant control

The transition from healthy to faulty operating condition with and without fault-tolerant control is shown in Figure 71.

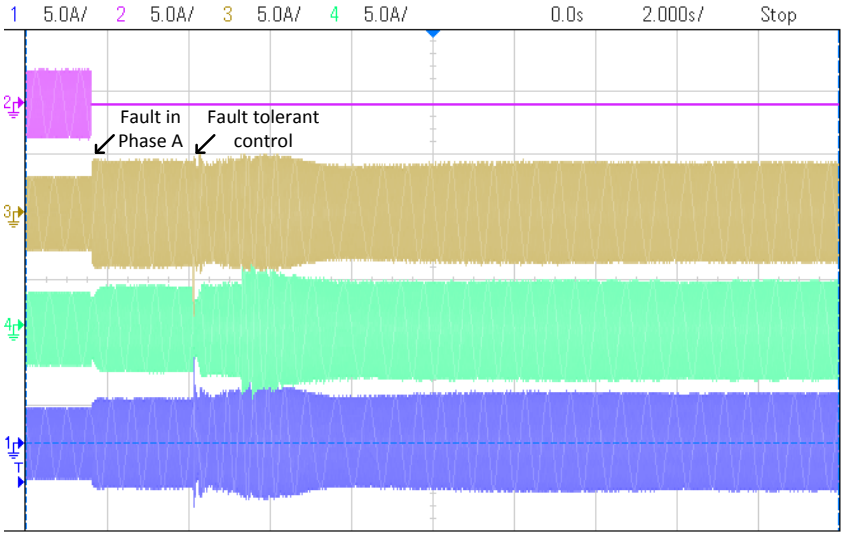

Figure 71. Transition from healthy to faulty to fault-tolerant operation

7. CONCLUSIONS AND FUTURE WORK

Reliability of the electric motor drive system is of prime importance in various cost sensitive and safety-critical applications.

Multiphase motors specifically five-phase motors, with their inherent ability to operate with an open phase are a possible solution to designing more reliable, fault-tolerant systems. However to exploit its fault-tolerant capability a five-phase motor drive system must be able to detect, identify and isolate the fault. Stator winding faults which originate as turn-to-turn faults within a phase have been identified as a major cause of failure in induction motors.

To solve this problem, a low-cost non-intrusive inter-turn fault detection method has been integrated with the fault-tolerant control scheme for a five-phase induction motors. The main advantage of the proposed DC injection method for fault detection is that it does not rely on magnetic imbalances created in the motor that have been shown to have more than one cause leading to false positives. By applying balanced DC voltages across two pairs of phases it has been shown to be truly non-intrusive in terms of its impact on the motor torque production.

To design the motor to be more tolerant to stator faults, fractional slot concentrated windings (FSCW) or tooth windings are being widely used for permanent magnet motors. This winding configuration eliminates the overlap between the different phases at the stators end connection, in addition to providing several other performance related benefits. From a reliability standpoint this provides physical isolation between the phases. An

FSCW configuration has been developed for outer rotor induction motors. In addition to eliminating overlap in the end windings the proposed design reduces the copper utilization by 11% when compared to a conventional distributed winding.

The widespread use of condition monitoring systems for motor drives has been mainly restricted by the added cost and complexity making it justifiable only for a handful of applications. However DSP based condition monitoring methods provide a low-cost alternative and have become more realizable due to the availability of fast and powerful microcontrollers. Such a system would also be suitable for applications that require integration of the motor and drive into a single package, where condition monitoring and reliably gain importance. Although this dissertation only introduced a stator inter-turn fault detection method there is still a need for DSP based monitoring methods for several other motor faults including eccentricity faults, broken bar faults and demagnetization in PM motors.

On the motor side, this dissertation illustrated possible FSCW configurations for induction motors. In addition to the improved copper utilization and magnetic isolation, FSCW allows for the use of hair-pin type bar windings. Bar wound coils can handle higher current densities due to better thermal contact with the slot walls and are less prone to burn out during inter-turn faults. With the absence of magnets (demagnetization) in an induction motor, a bar wound stator would result in a true fault-tolerant, torque dense design. This is one aspect that has to be further explored.

REFERENCES

[1] S. Nandi, H. A. Toliyat and X. Li, "Condition monitoring and fault diagnosis of electrical motors-a review," in *IEEE Transactions on Energy Conversion*, vol. 20, no. 4, pp. 719-729, Dec. 2005.

[2] F. Filippetti, G. Franceschini, C. Tassoni, S. Meo, and A. Ometto, “A simplified model of induction motor with stator shorted turns oriented to diagnostics,” in *Proc. ICEM*, Vigo, 1996, pp. 410–413.

[3] C. Gerada *et al*., "The results do mesh," in *IEEE Industry Applications Magazine*, vol. 13, no. 2, pp. 62-72, March-April 2007.

[4] S. M. A. Cruz and A. J. M. Cardoso, “Multiple reference frames theory: A new method for the diagnosis of stator faults in three-phase induction motors,” in *IEEE Transactions on Energy Conversion.*, vol. 20, no. 3, pp. 611–619, Sep. 2005.

[5] EL-Refaie, A.M., "Fractional-Slot Concentrated-Windings Synchronous Permanent Magnet Machines: Opportunities and Challenges," in *IEEE Transactions on Industrial Electronics*, vol.57, no.1, pp.107-121, Jan. 2010

[6] R. Maier, “Protection of squirrel-cage induction motor utilizing instantaneous power and phase information,” in *IEEE Transactions on Industry Applications*, vol. 28, no. 2, pp. 376-380, March/April, 1992.

[7] J. S. Hsu, “Monitoring of defects in induction motors through air-gap torque observation,” in *IEEE Transactions on Industry Applications*, vol. 31, no. 5, pp. 1061-1021, Sept./Oct., 1995.

[8] G. B. Kliman, W. J. Premerlani, R. A. Koegl and D. Hoeweler, "A new approach to on-line turn fault detection in AC motors," *Industry Applications Conference, 1996. Thirty-First IAS Annual Meeting, IAS '96., Conference Record of the 1996 IEEE*, San Diego, CA, 1996, pp. 687-693 vol.1.

[9] J. Sottile and J. L. Kohler, "An on-line method to detect incipient failure of turn insulation in random-wound motors," in *IEEE Transactions on Energy Conversion*, vol. 8, no. 4, pp. 762-768, December, 1993.

[10] F. C. Trutt, J. Sottile, and J. L. Kohler, "Online condition monitoring of induction motors," in *IEEE Transactions on Industry Applications*, vol. 38, no. 6, pp. 1627-1632, Nov./Dec., 2002.

[11] S. Williamson and K. Mirzoian, "Analysis of Cage Induction Motors with Stator Winding Faults," in *IEEE Transactions on Power Apparatus and Systems*, vol. PAS-104, no. 7, pp. 1838-1842, July 1985.

[12] A. J. Marques Cardoso, S. M. A. Cruz and D. S. B. Fonseca, "Inter-turn stator winding fault diagnosis in three-phase induction motors, by Park's vector approach," in *IEEE Transactions on Energy Conversion*, vol. 14, no. 3, pp. 595-598, Sep 1999.

[13] S. M. A. Cruz and A. J. M. Cardoso, "Stator winding fault diagnosis in three-phase synchronous and asynchronous motors, by the extended Park's vector approach," in *IEEE Transactions on Industry Applications*, vol. 37, no. 5, pp. 1227-1233, Sep/Oct 2001.

[14] Bellini, A.; Filippetti, F.; Tassoni, C.; Capolino, G.-A., "Advances in Diagnostic Techniques for Induction Machines," in *IEEE Transactions on Industrial Electronics*, vol.55, no.12, pp.4109-4126, Dec. 2008

[15] A. M. da Silva, R. J. Povinelli and N. A. O. Demerdash, "Induction Machine Broken Bar and Stator Short-Circuit Fault Diagnostics Based on Three-Phase Stator Current Envelopes," in *IEEE Transactions on Industrial Electronics*, vol. 55, no. 3, pp. 1310-1318, March 2008.

[16] S. M. A. Cruz, H. A. Toliyat and A. J. M. Cardoso, "DSP implementation of the multiple reference frames theory for the diagnosis of stator faults in a DTC induction motor drive," in *IEEE Transactions on Energy Conversion*, vol. 20, no. 2, pp. 329-335, June 2005.

[17] R. Maier, "Protection of squirrel-cage induction motor utilizing instantaneous power and phase information," in *IEEE Transactions on Industry Applications*, vol. 28, no. 2, pp. 376-380, Mar/Apr 1992.

[18] J. S. Hsu, "Monitoring of defects in induction motors through air-gap torque observation," in *IEEE Transactions on Industry Applications*, vol. 31, no. 5, pp. 1016-1021, Sep/Oct 1995.

[19] J. L. Kohler, J. Sottile, and F. C. Trutt, “Alternatives for assessing the electrical integrity of induction motors,” in *IEEE Transactions on Industrial Applications*, vol. 28, no. 5, pp. 1109–1117, Sep./Oct. 1992.

[20] S. B. Lee, R. M. Tallam, and T. G. Habetler, “A robust, on-line turnfault detection technique for induction machines based on monitoring the sequence component

impedance matrix," in *IEEE Transactions on Power Electronics*,vol. 18, no. 3, pp. 865–872, May 2003.

[21] M. Cash, T. Habetler and G. Kliman, "Insulation failure prediction in AC machines using line-neutral voltages", *IEEE Transactions on Industry Applications*, vol. 34, no. 6, pp. 1234-1239, 1998.

[22] Nandi, S.; Toliyat, H.A., "Novel frequency-domain-based technique to detect stator interturn faults in induction machines using stator-induced voltages after switch-off," in *IEEE Transactions on Industry Applications,* vol.38, no.1, pp.101-109, Jan/Feb 2002

[23] Briz, F.; Degner, M.W.; Diez, A.B.; Guerrero, J.M., "Online diagnostics in inverter-fed induction machines using high-frequency signal injection," in *IEEE Transactions on Industry Applications,* vol.40, no.4, pp.1153-1161, July-Aug. 2004

[24] A. Bellini, F. Filippetti, G. Franceschini and C. Tassoni, "Closed-loop control impact on the diagnosis of induction motors faults", *IEEE Transactions on Industry Applications*, vol. 36, no. 5, pp. 1318-1329, 2000.

[25] R. M. Tallam, T. G. Habetler, and R. G. Harley, "Stator winding turn-fault detection for closed-loop induction motor drives," in *IEEE Transactions on Industry Applications*, vol. 39, no. 3, pp. 720-724, May/June, 2003.

[26] F. C. Trutt, J. Sottile, and J. L. Kohler, "Online condition monitoring of induction motors," in *IEEE Transactions on. Industry Applications*, vol. 38, no. 6, pp. 1627-1632, Nov./Dec., 2002.

[27] E. Levi, R. Bojoi, F. Profumo, H. Toliyat and S. Williamson, "Multiphase induction motor drives – a technology status review", *IET Electric Power Applications*, vol. 1, no. 4, p. 489, 2007.

[28] Huangsheng Xu, H. A. Toliyat and L. J. Petersen, "Rotor field oriented control of five-phase induction motor with the combined fundamental and third harmonic currents," *Applied Power Electronics Conference and Exposition, 2001. APEC 2001. Sixteenth Annual IEEE*, Anaheim, CA, 2001, pp. 392-398 vol.1.

[29] Huangsheng Xu, H. Toliyat and L. Petersen, "Five-phase induction motor drives with DSP-based control system", *IEEE Transactions on Power Electronics*, vol. 17, no. 4, pp. 524-533, 2002.

[30] H. A. Toliyat and Huangsheng Xu, "A novel direct torque control (DTC) method for five-phase induction machines," *Applied Power Electronics Conference and Exposition, 2000. APEC 2000. Fifteenth Annual IEEE*, New Orleans, LA, 2000, pp. 162-168 vol.1.

[31] Iqbal, A., Levi, E., Jones, M., and Vukosavic, S. N., "Generalised Sinusoidal PWM with Harmonic Injection for Multi-Phase VSIs," *Power Electronics Specialists Conference, 2006. PESC '06. 37th IEEE*, Jeju, 2006, pp. 1-7.

[32] P. S. N. de Silva, J. E. Fletcher and B. W. Williams, "Development of space vector modulation strategies for five phase voltage source inverters," *Power Electronics, Machines and Drives, 2004. (PEMD 2004). Second International Conference on (Conf. Publ. No. 498)*, Edinburgh, UK, 2004, pp. 650-655 Vol.2.

[33] J. R. Fu and T. A. Lipo, “Disturbance free operation of a multiphase current regulated motor drive with an opened phase,” in *IEEE Transactions on. Industrial Applications*, vol. 30, no. 5, pp. 1267–1274, Sep./Oct. 1994

[34] Jacobina, C.B.; Freitas, I.S.; Oliveira, T.M.; da Silva, E.R.C.; Lima, A.M.N., "Fault tolerant control of five-phase AC motor drive," in *Power Electronics Specialists Conference, 2004. PESC 04. 2004 IEEE 35th Annual* , vol.5, no., pp.3486-3492 Vol.5, 20-25 June 2004

[35] A. Tani, M. Mengoni, L. Zarri, G. Serra, and D. Casadei, “Control of multi-phase induction motors with an odd number of phases under open-circuit phase faults,” in *IEEE Transactions on Power Electronics*, vol. 27, no. 2, pp. 565–577, Feb. 2012.

[36] L. Alberti and N. Bianchi, “Experimental tests of dual three-phase induction motor under faulty operating condition,” in *IEEE Transactions on Industrial Electronics*, vol. 59, no. 5, pp. 2041–2048, May 2012.

[37] H. M. Ryu, J.W. Kim, and S. K. Sul, “Synchronous-frame current control of multiphase synchronous motor under asymmetric fault condition due to open phases,” in *IEEE Transactions on Industrial Applications*, vol. 42, no. 4, pp. 1062–1070, Jul./Aug. 2006.

[38] H. Guzmán, M. J. Durán and F. Barrero, "A comprehensive fault analysis of a five-phase induction motor drive with an open phase," *Power Electronics and Motion Control Conference (EPE/PEMC), 2012 15th International*, Novi Sad, 2012, pp. LS5b.3-1-LS5b.3-6.

[39] H. Guzman, M. Duran, F. Barrero, L. Zarri, B. Bogado, I. Gonzalez Prieto and M. Arahal, "Comparative Study of Predictive and Resonant Controllers in Fault-Tolerant Five-Phase Induction Motor Drives", in *IEEE Transactions on Industrial Electronics*, vol. 63, no. 1, pp. 606-617, 2016.

[40] A. G. Yepes *et al.*, "Effects of discretization methods on the performance of resonant controllers," in *IEEE Transactions on Power Electronics*, vol. 25, no. 7, pp. 1692–1712, Jul. 2010.

[41] Haylock, J.A.; Mecrow, B.C.; Jack, A.G.; Atkinson, D.J., "Operation of a fault tolerant PM drive for an aerospace fuel pump application," in *Electrical Machines and Drives, 1997 Eighth International Conference on (Conf. Publ. No. 444)* , vol., no., pp.133-137, 1-3 Sep 1997

[42] A. M. El-Refaie and M. R. Shah, "Comparison of Induction Machine Performance with Distributed and Fractional-Slot Concentrated Windings," *Industry Applications Society Annual Meeting, 2008. IAS '08. IEEE,* Edmonton, Alta., 2008, pp. 1-8.

[43] M. V. Cistelecan, F. J. T. E. Ferreira and M. Popescu, "Three phase tooth-concentrated multiple-layer fractional windings with low space harmonic content," *2010 IEEE Energy Conversion Congress and Exposition*, Atlanta, GA, 2010, pp. 1399-1405.

[44] L. Alberti and N. Bianchi, "Design and tests on a fractional-slot induction machine," *2012 IEEE Energy Conversion Congress and Exposition (ECCE)*, Raleigh, NC, 2012, pp. 166-172.

[45] T. Lipo, *Introduction to AC machine design*. [Madison, Wis.]: Wisconsin Power Electronics Research Center, University of Wisconsin, 2004.

[46] Zmood, D.N.; Holmes, D.G., "Stationary frame current regulation of PWM inverters with zero steady-state error,", in *IEEE Transactions on Power Electronics*, vol.18, no.3, pp.814,822, May 2003

[47] H. A. Toliyat and T. A. Lipo, "Transient analysis of cage induction machines under stator, rotor bar and end ring faults," in *IEEE Transactions on Energy Conversion*, vol. 10, no. 2, pp. 241-247, Jun 1995.

[48] Pyrhonen, J., Jokinen, T., Hrabovcova, V., *"Design of Rotating Electrical Machines"*, Chichester, UK: Wiley, 2008

[49] Xiaogang Luo, Yuefeng Liao, H. A. Toliyat, A. El-Antably and T. A. Lipo, "Multiple coupled circuit modeling of induction machines," in *IEEE Transactions on Industry Applications*, vol. 31, no. 2, pp. 311-318, Mar/Apr 1995.

[50] Lee, Y. (2007). *A stator turn fault detection method and a fault-tolerant operating strategy for interior PM synchronous motor drives in safety-critical applications* (Doctoral dissertation, Georgia Institute of Technology).

[51] J. Penman, H. G. Sedding, B. A. Lloyd and W. T. Fink, "Detection and location of interturn short circuits in the stator windings of operating motors," in *IEEE Transactions on Energy Conversion*, vol. 9, no. 4, pp. 652-658, Dec 1994.

[52] Pinjia Zhang; Bin Lu; Habetler, T.G., "An Active Stator Temperature Estimation Technique for Thermal Protection of Inverter-Fed Induction Motors With

Considerations of Impaired Cooling Detection," in *IEEE Transactions on Industry Applications,* , vol.46, no.5, pp.1873-1881, Sept.-Oct. 2010

[53] Marčetić, Darko, Marko Gecić, and P Cistelecan etar Matić. "Robust Online Stator Resistance Estimation of High-Speed Vector Controlled Induction Motor", in *Proc. Scientific-Professional Symposium INFOTEH-JAHORINA* vol.13, March 2014.

[54] J. Plotkin, M. Stiebler and D. Schuster, "A novel method for online stator resistance estimation of inverter-fed ac-machines without temperature sensors," *Optimization of Electrical and Electronic Equipment, 2008. OPTIM 2008. 11th International Conference on*, Brasov, 2008, pp. 155-161.

[55] B. Heller and V. Hamata, *Harmonic field effects in induction machines*. Prague: Academia, 1977.

[56] G. Dajaku and D. Gerling, "Eddy current loss minimization in rotor magnets of PM machines using high-efficiency 12-teeth/10-slots winding topology," *Electrical Machines and Systems (ICEMS), 2011 International Conference on*, Beijing, 2011, pp. 1-6.

[57] G. Dajaku and D. Gerling, "A Novel 24-Slots/10-Poles Winding Topology for Electric Machines," *2011 IEEE International Electric Machines & Drives Conference (IEMDC)*, Niagara Falls, ON, 2011, pp. 65-70.

[58] Alberti, L., Bianchi, N., "Theory and Design of Fractional-Slot Multilayer Windings," in *IEEE Transactions on Industry Applications*, vol.49, no.2, pp.841, 849, March-April 2013.

[59] A. G. Yepes *et al*., "Parameter Identification of Multiphase Induction Machines With Distributed Windings—Part 1: Sinusoidal Excitation Methods," in *IEEE Transactions on Energy Conversion*, vol. 27, no. 4, pp. 1056-1066, Dec. 2012.